Describing Shrivel Development in 'SunGold™' kiwifruit using Fringe projection and Three-dimension Scanner

A thesis presented in partial fulfilment of the requirements for the degree of

Master of Food Technology

at Massey University, Manawatu,

New Zealand.

Ruishu Cao

2021

Abstract

Postharvest kiwifruit shrivel decreases customer satisfaction and is highly correlated with weight loss during storage after harvest. The wrinkled skin has been mainly attributed to the water loss from cells near the epidermis on the kiwifruit surface. This thesis investigated the impact of rate of weight loss on kiwifruit shrivel symptoms, and the use of skin topography to non-destructively and quantitatively describe shrivel severity. Three regimes (20℃, 47% RH; 20℃, 53% RH; 1℃, 80% RH) were evaluated over a 6% weight loss range to assess kiwifruit skin topography parameters using fringe projection.

Generally, a higher weight loss induces more severe shrivel symptoms. Kiwifruit with 4-5% weight loss were regarded as being at risk of shriveling and a shriveled kiwifruit normally has 1- 6% relative mass loss. Skin topography parameters could identify the shrivel occurrence but cannot classify the severity of shrivel. The vertical parameters represented by root mean square average of height of roughness (Rq) could indicate the shrivel occurrence at 73.7% accuracy, whereas Peak density (PC) gave an accuracy of 81.9%. Also, fringe projection showed obvious differentiation surface changes at each weight loss treatment in each storage period. Advanced 3D technology was applied in physically recreating 3D samples of fruit at different levels of shrivel severity. This investigation showed obvious distinctions between shrivel categories in the 3D fruit surfaces, however it lacked accuracy.

It is concluded that the shrivel appearance can be identified by skin topography parameters. 3D technology has the potential ability to record and reproduce the shrivel severities which are measurable using surface imaging technologies such as fringe projection.

ACKNOWLEDGEMENT

First and foremost, I would like to express my sincere gratitude to my research supervisors, Dr. Mo Li, and Prof. Andrew East, for offering me the precious opportunity to do this research and providing clear guidance on experiments and thesis. I have been deeply inspired by their expertise, enthusiasm, patience, and sincerity in the past year. I am very much thankful to Dr. Mo Li for her invaluable advice that made the thesis much more academic and for indicating a correct direction on my academic career. I am extremely grateful to Prof. Andrew East for guiding me to carry out the research and for sacrificing his precious time to make further discussion on my thesis. It was a great honor to work and study under their guidance.

I would like to express my gratitude to Dr. Mo Li, Prof. Andrew East, Prof. Johan Potgieter, Jeans Odendaal, and Dr. Gabe Redding for supporting me to do 3D scanning and printing, which is of great help to the research. Many thanks to Johan and Jeans for the expert advice and help, I would not have been able to complete my 3D printing without their assistance. I would also like to express gratitude to Gabe who provided professional guidance on how to use the blender (version 2.79, Blender foundation, Amsterdam, Netherlands, 2020), which without I would not have been able to experiment successfully.

I am extending my heartfelt thanks to my friends and research colleagues, Zoe, Han, Raquel, Talon, Jeans Henri Odendaal, Mr. Peter Jeffery for their support and encouragement throughout the research. My gratitude also to my friend Brenda who gave me motivation when I was upset in daily life.

I would like to say thanks to the MAF team for the opportunities, the support, and the expert guidance, I would not have been able to access the research work and achieve the objective that I set up without my team.

List of Abbreviations

AFM	Atomic Force Microscope
AM	Additive Manufacturing
AR	Augmented Reality
℃	Degree Celsius
EP	Epidermis
FOB	Freight On Board
FTP	Fourier Transforms Profilometry
h	Hour (s)
IP	Inner pericarp
jpg	Joint Picture Group
kg	Kilogram (s)
LCoS	Liquid Crystal on Silicon
mg	Milligram
MJ	Material Jetting
BJ	Binder Jetting
DED	Directed Energy Deposition
ME	Material Extrusion
MJ	Material Jetting
PBF	Powder Bed Fusion
SL	Sheet Lamination
VP	Vat Photopolymerization
MIFST	Massey Institute of Food Science and Technology
mm	Millimeter (s)
µm	Micrometer
MTL	Wavefront Material Template Library
m2	Square Metre
OP	Outer Pericarp

%	Percent
PSP	Phase Stepping Profilometry
RH%	Relative Humidity
RWL	Relative Weight Loss
SFP	Spatial Filtering Profilometry
STL	Standard Template library
TCR	Temperature-Controlled Room
USA	United States
WTP	Wavelet Transforms Profilometry
WVPD	Water Vapour Pressure Deficit

Table of Contents

List of Figures

List of Tables

Chapter 1. Introduction

The gold fleshed Zespri® 'SunGold™' kiwifruit (Actinidia *chinensis* var. *chinensis* 'Zesy002') Was first registered in 2009 and has since become a market staple (Costa et al., 2017). 'SunGold™' replaced 'Hort16A' as the commercial yellow fleshed kiwifruit cultivar in New Zealand and is increasingly exported overseas (Ferguson & Huang, 2016; Costa et al., 2017). As a newly released variety, 'SunGold™' is not only PSA-resistant but also has higher Vitamin C and a more subtropical flavour than classic green kiwifruit (Ferguson & Huang, 2016).

As kiwifruit popularity increased, research focused on preserving fresh kiwifruit became a hotspot in recent decades. Maintenance of supply chain management aimed at reducing kiwifruit losses is a priority for the industry within the competitive global trade. Postharvest losses can occur due to mechanical injury, physiological, pathological and environment factors. To reduce commercial losses, the capability to distinguish poor and sound quality fruit in the sorting line could significantly improve inventory management (East, 2011).

Shrivel as a potential storage quality problem is a factor that affects customer preferences that is associated with softening and weight loss, but can be instigated by injuries such as bruises, during storage (Burden et al., 2014). In general, water loss in fruit and vegetables is the major cause of postharvest loss that are estimated to range from 45 to 55% along the value chain each year (Lufu et al., 2020). Shrivel is an aesthetic disorder resulting from epidermal cell shrinkage (Burden et al., 2014; Wei et al., 2019). Shrivelled 'Gold9' kiwifruit generally had a 1-6% weight loss, but not all 'Gold9' kiwifruit with 6% weight loss exhibited shrivel symptoms (Burden et al., 2014). Therefore, the correlation between shrivel and weight loss is variable in 'Gold9'. However, weight loss does induce shrivel occurrence, and higher weight loss may result in severe shrivel symptoms. However, research to date has not yet determined the correlation between shrivel and weight loss in 'SunGold™'. One of the aims of this research is to explore the relationship between mass loss and shrivel in 'SunGold™'.

This research aims to evaluate the possible interactions between shrivel, skin topography parameters, and weight loss during kiwifruit postharvest. The shrivel conditions of kiwifruit were assessed in this work with a focus on visualizing skin topographical changes resulting from weight loss.

The main objectives defined for the present study are as follows:

1) Determine shrivel categories, and the influential skin topography parameters produced by fringe projection to classify shrivel categories

2) Setting up 3D shrivel library for the kiwifruit industry and ascertain what extent shrivel can be captured by 3D technology (scanning and printing) and fringe projection

Chapter 2. Literature review

This chapter gives a brief overview of how a pivotal role the kiwifruit industry plays in New Zealand, how water loss and weight change influence kiwifruit shrivel during kiwifruit development postharvest storage, and the impact of fruit shriveling on customers' preference. It also summarizes the different factors, including preharvest, harvest, and postharvest factors influencing kiwifruit water loss. Also, for decreasing the impact of shrivel, a review of fringe projection as a non-destructive method to monitor and determine kiwifruit skin topographical changes is presented. The three-dimensional scanning and printing to record the skin topography for indicating the shrivel categories are also reviewed. The examination of the literature offers the essential basis for future experimental enquiry in order to discover further research topics.

2.1. Kiwifruit history and importance in NZ

Kiwifruit (*Actinidia deliciosa and Actinidia chinensis*) is an edible berry in the genus *Actinidia*. It has high nutritional value and contains vitamins C and E, folate, and potassium, with high antioxidant capacity (Drummond, 2013). It by far only takes up small proportion of the global fruit bowl, representing 0.62% of the total production of crops globally in 2017 (FAOSTAT, 2020). However, it has a potential to be a successful commercial crop in the future. By 2019, the kiwifruit harvest area around the world had reached around 278,788 ha (FAOSTAT, 2020).

Kiwifruit originates from central and eastern China. Seed of kiwifruit was brought to New Zealand in the early 20th century, and the crop became a pillar industry in the horticultural economy of New Zealand (Schroeder & Fletcher, 1965). Eighty-seven percent of kiwifruit was produced by China, Italy, New Zealand, and Iran.

The kiwifruit industry is the largest fresh horticultural export industry from New Zealand (Mazzaglia et al., 2012). New Zealand had 12,905 ha of kiwifruit in 2020 (New Zealand Horticulture, 2020). In 2000, Exports of kiwifruit worth $462 million (FOB) was achieved and this value continues to rise. It achieved $ 2,533.6 million (FOB) in 2020, accounting for almost

69% of New Zealand's total fresh fruit exports (New Zealand Horticulture, 2020). Zespri International Limited, the world's largest kiwifruit marketer, is the sole global exporter of New

Zealand-grown kiwifruit (Burdon & Lallu, 2011). Zespri's kiwifruit was sold in more than 53 countries and accounting for 30% of global volume (FAOSTAT, 2020). Zespri kiwifruit is the most recognized fruit brand in China's largest cities, such as Beijing and Shanghai (Tait et al., 2018). Zespri not only put effort into kiwifruit marketing but also into the development of kiwifruit cultivars, such as 'SunGold™' and 'Red19' ('Zespri™RED').

"Hayward" kiwifruit (*Actinidia deliciosa* C.F. Liang and A.R. Ferguson var. *deliciosa*) was bred in 1927 and accounted for 90% of kiwifruit production worldwide until 2019. The cultivar 'Zesy002', commonly known as 'SunGold™', is marketed as Zespri® 'SunGold™' kiwifruit. Compared to Hayward, 'SunGold™' kiwifruit as a newly released cultivar is not only less susceptible to PSA but also an earlier maturing fruit, greater storage life, and a sweeter taste than 'Hayward' (Vanneste, 2012). While Hayward is still the most produced and sold kiwifruit cultivar throughout the world, making it currently numbers-wise the most popular. 'SunGold™' has the potential to be the most popular cultivar shortly (Costa et al., 2017).

2.2. Kiwifruit Anatomy

Kiwifruit consists of a core, inner pericarp (IP), outer pericarp (OP), and epidermis (EP) from inner to outer (Wei et al., 2019) (Fig. 2.1). Compared with the other regions, the core has the lowest water content but possesses high fiber content (Taglienti, et al., 2009; Wei et al., 2019), followed by IP cells containing seeds. The outer pericarp is the largest proportion of the kiwifruit (Burdon & Clark, 2001). The outer regions (OP and EP) contain water with greater mobility than the inner tissues (Taglienti, et al., 2009). Thus, the epidermal region followed by the OP is more susceptible to water loss than the inner tissues (DíazPérez et al., 2007). Therefore, the epidermis plays a vital role in controlling water loss in kiwifruit.

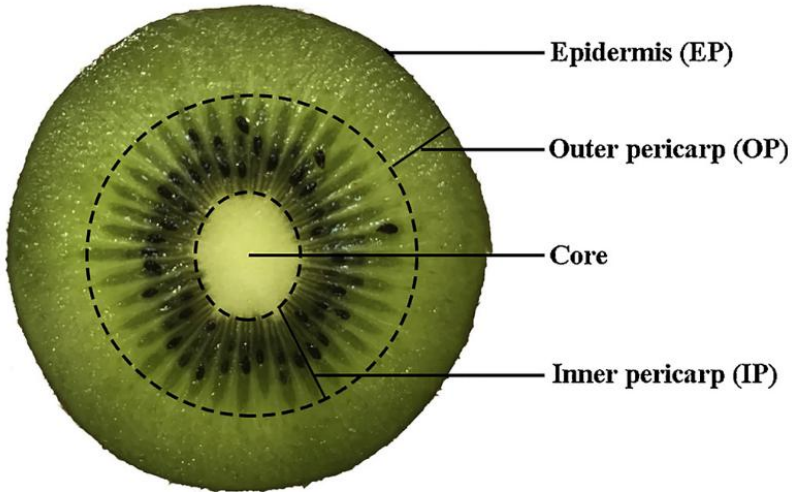

Figure 2.1. Transverse image of kiwifruit with tissue annotation retrieved from Wei et al (2019) with permission.

Common quality issues within the kiwifruit industry are shrivelled, soft fruit, decay, and development of disorders after harvest. Unblemished produce is required at a sale to achieve consumer acceptance (Wei et al., 2019). The occurrence of wrinkled skin is referred to as shrivel. Shrivel is a commercial risk as it impacts fruit appearance. Previous research has established that shrivel appearance in yellow-fleshed cultivar 'Gold9' (Actinidia chinensis) could be related to water status (free or bound water) on the fruit surface, water loss, and fruit softening (Burdon et al., 2014; Burdon et al., 2015).

Water loss results in the products developing shrivel, due to associated shrinkage of epidermal cells. Therefore, water loss of kiwifruit in the supply chain before the sale is important to manage. There are many factors affecting water loss during the entire period of fruit growing and marketing that have been summarised, which consists of preharvest, harvest, and postharvest factors. Those factors could increase susceptibility to moisture loss of fruit during the postharvest period.

2.3 Factors affecting water loss

2.3.1 Preharvest factors

Fruit cultivar, fruit size and orchard practices can affect water loss rate, directly or indirectly, during postharvest storage (Lufu et al., 2020). Water loss of fruit is highly correlated with the water vapor pressure deficit (WVPD). Factors that impact WVPD tend to affect water loss.

The weight loss rate is influenced by skin permeance, the surface area of fruit, and driving force (Maguire et al., 2001). Maguire et al. (2001) mentioned an equation that the correlation between surface area (m^2) and weight of the fruit (kg) is $A=0.058W^{0.685}$ in apple. This indicates that large fruit has a larger mass compared to smaller fruit. Large fruit has a lower surface area volume ratio. A larger surface area to volume ratio results in a larger transpiration area per kg of fruit. It means that large fruit loses water slower than smaller fruit (Ben-Yehoshua & Rodov, 2002).

Different cultivars of the same fruit have different skin permeance, which results in differences in water loss rates. A notable example is that 'Gold9' kiwifruit has higher skin permeance than 'Hort16A' and 'Hayward' (Boyd et al., 2011). This difference is thought to partially explain 'Gold9' fruit has propensity to shrivel (Hernandez et al., 2012; Minchin et al., 2013). However, Burdon et al. (2014) suggest that shrivel formation is not only about the amount of water lost or the rate but also how the cells "react" and change shape as a function of that water loss. Hence permeance explains the water loss but not necessarily the propensity to shrivel.

Pre-harvest orchards practices influence fruit water loss in postharvest storage as well. Fertilizer application on grapes (cv. Monukka) can minimize the moisture loss during postharvest storage (Zhang et al., 2017). This is because that the spray can minimizes the enzymatic disintegrations and maintain the integrity of cell structure (Lufu et al., 2020). Also, the calcium, magnesium and titanium ions from the spray can reduce moisture loss in peaches (cv. Early Swelling, cv. Sevilla) (Gayed et al., 2017; Serrano et al., 2004). A sudden change in water status of the fruit trees can initiate fruit cracking, enhancing fruit moisture and water loss in apples (Maguire et al., 2010).

2.3.2 At-harvest factors

Different orchard management practices at harvest, for instance, fruit maturity, the weather and climatic condition of harvest seasons, and the harvest technique, would impact the water loss of fruit in postharvest.

Well-matured fruit compared with over matured or less matured fruit tend to have a complete peel structure with proper cuticle permeability as essential barriers to water loss (Lufu et al., 2020). Harvesting as early as possible after fruit reach quality standards could avoid cracking of peel (Maguire et al., 2001). During the ripening process, the assimilates in the pulp will gradually increase and thus a decrease of osmotic potential, leading to a higher rate of water absorption in the pulp. This process increases the turgor pressure of the pulp and thus the flesh bulges, causing the pericarp to break.

Also, weather events, such as heavy rainfall before fruit harvest, would increase the turgor pressure within fruit tissues. The fruit would have high respiration and transpiration rates triggered by the high temperature at harvest. Thus, the harvest environment should be considered to minimize the product's weight loss after harvest. In addition, the harvest technique, for instance, mechanical harvest, could increase the forces on harvested fruit and cause tissue damage on the surface, increasing peel permeance (Li & Thomas, 2014).

2.3.3. Postharvest factors

Transpiration causes water loss in fruit and vegetable during postharvest. Water flows from the fruit tissue to the ambient environment are induced by the water gradient between the ambient air and epidermis (Maguire et al., 2001; Daz Pérez et al., 2007). The water gradient equals the water vapour pressure deficit if the air within the fruit is saturated (WVPD in Pa). The external environment: temperature, humidity, and airflow, all influence the water vapour pressure immediately external to the fruit and hence affect the water loss rate (Lufu et al., 2020).

Temperature is one of the most influential factors affecting mass loss from fresh commodities. High temperature decreases the relative humidity of the surroundings and increases the water potential of

the produce. High flesh temperature facilitates respiration and the evaporation of water from the skin surface, and thus inducing weight loss ((Talbot & Baird, 1993; Lufu et al., 2020). High temperatures also induce disorders in the interface of the polymer matrix and the soluble cuticular lipids, thus increasing the skin's water permeability (Maguire et al., 2001). However, low temperatures below optimum can result in freezing or chilling injury. Hence, controlling the temperature at an optimal range is vital to maintain the quality of fresh commodities.

Changes in relative humidity can affect the shelf-life significantly at a certain temperature (Lufu et al., 2020). An example is that when 'Gold9' fruit has been stored in high humidity for a long time and has softened while losing just a little amount of water, the soft fruit may shrivel after only a modest amount of water loss (Burdon et al., 2014). The water content of fruit is very high at harvest, generally in the range of 70-90%, for example, kiwifruit and apples possess water contents of 82 and 84%, respectively (Holcroft, 2015). Harvesting removes the fruit water supply, thus after harvest, fruit begin a self-consumption process. The ratio of the partial pressure of water vapour in the air to the saturation partial pressure at the ambient temperature is known as relative humidity (RH) (Maguire et al., 2010). Relative humidity（RH）lower than the stored fruit water content results in a difference between the amount of moisture in peel and the moisture content in the environment. Thus, it increases the water-holding capability of peel and water vapour pressure deficit (WVPD) (Lufu et al., 2020; Talbot & Baird, 1993). A high WVPD improves the driving force for water loss, and thus promotes the movement of water from fruit to surrounding (Maguire et al., 2001). At 0℃, 'Spadona' pears with 519 pa loss weight are faster than that in 6pa (Hertog et al., 2004).

Higher airflows tend to increase the rate of moisture loss on produce peel (Maguire et al., 2001; Lufu et al., 2020). Airflow affects water loss by influencing the boundary layer and WVPD. Some studies have used fans to regulate airflow and then reduce the relative humidity, such as Burdon & Clark (2001) and Lai et al. (2019). However, airflow can be an issue as it is used in cooling systems to facilitate cooling of the product but can potentially result in water loss if not managed properly. To prevent water loss in the kiwifruit industry, polyliners and other packaging materials are utilized (Mukama et al., 2020).

2.4 How does water loss affect shrivels

Shrivel is the description used for the visual skin wrinkling of bulky (spherical) crops (Fig. 2.2). Normally, the shrivel tends to occur as a firm fruit loses sufficient amounts of water (>6% absolute water loss) (Minchin et al., 2013; Burdon et al., 2015). The fruit skin can defend against water vapour diffusion; however, it must be porous enough to exchange oxygen and carbon dioxide in order for regular aerobic respiration to occur (Maguire et al.,2001). The permeance determines the ease with which water vapour can escape from fruit. Estimating the rate of water loss, surface area, and driving force are all essential part to determine permeance. This is the variable that is the most difficult to precisely measure; driving force data frequently contains major inaccuracies (Gaffney et al., 1985). Bell (1937) defined a general fruit skin as having four layers of tissue: an epidermal hair coating (missing in ripe apples), cuticle, epidermis, and hypodermis. The epidermis and hypodermis of the fruit skin are all cellular components, so they are the most permeable layers; unaltered cellulose walls are particularly permeable to water migration (Burton, 1982). Water can also effortlessly pass through semi-permeable membranes that surround cell vacuoles and cells (Burton, 1982). If these were the only barriers to transpiration, the fruit surface would quickly become dry. For a mature fruit, the cuticle is the outermost layer of the skin. An extracellular coating that protects leaves, primary stems, flowers, petioles, fruit, hairs, and even glands from the environment (Lendzian & Kerstiens 1991). The cuticle serves as a barrier between the plant and its environment, preventing excessive water loss through evaporation (Holloway, 1982). Permeance of fruit is considered as a crucial predictor of relative rates of weight loss in harvested apples, and consequently fruit within the population will shrivel (Maguire et al.,2001).

Figure 2.2. Kiwifruit shrivel symptom.

It has previously been observed that shrivelled 'Gold9' kiwifruit tends to have a 1-6% weight loss (Burdon et al., 2014), although weight loss of 1-6% did not always result in shrivel symptoms. Water loss is not the only factor that determine shrivel. This makes it difficult to identify the severity of shrivel directly by weight loss. 'Gold9' kiwifruit with 5.6% weight loss could be none, slightly or moderately shrivelled (Burdon et al., 2014). Thus, the correlation between weight loss and shrivel response of a wide variety of kiwifruit is not invariably moderate. The occurrence of shrivel is due to the deformation of fruit skin and tissues under the skin. The loss of water within the fruit can only become a problem if redistributing the water within the fruit does not preserve the hydration state of the fruit tissue under the skin. Thus, shrivel appearance is related to the water characteristics of the outer pericarp of fruit (Burdon et al., 2014).

The exterior pericarp with a higher water-binding capacity collects water, re-equilibrates water within the fruit when water is lost, and therefore inhibits water flow (Burdon et al., 2015). As the water evaporation occurs on the fruit surface, better water-holding capability prevents the water from flowing to the surface in 'Gold9'. Lower water mobility means there is limited transfer of water within the OP tissue, and therefore can replace water faster reducing the risk of shrivel appearance. In this case, the OP of 'Gold9' kiwifruit with high-water binding capacity appears more susceptible to shrivel than 'Hort16A' and 'SunGold™'.

Alternatively, firmer fruit had less severe shrivel symptoms compared with soft fruit. For instance, with weight loss >6%, the fruit with ~18 N firmness had no shrivel, but fruit in the range of 8~12N

showed shrivel symptoms (Burdon et al., 2015). Thus, controlling softening of fruit can help to manage shrivel appearance, although once the fruit is already soft, the potential to manage shrivel is limited. However, water loss is the main reason for firmness change in fruit (Holcroft, 2015). Hence, water loss could be the most significant index which needs to be considered in this essay.

2.5 Non-destructive method (Fringe Projection) indicating shrivel

2.5.1 The history of fringe projection

Fringe projection is a rapid and non-destructive technology that can perform high-resolution (μm) three-dimensional surface topographical imaging (Lai et al., 2019). The first use to determine surface topography was introduced by Rowe & Welford (1967). Fringe projection can measure the contouring of objects. Fringe projection provides a structured light of parallel stripes to the objective surface. The difference of the surface micro-topography on the objective surface can be modulated as fringe patterns and captured by the camera (Creath & Wyant, 1992).

In the last two decades, the use of fringe projection technology to generate 3D surface images has been an active research area in optical metrology (Gorthi, & Rastogi, 2010). Many applications are on quality control of manufactured surface and reverse engineering.

2.5.2 Principles of operation

The fringe projection applies active 3D morphometry where the artificial light source projects a structured pattern onto the surface of the measured objects (Gorthi & Rastogi, 2011). The fringe pattern is phase-modulated by the shape of the object surface, and the structured light with the deformation being captured by the camera from another angle (Fig. 2.3). The three-dimensional topography of the object can be determined by the position relationship between the light sources of the camera and the degree of deformation of structured light. The phase modulation was automatically calculated from the images of the distorted light (e.g. Fourier transform, etc) (Gorthi & Rastogi, 2011). A moderate repots on the use of fringe projection techniques for micrometer measurements. Fringe projection technology applies point-to-point operation to solve the initial phase of the object. That is, in principle, the phase value of the center point is not affected by the

light intensity value of adjacent points, to avoid the error caused by the uneven reflective rate of the object surface or the deviation of the viewing angle. Notably, its dense reconstruction of the point cloud can vividly restore the physical object, and its texture mapping function can make the reconstructed 3D model closer to the real objective the color, texture, and detail characteristics (Salvi et al., 2010; Feng et al., 2018; Yin et al., 2015).

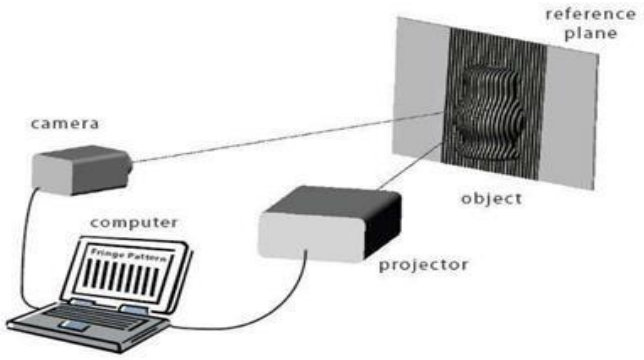

Figure 2.3. Fringe projection profilometry system retrieved from Gorthi &Rastogi (2010) with permission.

2.5.3 Resolution

The resolution of the fringe projection system can be divided into lateral and vertical resolution (Samara, 2005). They are determined by the camera and optics resolution. Optical resolution is used to describe the ability of an optical imaging system to resolve the details of an object. The level of detail a camera can capture is called resolution and is measured in pixels. The higher the pixel, the more detail the camera captures. Exorbitant optical resolution without a certain high image resolution can reduce actual resolution below camera resolution, the same condition as a higher camera resolution with a relatively low optical resolution. The vertical resolution is also based on the gratings' frequency. The spatial light modulator of fringe projection can generate variable gratings and thus variable system resolutions applicable for a wide variety of surfaces and objects. In fringe projection systems, a typical vertical resolution reported is approximately 1 μm in the literature (Samara, 2005).

2.5.4 Image analysis techniques used for analyzing data obtained from fringe projection systems

Fringe projection topography has been widely developed and utilised in a variety of industrial sectors, such as quality control, reverse engineering, and medical diagnostics, to name a few (East et al., 2016). Pattern design or structure applied in projection (Salvi et al., 2004), generating method and projecting the patterns, studying and correcting the equipment, developing new fringe analysis methods to extract underlying phase distribution, and improving existing fringe analysis methods have all seen significant advancements in last three decades. Fringe projection techniques are classified as Phase stepping profilometry (PSP), Fourier transforms profilometry (FTP), Wavelet transforms profilometry (WTP), Spatial filtering profilometry (SFP), and so on, depending on the fringe analysis method employed in the measurement (Gorthi &Rastogi, 2010).

The surfaces of machined components have a complicated form that is made up of a sequence of peaks and troughs with different heights, depths, and spacing (Keyence Corporation of America, 2012). The shorter frequency of actual surfaces relative to the troughs is known as surface roughness. The parameters of skin topography are automatically calculated by Primos™ software (Lai et al., 2018). The surface parameters can be evaluated by line roughness data and surface roughness data. Line roughness parameter (Appendix Table A.1) and surface roughness parameter (Appendix Table A.2) are described below. A detailed explanation of these parameters is described by Gadelmawla et al. (2002). Among these parameters, Ra, as 2D vertical parameters of line parameter (y and z), describing the arithmetical mean height, is the most common parameter that evaluate tropically superfinished surfaces (Fig. 2.4). Lai et al (2018) determined the skin topography changes during kiwifruit developments in different weather conditions by looking at Sa and Rsm (Table 2.1).

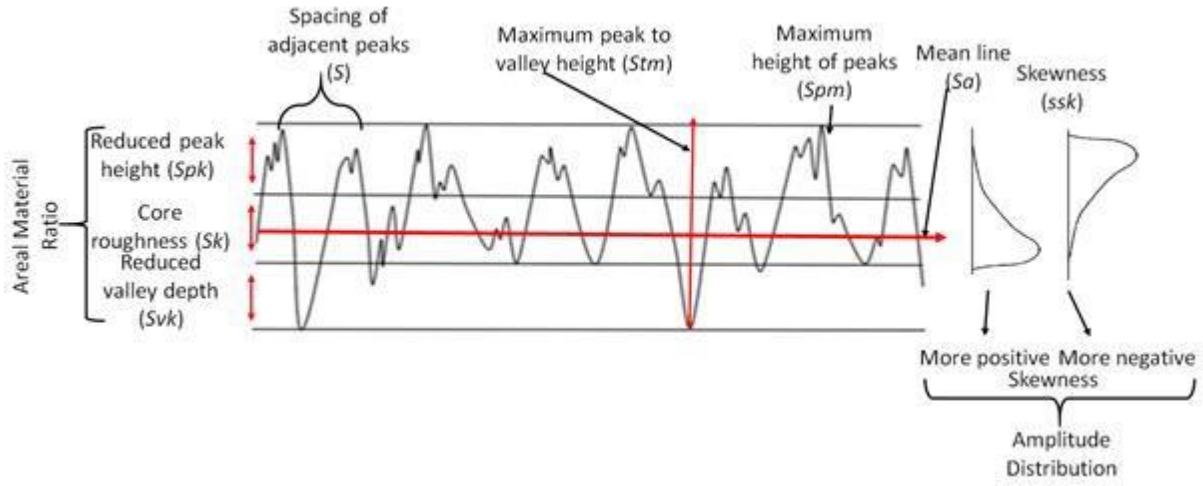

Figure 2.4. The definition of Reduced peak height (Spk); roughness (Sk); Reduced valley depth (Svk); Spacing of adjacent peaks(S); Maximum peak to valley height (Stm); Maximum height of peaks (Spm); Mean line (Sa); Skewness (Ssk).

Table 2.1. The definition of Ra and Rq. (Ra and Ra are the most common parameter in describing surface roughness).

Name of line parameters	Abbreviation	Explanation of the line parameters
Average roughness vertical direction.	Ra	Ra is the average of the absolute values of the profile heights of the roughness profile. Ra=$\frac{1}{lr}*\int_0^{lr}\|R(x)\|dx$
Root mean square roughness	Rq	Rq is the Root mean square average of the profile heights of the roughness profile. Rq is a vertical parameter, that is, it describes the roughness in a vertical direction. Rq=$\sqrt{\frac{1}{lr}*\int_0^{lr}R^2(x)}\ dx$
Average spacing of the roughness profile elements (horizontal parameter)	Rsm	The average distance between the profile components Xs is denoted by Rsm. Rsm is calculated using the following counting thresholds: in the vertical direction, 1% of the total measurement section. Rsm= $\frac{1}{n}*\sum_{i=1}^{n} Xsi$

2.5.5 Applications of fringe projection

2.5.5.1 Medical diagnostics

Fringe projection technology has been applied as a micrometer resolution imaging tool in the medical field due to its non-invasive imaging modality (Xiao et al., 2015). The fringe projection has been applied for measuring 3D surface characteristics in the mouth cavity (Chen & Huang, 2005), monitoring and reconstructing the 360 shapes of vascular segments caused by internal pressure (Genovese & Pappalettere, 2006), high-speed monitoring patient body shape, and position during the delivery of radiotherapy treatment for cancer (Lilley, Lalor & Burton, 2000), lower back (Hanafi, Gharbi & Cornu, 2005) and scoliosis detection (Berryman et al., 2008), non‐invasive and rapid

measurement of skin quality in cosmetology field (Jaspers et al., 1999), breast height imaging (Norhaimi et al., 2020).

A prototype using the principle of fringe projection and active triangulation method for 3D intra-oral scanner has been designed (Park, et al., 2016). The accuracy has achieved 25μm and it took around 180 sec for the full arc scan of the lower oral cavity. It uses LED as a light source, light from LED is radiated by liquid crystal on silicon (LCoS) into red, green, and blue light, and then strikes onto the collimating lens for the next step passing the optical deflectors. And it applies a four-step phase-shifting algorithm to calculate the phase distribution and unwrap the wrapped phase to get accurate images. The dentist can use CAD/CAM to check the scanned data for comparison with the denture prototype. The images can be printed out by a 3D printing machine for making prostheses or abutments directly.

The wide use of fringe projection in the medical field continues to be explored, however, the high accuracy and non-destructive advantages made it possible for fringe projection to be developed in variable industries.

2.5.5.2 Horticultural applications

The application of fringe projection monitoring surface quality of horticultural products is a recent trend in the horticultural industry. Fringe projection can be utilized to visualize the surface curvature of horticultural products for assessing fruit surface roughness and identify and quantifiably characterize protruding and depressed features on fresh produce surfaces (East, et al., 2016). It enables the non-destructive, contactless visualization of plant surfaces with high accuracy to the micrometer level. A depth resolution of 2 μm from the surface of the skin, 20×13 mm surface topography area, x-y resolution of 27 μm, and an acquisition time of 2s have been reported in kiwifruit (Lai, et al., 2019; East, et al., 2016), apple (López et al., 2017), peach, banana, mango, Persimmon, tomato, pear, lemon and orange (East, et al., 2016).

A feasibility study conducted by Lai et al. (2019) successfully captured the surface topography and lenticel changes of kiwifruit using fringe projection equipment (Primos^{TM} Lite, Cranfield

Image Systems, USA). Lai et al. (2019) estimated the impact of kiwifruit growing conditions (shade or sun-exposed side) by measuring the skin features of 'Zesy002' kiwifruit including roughness parameters (*Sa* and *S*) and lenticels using fringe projection. The fringe projection was used to work on olive fruit surface for determining surface functions in different cultivars as well (Diarte et al., 2019).

2.6 Three-dimensional Scanner

2.6.1 The development of a Three-dimensional Scanner

Three-dimensional scanning is a non-destructive, fast measurements device that captures high resolution data from objects. In the past five years, the 3D scanning market increased by 15 percent annually with the portable 3D scanning segment as the main developing direction (Creaform, 2015). The two main purposes of using the 3D scanner are to extract dimensions for reverse engineering or rapid prototyping and analyzing and documenting the object itself. The 3D scanner can be divided into several categories including white-light and structured light systems, scan arms, and portable handheld scanners. The scan arms and portable handheld scanners can capture multiple images continuously. The white-light and structured-light systems take single snapshots each time and organize all the images to generate a whole 3D model automatically.

2.6.2 Applications of Three-dimensional Scanner

The 3D scanner has been extensively employed in engineering, computer science, physics and astronomy, materials science, mathematics, medicine, social science, and another area for providing a complex model with low cost (Haleem & Javaid, 2019). For instance, 3D scanning technology is applied in recording the body structure for obtaining digital data in the medical area. The scanned objects saved as 3D files can be quickly viewed from 360°.

In horticulture, the handheld 3D scanner is portable, which was used to analyze plant growth regimes, for example, Handy SCAN 3D in the wheat crop growth cycle, and individual plant scanning for data documentation or augmented reality (AR) display. For the structured-light 3D scanners, the high-quality data collection with high resolution allows the scanners to capture the smallest features on the object surface. These applications include apple (Celik, Rennie & Akinci, 2011, Rogge et al., 2015), pear (Rogge et al., 2015), kiwifruit (Olatunji et al., 2020), sweet potato (Villordon, Gregorie & LaBonte, 2020), etc. These scanners have been used in looking at the deformation behavior of golden delicious apples under a drop case (Celik, Rennie & Akinci, 2011). Also, a 3D model was established by a structure 3D scanner (Occipital Inc.) in analyzing the shape, volume, surface area of sweet potatoes (Villordon, Gregorie & LaBonte, 2020). In the kiwifruit industry, Olatunji et al. (2020) applied a 'Sense™ 3D' scanner with 0.9 mm resolution in recording the kiwifruit's skin topography. The model has successfully been used in developing an estimation tool that can non-destructively predict the weight, size, and shape of fruit on-tree with a less than 5% error in mean absolute percentage. These applications focus on the relatively detailed surface data collection, thus a structured light 3D scanner with higher accuracy is more reliable. EinScan-SE (Shing 3D Tech Co., Ltd, 2019) is a high-resolution structured 3D scanner with a single shot accuracy of 0.1 mm. The accuracy of EinScan-SE is much higher than that of the 'Sense™ 3D' scanner, which was used in capturing shrivel data on the kiwifruit surface in this research.

2.7 3D Printing Technology

2.7.1 The history of 3D printing

3D printing, as an additive manufacturing (AM) technique, is a technology to print the saved digital 3D model to a physical object (Varotsis, 2021). The technology for printing physical 3D objects from digital data was first released by Charles Hull in 1984. The 3D printer is popular in engineering, architecture, and manufacturing, and is employed in producing mock-ups parts of patients' bodies for operations in the medical industry in the recent decade. There are seven types of 3D printers (Ngo et al., 2018) (Fig. 2.5). In this study, Material Jetting (MJ) technology is applied in printing 3D kiwifruit.

2.7.2 The principle of operation

Material Jetting (MJ) is one of the fastest and most accurate 3D printing technologies. The basic principle is to make parts by spraying liquid photopolymer droplets. The liquid photopolymer resin droplets can polymerise and solidify under ultraviolet light (Ngo et al., 2018). Photopolymer resins are sprayed as droplets before curing; thus, MJ is often compared to a 2D inkjet process. The 3D printing process is done layer by layer and an object can be printed in ProJet MJP 2500 system (3D Systems, Inc., Rock Hill, SC). The printing time for any 3D printed object is dependent on its total volume. This volume is decided by the geometry of the object. If the geometry of an object is complex and consists of many overhangs and / or bridges where support would be required to successfully print, then the total volume and hence the printing time would increase. This is common within 3D printing and is a major topic of research where printing time is desired to be minimized by reducing the amount of material required to successfully print an object. Furthermore, there are many guides and design methodologies for 3D printing in order to reduce or eliminate the need for support structures (which are removed after printing) and so minimize the time it takes for an object to be produced. Alongside design considerations, the 3D printing technique employed also impacts the time required print a specific object. Certain techniques call for specific support material structures which may reduce the time required to print an object. However, the final quality of the print is dependent on the print resolution and, the finer the print resolution of the print (<32 microns), the longer it will take to print, regardless of object size or total print volume within the parameters of the 3D printer (bed size, technique, etc.). Post processing (cleaning supports, etc) the 3D printed objects is another time-consuming process but is critical to the successful production of accurate and true-to-life objects, especially in the case of scanned models. The whole process is as similar as ink-jet printers. The tiny droplets are deposited precisely thus the thin layers can reach 0.013 mm in thickness, thus enabling the production of high accuracy features.

2.7.3 Resolution and Materials

Material Jetting printing has the highest resolution (15,200 elements mm^{-3}) and thus can identify the detailed information. MultiJet printing is a material jetting printing process. It uses a meltable, dissolvable material as the support, the support material can be removed efficiently by oil and Material jetting enables the creation of models with very high accuracy, as well as accurate visual

and haptic prototypes (Varotsis, 2021). Thus, in this research, the MultiJet printing technology was employed in printing high accuracy kiwifruit models with different shrivel conditions.

ProJet MJP 2500 system (3D Systems, Inc., Rock Hill, SC) using VisiJetP ®P M2R-CL resin supplied by the manufacturer, which was stated to be a USP Class VI certified material with ISO 10993 biocompatibility. The materials used for 3D Systems' MJ process include a range of engineering, rigid, elastomer, composite, and wax materials. VisiJet materials such as photopolymer resin are the main materials used in this 3D system. Resin VisiJet® M2R-CL has ideal flex and rigid function. It has been applied in surgical guides in the medical field.

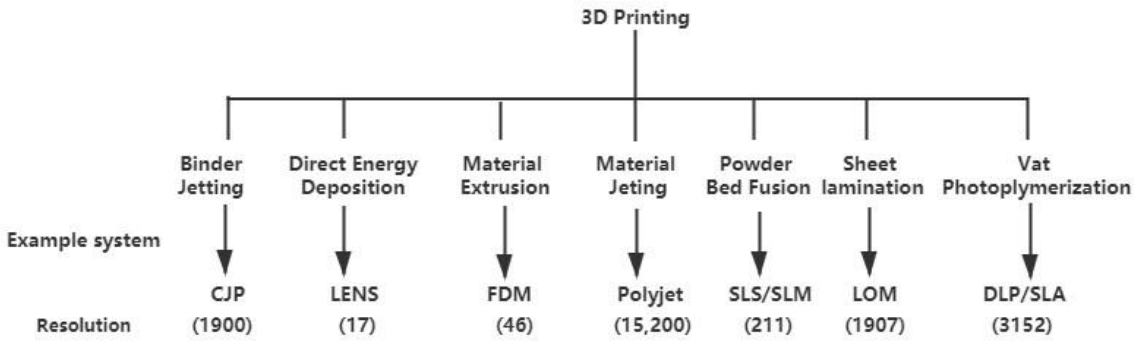

Figure 2.5. The standard from the International Organization for Standardization (ISO) and the American Society for Testing and Materials (ASTM) 52900:2015 divides typical additive manufacturing (AM) procedures into seven categories: binder jetting (BJ); directed energy deposition (DED); material extrusion (ME); (4) material jetting (MJ); powder bed fusion (PBF); sheet lamination (SL); and vat photopolymerization (VP), with example technology, the method in terms of Resolution (elements mm-3). The example system is Color Jet Printing (CJP); Laser Engineered, Net Shaping (LENS); Fused Deposition Modelling (FDM); Polyjet; Selective Laser Sintering/ Melting (SLS/SLM); Laminated Object Manufacturing (LOM); Stereo Lithography (SLA)/ Digital Light Processing (DLP).

2.7.4 The 3D printer applications

Material jetting could be applied to produce 3D anatomical models for the medical industry, such as the design of customised knee positioning orthosis (Santos et al., 2017). Furthermore, it is well-

suited for designers in producing molds and casting patterns, for instance, for verifying design quickly.

In horticulture and agriculture areas, the 3D printer has been widely used in mold manufacturing processing machine parts. For example, the Farmshelf company has developed an automated system that allows anyone to create a smart indoor farm (Griffin, 2017). New projects are difficult to develop and costly due to the lack of a sound ecological chain. FarmShelf is using 3D printing to design suitable parts, such as mounting brackets and plant hooks. They can print custom parts very quickly and test them, saving development time and cost. Existing research recognises the critical role played by the 3D printer in the agriculture industry. However, few studies have investigated whether 3D printers can record models with micrometer-level accuracy. This work will generate fresh insight into using a 3D printer recording the wrinkled skin on the kiwifruit surface with a high-accuracy 3D kiwifruit model.

2.8 Conclusion

The literature review shows that fringe projection has the potential to capture the changes of valleys and peaks on the fruit surface due to shrivel development. Different relative humidity and temperature in storage can lead to variable water vapour pressure deficit, which, in turn, influence the severity of shrivel symptoms. Alternatively, 3D technology is regarded as a non-destructive method to capture the shrivel changes of the fruit surface. This study investigates the possibility of using skin topography parameters measured by the fringe project to quantify shrivel development in kiwifruit stored under different RH and temperature conditions, and to classify shrivel severity categories. The accuracy of 3D technology (scanning and printing) in reproducing the shrivel symptoms on the fruit surface will also be investigated.

Chapter 3. Quantitative assessment of shrivel development in kiwifruit using fringe projection

3.1 Introduction

Kiwifruit shrivel is a quality issue in the kiwifruit industry. The development of shrivel was regarded to have a possible correlation with water loss. With the time in the storage, the water loss of kiwifruit tends to increase with more severe shrivel symptoms. The skin wrinkles caused by shrivel could affect customer's preferences. Shrivel severity of kiwifruit has been categorised through subjective visual measures. Burdon et al. (2014) divided shrivel symptoms into four categories including none, slight, moderate, and severe. However, the study is based on the area of skin wrinkles on the fruit surface without looking at the fruit surface roughness. The evaluation of skin wrinkles needs to consider the height, peak as well as the width of the valley as a result of surface roughness during shrivel development. Thus, in this work, shrivel severity was evaluated using the same skin surface area by looking at surface roughness from vertical and horizontal directions caused by shrivel.

The fringe projection is a new technology in the horticulture area and was first regarded as a quantitative method to look at the surfaces of horticulture products in 2016 (East et al., 2016). Subsequently, the fringe projection was used to successfully examine the surface characteristic including lenticels and roughness of three commercial kiwifruit cultivars (‘Zespri ‘SunGold™’’, ‘Zespri Charm™’; ‘and Zespri Gold™’) and hypothesised the potential influence of surface topography on gas transfer and therefore storage outcomes (Lai et al., 2019). These studies effectively applied fringe projection in kiwifruit surface characteristic monitoring. Thus, in this research, the fringe projection was employed as a monitoring tool to provide a mathematical description of shrivel development using the exported skin topography parameters.

The goal of this study was to determine whether there was a link between shrivel symptoms and kiwifruit skin topography, and whether the structured light approach that provides microtopography information is effective in quantitatively characterising shrivel objectively.

3.2 Materials and Methods

Fruit origin, storage condition, and data analysis are described in this section. In this research, different shrivel severities on the surface of kiwifruit were obtained separately in three storage locations: the lab, a water permeance cabinet, and a temperature-controlled room (TCR). This chapter details the methodology for measuring the shrivel of kiwifruit for the duration of the experiment. Weight loss measurements, fringe projection assessment methodologies are detailed in their respective chapters.

3.2.1 Fruit materials and preparation

'SunGold™' kiwifruit (A. *chinensis*) was supplied by Zespri ® International limited located in the bay of plenty, New Zealand, and collected from a standard commercial orchard. The harvested kiwifruit was commercially packed and then were transported to Massey Institute of Food Science and Technology (MIFST), Massey University, Manawatu on 6/05/2020 and stored in the cool store at 1℃.

3.2.2 Experimental design

90 'SunGold™' kiwifruit, from three grower lines 4788F 8M214A, 61508 M2GA3A, 64207M2GA2A were randomly chosen, each grower line containing 30 fruit. 30 kiwifruit (10 fruit from each grown line) were put into the trays. There are 3 trays in total. All the kiwifruit had been stored in the cool store at 1℃ in Massey Institute of Food Science and Technology (MIFST), Massey University for 18 weeks in the very same environment before the experiments.

The measurement preparation started 48h prior to the experiment (11/09/2020). Each of the trays was stored into the water vapor permeance cabinet, in the open air in the lab, and in the open air in a temperature-controlled room (TCR) (Fig. 3.1). The temperature was set at 20℃ for the first two conditions, but at 1 ℃ for TCR. The measurements were taken until all fruit had reached 6% weight loss. The measurement of fruit stored in the water permanence cabinet and lab conditions for 17

days and 19 days respectively. The fruit in the TCR were measured for 57 days due to the low-water loss rate. Fruit in cabinet supported on mesh racks was expose maximally to airflow.

The 90 kiwifruit were numbered on the fruit surface with a soft marker with water-soluble ink to keep track. Skin topography measurements were carried out parallel to the weight loss experiment (measuring weight at each measurement point to determine the rate of weight loss) in each fruit. Kiwifruit in 20℃ was tested by the sequence: photography, skin property, and weight loss every time (twice a day for the fruit in the permeance cabinet (or equivalent – exposed to a fan. Once a day for those sitting in the 20 ℃ room). The measurement of fruit in 1 ℃ cannot be carried out in TCR (1 ℃) room due to the cold temperature. Thus, fruit in 1 ℃ can be moved out from the TCR room at 9 am to the lab (20 ℃) for an hour under fans to ensure no influence of surface moisture on the weight loss and skin property measurement. Measurement was done at 10 and then fruit was returned to the cool room by 11 am each time.

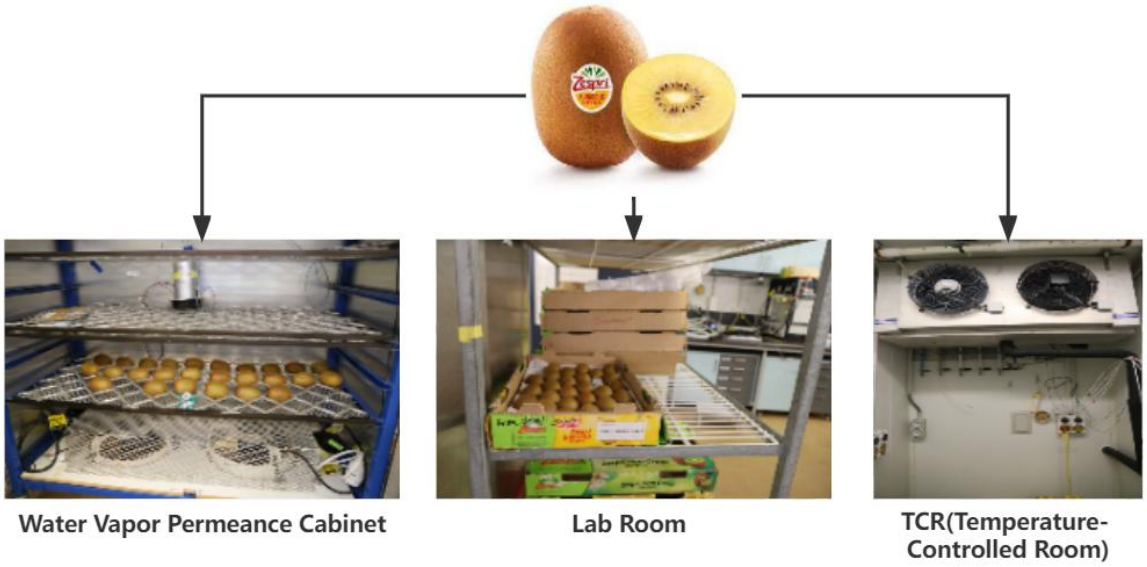

Figure 3.1. Experimental process (kiwifruit stored in Water Vapor Permeance Cabinet (fan to make a higher airflow for reducing the humidity in cabinet room), Lab Room, and TCR (Temperature-Controlled Room respectively).

Both weight loss and skin topography measurements were conducted in a 20°C laboratory. The Micro-topography was captured by fringe projection (Primos^{TM} Lite, Canfield Image Systems, USA).

The frequency of measurements will be different due to the different rates of weight loss caused by the different storage conditions. The fruit stored in the water vapor permeance cabinet will be measured two times per day at 9 am and 3 pm. Fruit stored in the open air in the lab will be tested at 9 am every day. The fruit stored at 1℃ is going to be measured on Monday weekly. Relative humidity (RH) and temperature in all conditions were measured using dual i-buttons (DS1923-F5 Hygrochron Temperature & Humidity I Button, Maximus Technologies, New Zealand ----two i-button per condition).

Table 3.1. 'SunGold™' Kiwifruit stored conditions (the mean ± standard deviation of stored temperature and humidity) in this experiment for obtaining variable shrivel categories.

Mean	Temperature ℃	Humidity (RH%)
Cabinet	20.35 ± 0.35	47.38 ± 9.07
Lab	20.40 ± 0.22	52.91 ± 8.39
TCR	0.92 ± 2.51	79.46 ± 4.33

3.2.3 Weight loss measurement

Figure 3.2. Weight loss measurement (A digital balance (S-4002, Denver instruments, Colorado, USA, with a precision of 0.001g).

Relative Weight Loss (RWL%) was obtained for each kiwifruit following the method described in Burdon et al. (2014), as the difference between the m_0 and m of fruit. The m_o (the initial weight) is the experimental beginning weight, not the at-harvest weight, due to the study starting time in September and the harvest time of kiwifruit in New Zealand is in May. The *m* is the mass at any given time. The WL% was expressed as a percentage of weight loss (Eq. 3.1). To allow for

condensation clearance, the sample for assessment was conditioned at room temperature (20°C) for 1 hour before recording the final weight on each measurement day. To determine the weight, a digital balance (S-4002, Denver Instruments, Colorado, USA) with a precision of 0.001g was utilised (Fig. 3.2).

$$\% \text{ WL} = ((m_o - m)/(m_o))(100) \qquad \text{(Eq. 3.1)}$$

3.2.4 Fringe projection instrumentation and image capture

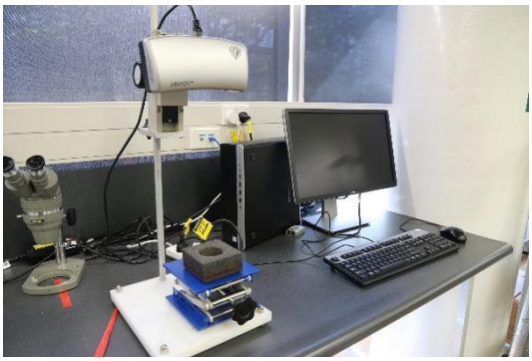

Figure 3.3. Fringe projection equipment (Primos™ Lite, Canfield Image Systems, USA).

The skin topography measurement method was provided by Lai et al. (2018). Microtopography of kiwifruit was measured at two locations (180° apart) in the equatorial region. The area that skin topography measured was labelled by water-soluble ink before the first-time measurement to guarantee the same area to be measured each time. The two locations were always identical at each of the measurement time points. Two points were drawn at the diagonal corner of the rectangle. The fruit was supported on a soft sponge to fix the position before the measurement. The assessment window was a 20.07×12.88 mm (260 mm^2) quadrilateral shape. The topography image within this window was captured. The Fringe projection has an x-y resolution of 26.83 µm and z (vertical) resolution of 2 µm. A detailed description of the fringe projection system was provided by Berardesca, et al. (2013). Before the image was captured, the distance between the kiwifruit surface and sensor needs to be adjusted for a high image resolution.

3.2.5 Image processing and analysis

The surface curve was captured by the 260mm^2 window of the fringe projection equipment. The surface 3D image was extracted to surface topography descriptive parameter data by Primos version 5.8 (Canfield Image Systems), a proprietary software package. The original image (Fig. 3.4 A; B) was captured with the natural curve of the fruit, which is low-frequency components. A high resolution for data analysis is needed. Thus, the raw image experiences a robust high-pass filter to remove the fruit surface curvature, noise and to generate a flat surface with high roughness resolution (Lai et al., 2019) (Fig. 3.4 C; D).

For obtaining line parameters, ten lines were inserted into the images for obtaining the line parameters from the surface roughness (Fig. 3.6). The line set was saved and applied to all the images automatically to guarantee the data from the same location were analysed for each image. The first line position is from x=2mm, y=1mm to x= 2mm, y=12mm; the final line (10th line), from x=18mm, y=1mm to x=18, y=12, and the gap between two close lines is 1.8mm (Fig. 3.6).

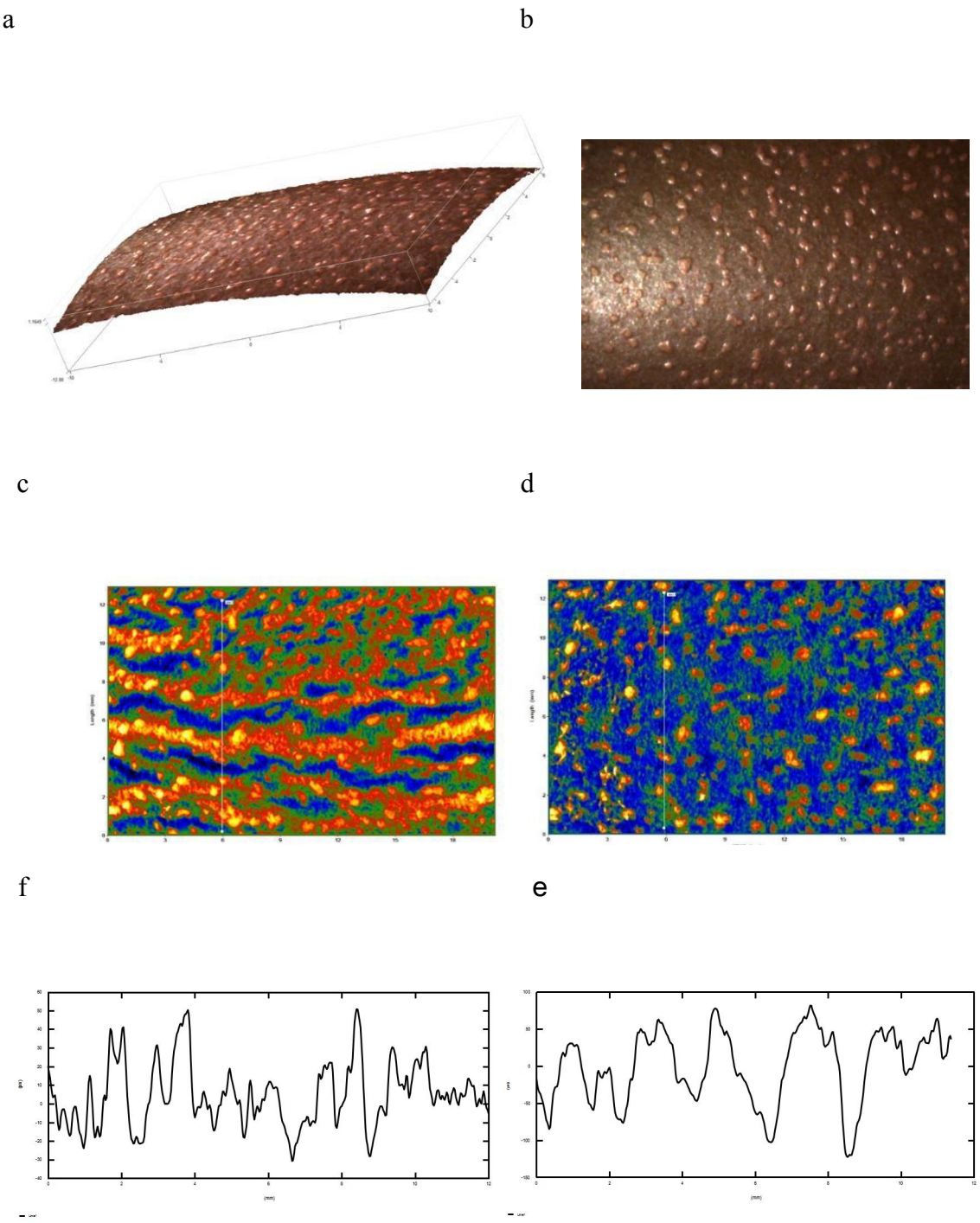

Figure 3.4. Surface topography information. (A), (B) A 3D raw image output example; (C), (D) The result of the robust high-pass filter from a raw image-----A flat micro-topography image for a fruit example in the initial day and the final day of study (This image include line drawn for looking at the line roughness) (E), (F) roughness data for the line drawn in (C) and (D).

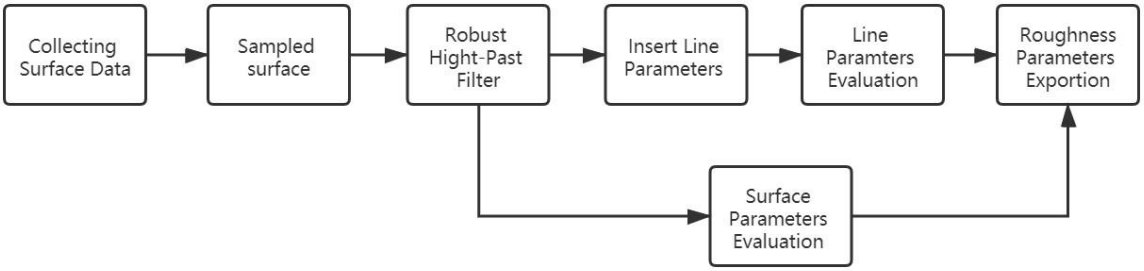

Figure 3.5. General procedure for assessing line/surface parameters of surface topography.

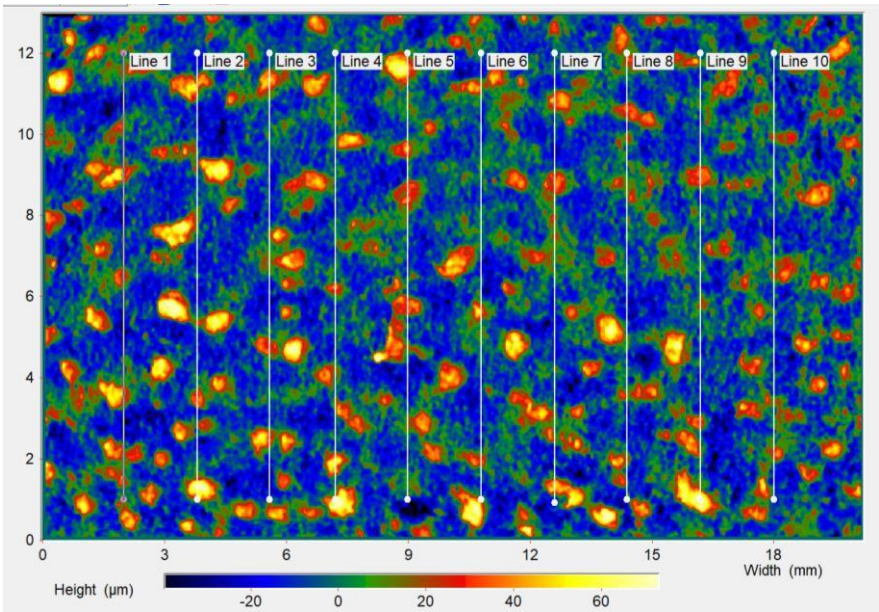

Figure 3.6. Draw line in skin topography to look at the accurate change of the shrivel in kiwifruit surface each day.

3.2.6 Shrivel

The shrivel category has been divided into 4 subjective ranges visually with the naked eye from 0 to 3 (Fig. 3.7); level 0- the non-shrivelled fruit with no sign of skin deformation, level 1 - slight shrivel with very shallow skin deformation, level 2 with moderate shrivel with obvious skin deformation (area is greater than 2 cm^2), level 3 with severe skin deformation.

Figure 3.7. Selected representative kiwifruit showing the shrivel categories from level 0 to level 3 from left to right. (Same fruit in different timeline).

3.2.7 Data analysis

Data analysis was performed with R Studio (v. 1.4.1106, R Studio Inc., Boston, MA) using R version 4.0.3 (R Development Core Team, 2020). PCA was applied to group the skin topography parameters and could imply the most influential parameters to indicate shrivel. The correlations of weight loss and surface parameters were analyzed by Pearson's correlation test. The effect of storage conditions (temperature, humidity) on surface roughness and on shrivel category was analyzed using a one-way ANOVA to measure differences among means. Tukey's test (a confidence interval of 95%) was applied in performing the significant differences that treatments caused.

3.3. Results and Discussion

3.3.1 Relative Weight loss

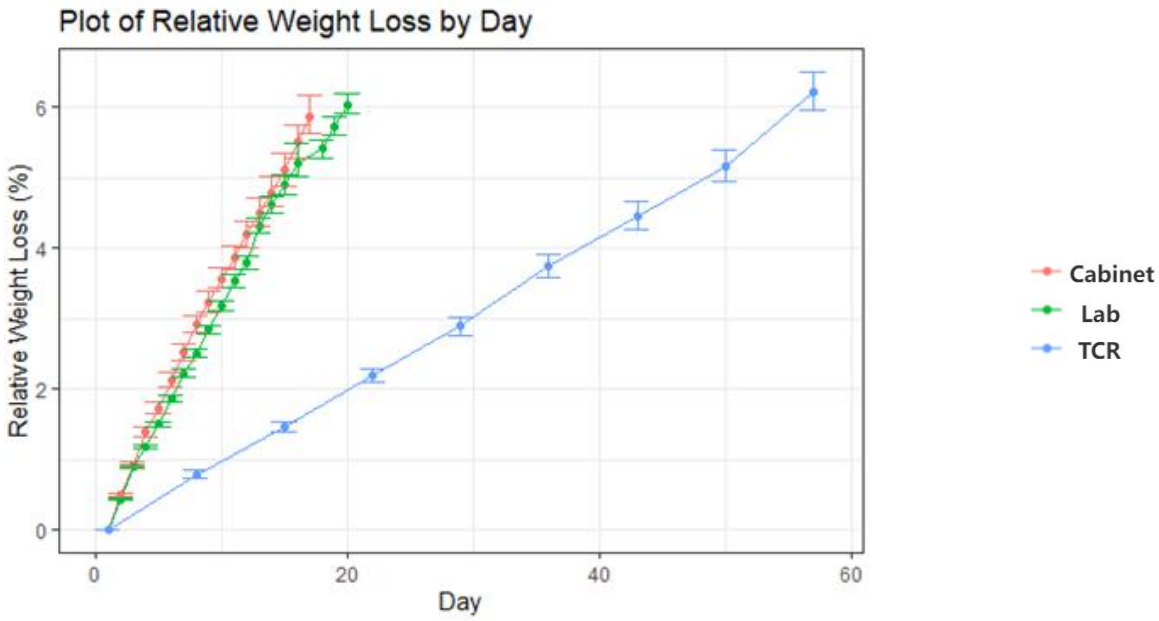

Figure 3.8. 'SunGold™' Kiwifruit stored in three conditions (lab, water permeance cabinet, and TCR room) relatively weight loss%.

For obtaining 6% relative weight loss, 'SunGold™' kiwifruit was stored in cabinet (20℃, 47% RH) lab (20℃, 53% RH), and TCR room (1 ℃, 80% RH) spend 17d in 19d and 57d respectively. Weight loss increased during the storage for all three treatments (Fig. 3.7), with the highest weight loss rate in increased airflow rates, following by fruit stored in the lab and then in cool room storage (1℃) (Fig. 3.8) as expected from the experimental design.

The initial weight is not at-harvest weight. Thus, the relative weight loss value of kiwifruit in this research cannot represent the actual weight loss after harvest but is still meaningful to detect the weight altering in the different storage environments.

3.3.2 Weight loss rate

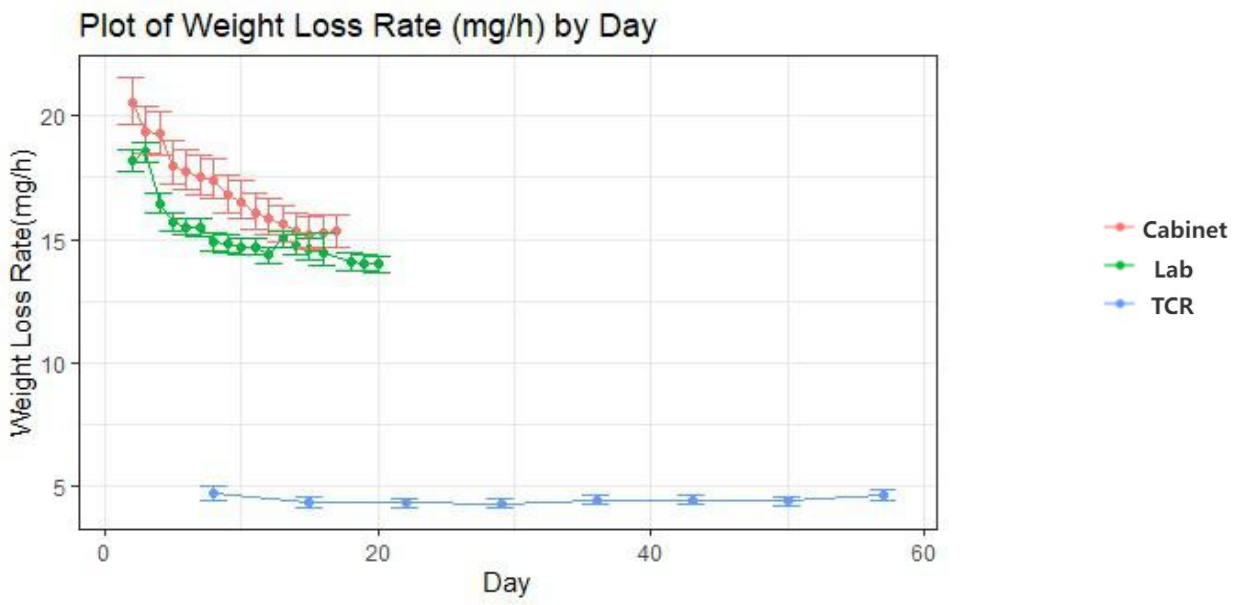

Figure 3.9. Weight loss rate(mg/h) of 'SunGold™' kiwifruit in three treatments (lab, water permeance cabinet, and TCR room).

The weight loss rate of 'SunGold™' decreased dramatically (from over 20mg/h to around 15mg/h) in cabinet and (from 17mg/h to 14mg/h) lab conditions. In the TCR room, the weight loss rate had not variated during the whole storage period. According to Burdon & Clark, 2001, the water loss rate is higher at the beginning and reduces with the storage duration. The water loss of vegetables or fruit normally results in weight loss. Thus, the reduction of water loss could generate a lower weight loss rate. Also, 10 days of 20℃ storage increased the weight loss rate of kiwifruit previously stored in the cool room for 3 weeks compared with the fruit which were continually stored in the cool room for 14 weeks (Burdon et al., 2015). The weight loss of the former treatment is 6 times that of the latter. Thus, room temperature storage can result in a more rapid weight loss compared to cool storage. Hence, the rate of weight loss was much higher for fruit stored at 20 ℃, which have been observed similar results in this work. The average weight loss rate of 'Gold9' in the 10d is 20.83mg/h (Burdon et al, 2015), which is slightly higher than the highest value of relative weight loss rate of 'SunGold™' in this research (Fig. 3.9). However, the weight loss rate values generated in this study seemed reasonable based on the previous research.

Despite the consistent circumstances pushing water loss from the fruit, the experiment's fruit water loss rate reduced. This might be due to changes in the fruit's internal water environment (reduced water mobility) or to the fruit skin's or harvest scar's enhanced resistance to water loss. Fruit skin desiccation may limit water vapour permeability by drying cell wall material (Ben Yehoshua et al., 1983).

3.3.3 Shrivel developments

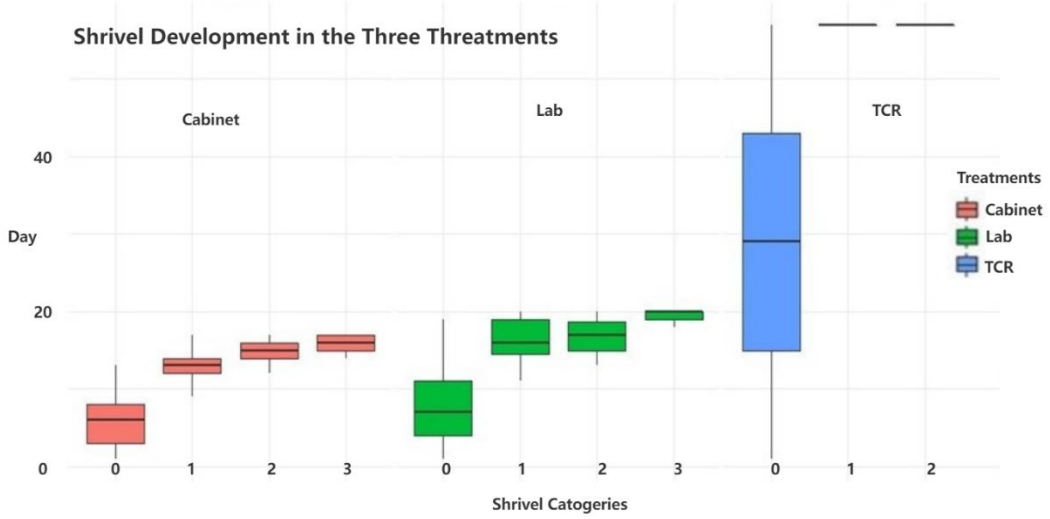

Figure 3.10. Boxplot of shrivel severity development of ''SunGold™' kiwifruit in three treatments (lab at 20℃, 52.9% RH; cabinet at 20℃, 47.4% RH; TCR at 1℃, 79.5% RH). No kiwifruit stored in TCR showed shrivel 3, and merely two fruit had shrivel symptoms, because 57-day storage in TCR cannot induce a severe shrivel kiwifruit.

The progression of shriveling during storage was dissimilar between the three treatments (lab, cabinet, and TCR treatments) (Fig. 3.10). 'SunGold™' stored in cabinet (20℃, 47% RH treatment) showed slight shrivel (1 degree) in nine days, and in TCR (1℃, 80%) treatment with two months of storage. An increase in shrivel severity (1, 2 degrees) was seen after two weeks of storage for lab (20℃, 53% RH) treatment, and these differences caused by the three treatments were statistically significant from kiwifruit to shrivel (P <2e-16 ***). Interestingly, fruit stored in the lab took similar storage days to reach slight shrivel and moderate shrivel, though median of the storage days is

higher for moderate shrivel. After two-week storage in the cabinet, all the kiwifruit got shrivel with 65% of them having moderate symptoms and 3.8% of them having severe symptoms. 61% of kiwifruit finally occurred severe shrivel symptoms after 17d of cabinet storage and 38.5% of fruit in the lab had 3 degrees shrivels in around three weeks storage, respectively. However, for kiwifruit stored in 1℃ TCR room shrivel only occurred 8 weeks after storage, with 36.7% and 13.3% of fruit having slight and moderate symptoms after 60d of cool storage. No severe symptoms were observed during this treatment.

3.3.4 PCA (Principal Component Analysis) of Skin Topography

3.3.4.1 PCA for line parameters

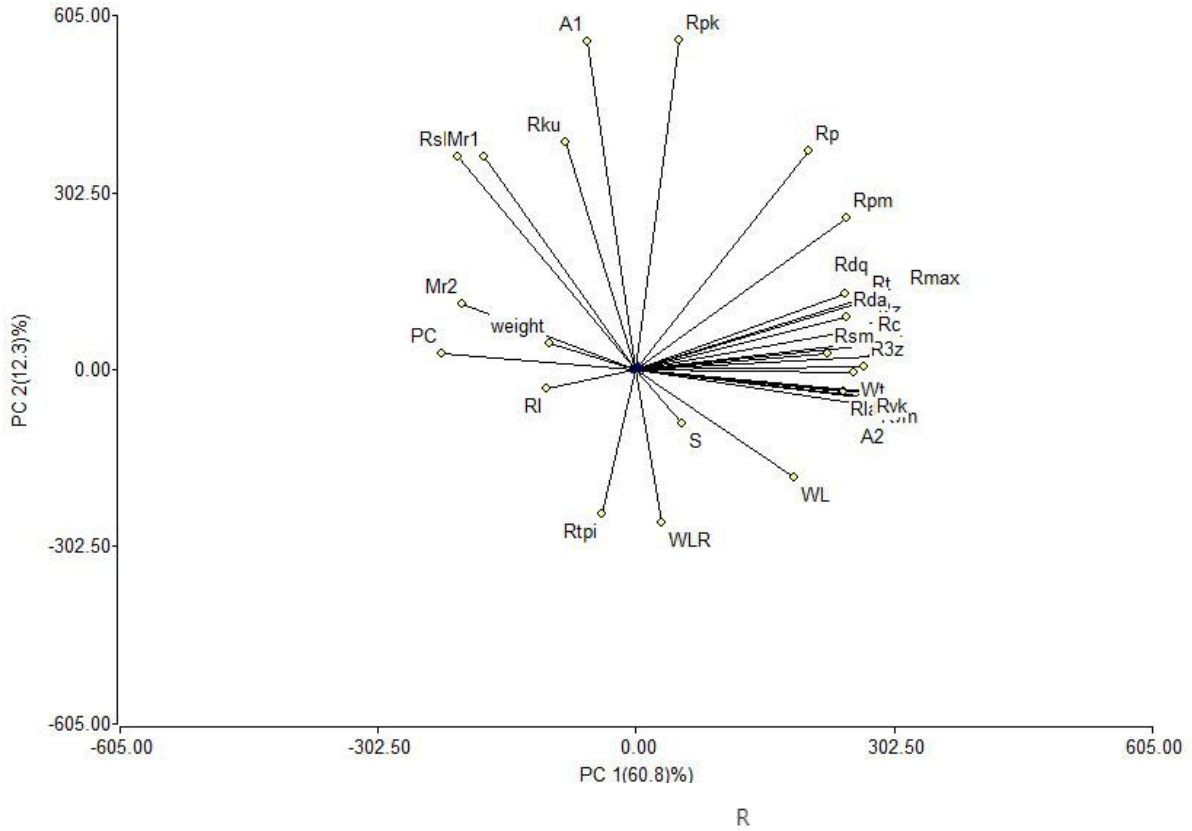

Figure 3.11. The PCA analysis of skin line topography parameters (Ra, Rl, Rq, Rmax, R3z, Rt, Rz, Rp, Rpm, Rv, Rvm, Rsk, Rku, Rsm, S, Rda, Rdq, Rla, Rc, Rtpi, Wt, PC, Mr1, Mr2, Rk, Rpk, Rvk, A1, A2) and Relative weight loss (RWL), the weight loss rate (WLR) of kiwifruit stored in three conditions without treatment variations (the details of skin line parameters are described in Appendix Table B.1).

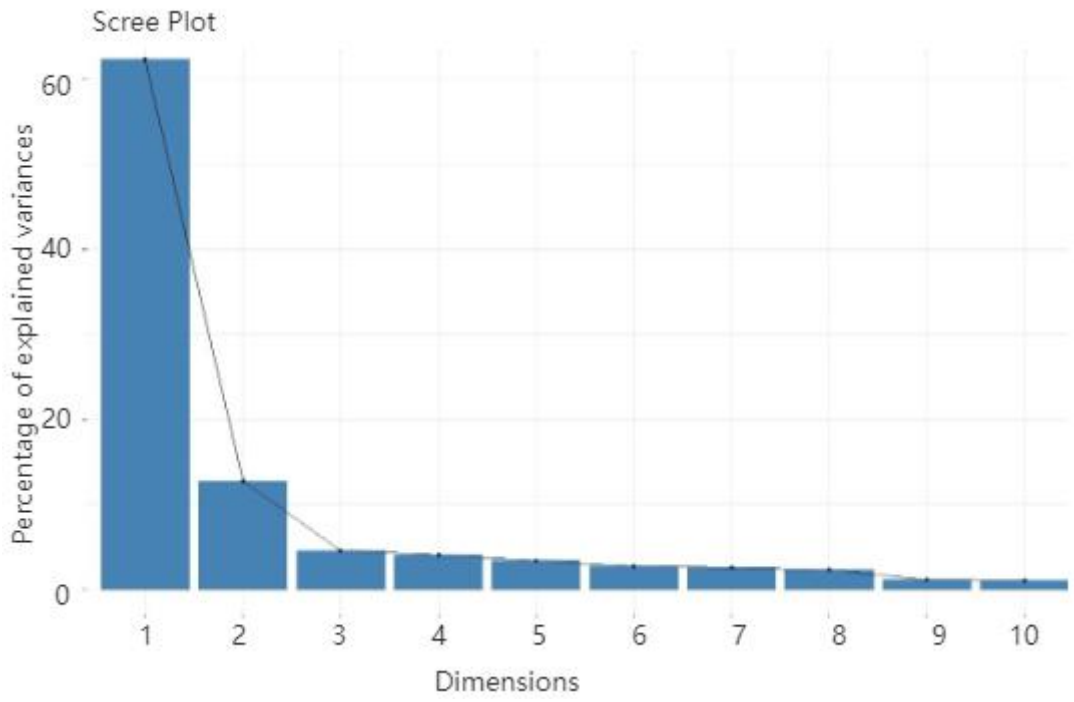

Figure 3.12. Scree plot of principal component analysis of skin line topography parameters between eigenvalues and principal components (The skin line topography parameters include Ra, Rl, Rq, Rmax, R3z, Rt, Rz, Rp, Rpm, Rv, Rvm, Rsk, Rku, Rsm, S, Rda, Rdq, Rla, Rc, Rtpi, Wt, PC, Mr1, Mr2, Rk, Rpk, Rvk, A1, A2.).

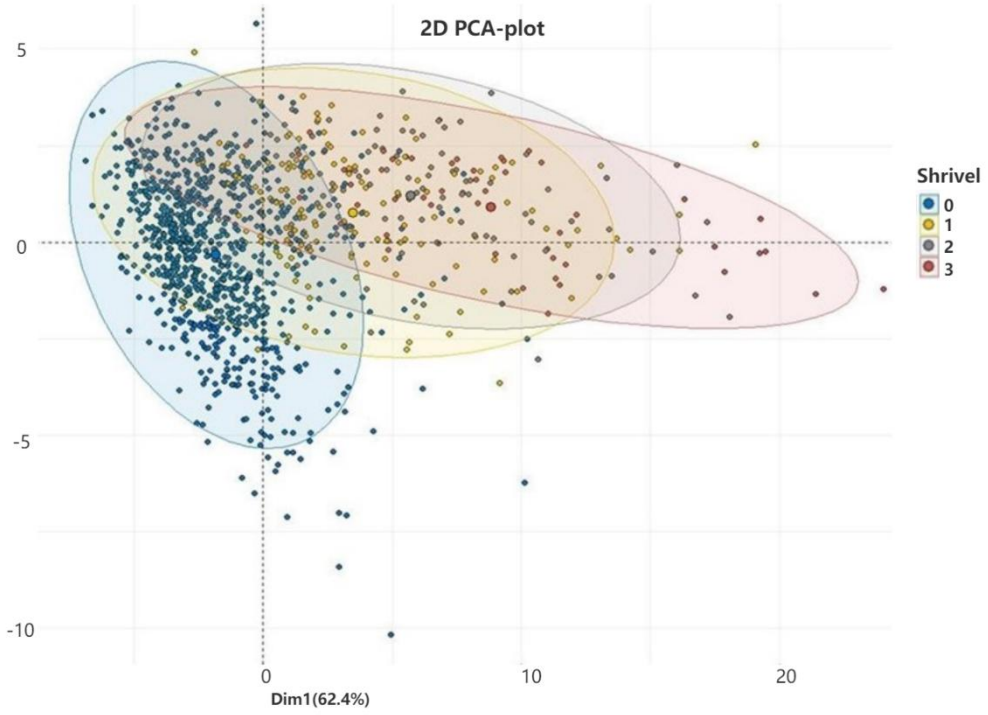

Figure 3.13. 2D PCA-plot of shrivel categories for the investigated skin line topography parameters in different shrivel categories. The skin line topography parameters include Ra, Rl, Rq, Rmax, R3z, Rt, Rz, Rp, Rpm, Rv, Rvm, Rsk, Rku, Rsm, S, Rda, Rdq, Rla, Rc, Rtpi, Wt, PC, Mr1, Mr2, Rk, Rpk, Rvk, A1, A2.

The detailed process of factor selection in PCA is described in Appendix A. PC1 (Fig. 3.11) explains the maximum amount of variability in the data and should be selected. Based on the 2D PCA-plot (Fig. 3.13), from parallel comparison, shrivel 0 group has an apparent difference from the other shrivel categories, but from the vertical line, the difference from different shrivel categories is not distinguished clearly. Thus, based on Fig. 3.12 and Fig. 3.13., the PC1 could play a critical role on distinguishing the shrivel differences. In linear, Rq, Rc, Rz, Rt, Ra, Rmax, Rvm, Rvk, Rv, Wt, A2, Rk, R3z, Rla, Rpm, Rsm, PC, Rdq, Rda, Mr2, Rp, Rsk belongs to vertical parameters and are significant variables in PC1, which could be identified as the relatively important line parameters on the shrivel categories distinguished. Among those parameters, Rq showed the longest line on the PCA plot, which could be the most influential parameter in PC1 for indicating skin topography in the vertical direction.

3.3.4.2 PCA for Surface parameter

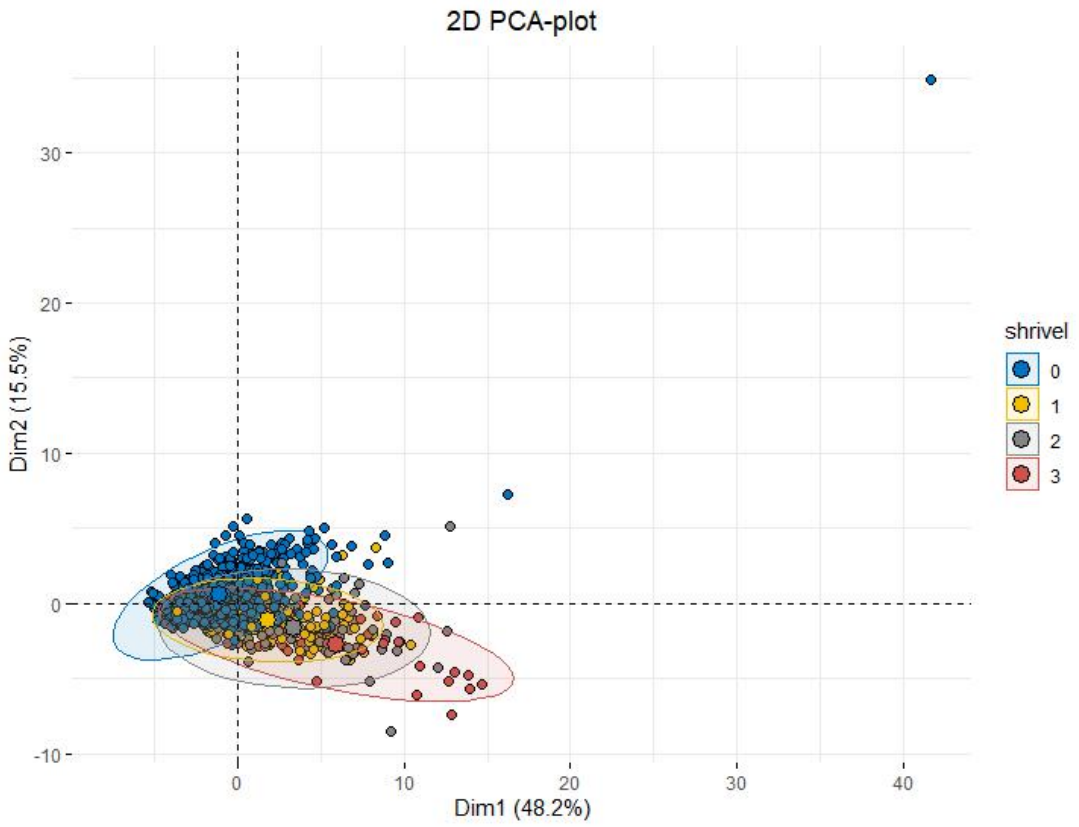

Figure 3.14. 3D PCA-plot of shrivel categories for investigated parameters of the skin topography in different shrivel categories. The skin surface topography parameters include Sc, Sa, Sk, Sq, Svk, V2, Sda, Sdr, Sla, Sku, St, Stm, Sv. Svm, Ssk, Sdq, Sp. Spm, V1, Spk, S, PC, Smax Sz (the details of surface parameters are described in Appendix Table A.3).

Based on the 3D PCA plot of surface roughness (Fig. 3.14), the shrivel categories could not be distinguished by surface parameters as clear as the line roughness. For surface parameters, PC1 could only explain 48.2% of the total variation with 15.5% in PC2, 11% in PC3. The PC1 of surface parameters explained less compared to the line parameters. Considering that 75% could be a better value, the selection of lines from PC1, PC2 and PC3 could need to be considered in this case. Also, looking at the 3D PCA-plot of surface parameters, shrivel categories did not be distinguished clearly in both PC1 and PC2 directions. Thus, in this research, surface parameters would not be considered in the following sections.

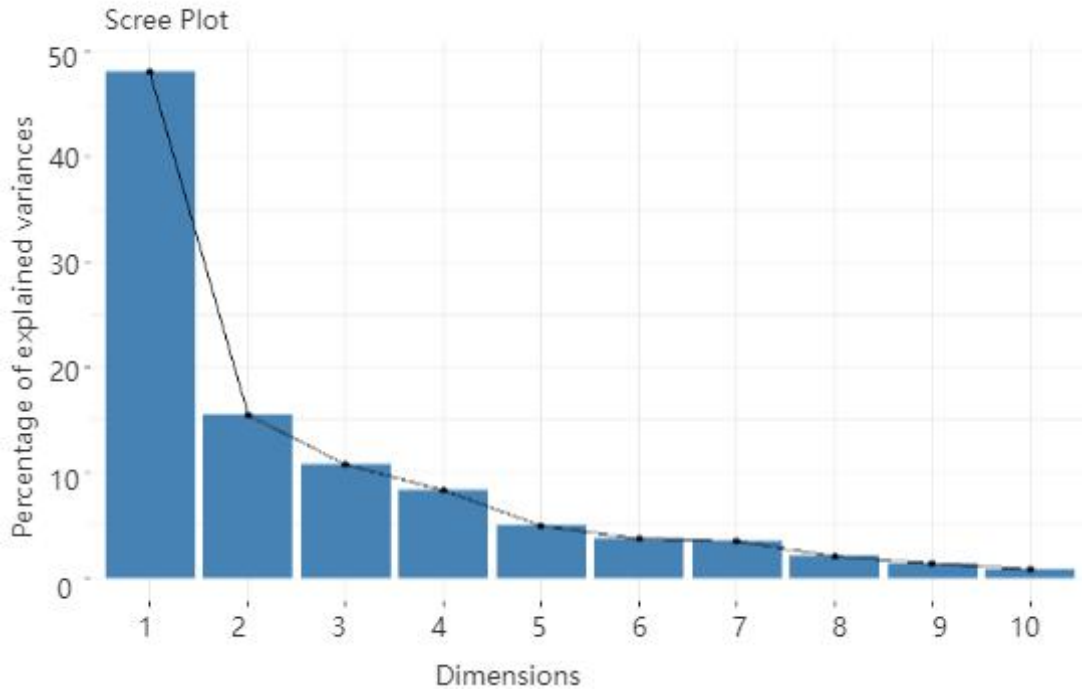

Figure 3.15. Scree plot of principal component analysis of skin surface topography parameters between eigenvalues and principal components (The skin line topography parameters include Sc, Sa, Sk, Sq, Svk, V2, Sda, Sdr, Sla, Sku, St, Stm, Sv. Svm, Ssk, Sdq, Sp. Spm, V1, Spk, S, PC, Smax Sz.).

3.3.4.3 Pearson Correlation coefficient analyze of skin line parameters

Pearson's Correlation coefficient analyze was used to deleting the parameters (Fig. 3.16). On the basis of Pearson's correlation coefficient, Rq has remarkably correlated linearly with Ra, Rz, Rt, Rc, Rmax, Rvm, Rvk, Rv, Rk, R3z, Rda, Rpm, Wt, Rdq, Rla, A2 (coefficient ≥ 0.8). Features with high correlation are more linearly dependent and hence have almost the same effect on the dependent variable. So, when two features have a high correlation, we can drop one of the two features. Also, given that the result of PCA, Rq could be the most influential parameter in PC1 for indicating skin topography in the vertical direction. Thus, Rq as a vertical parameter could be selected as a representative.

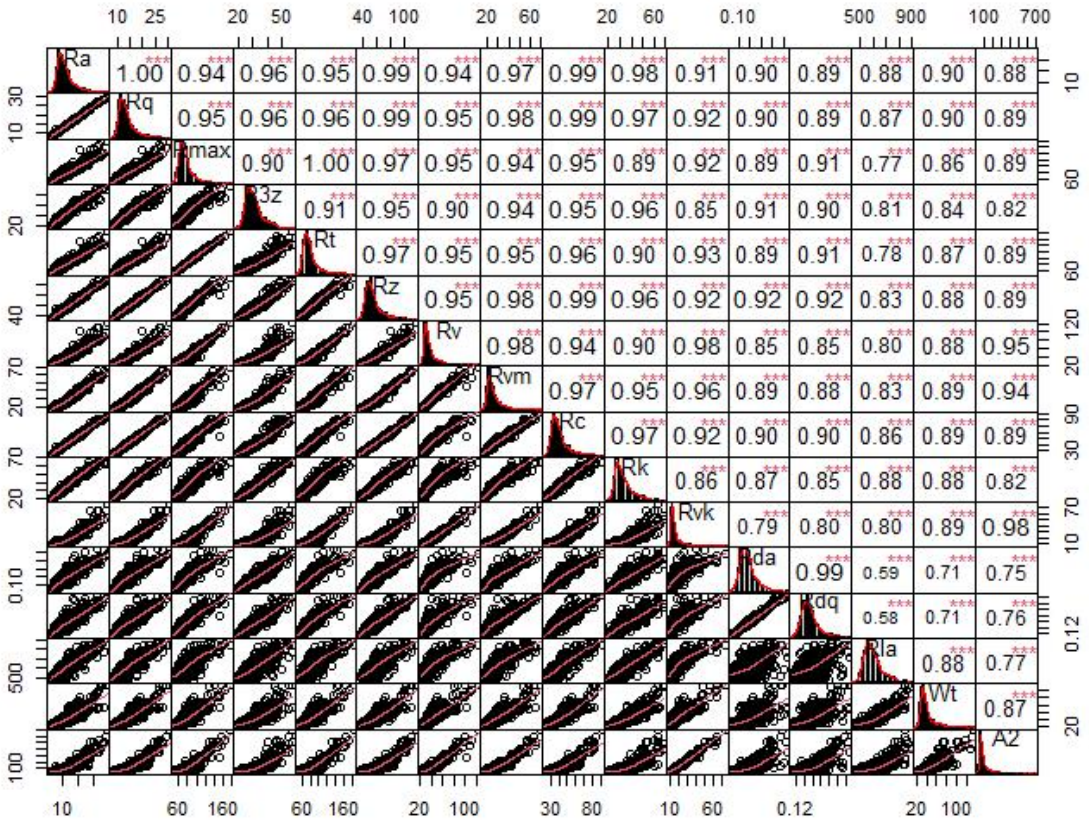

Figure 3.16. A Pearson correlation. This table shows a high correlation between with Ra, Rq, Rmax, R3z, Rt, Rz, Rv, Rvm, Rc, Rk, Rvk, Rda, Rdq, Rpm, Rla, Wt, A2.

Also, Rp, Rsk, seems to account for a vital role in influencing the PC1. Thus, Rp and Rsk would be selected to represent. Besides, PC (Peak number) showed a vital role in PC1 play a negative correlation with Rq (Fig. 3.11). Thus, PC would also be described in the following sections. The skin line topography parameters have been classified into seven groups as above, Among the seven groups, Rq, Rpk, Rpm, WL, Rtpi, PC, Rsk were considered as relatively more influential parameter in each group. The alteration of those parameters as the severity of shrivel categories would be present as follow.

3.3.5 Relationship between Skin Topography, and Shrivel Symptoms

a.

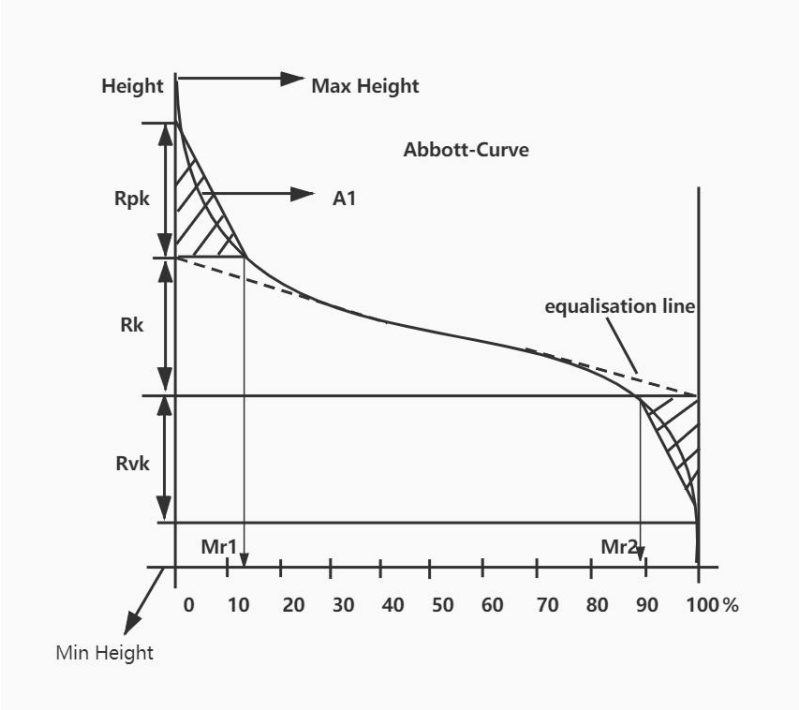

b.

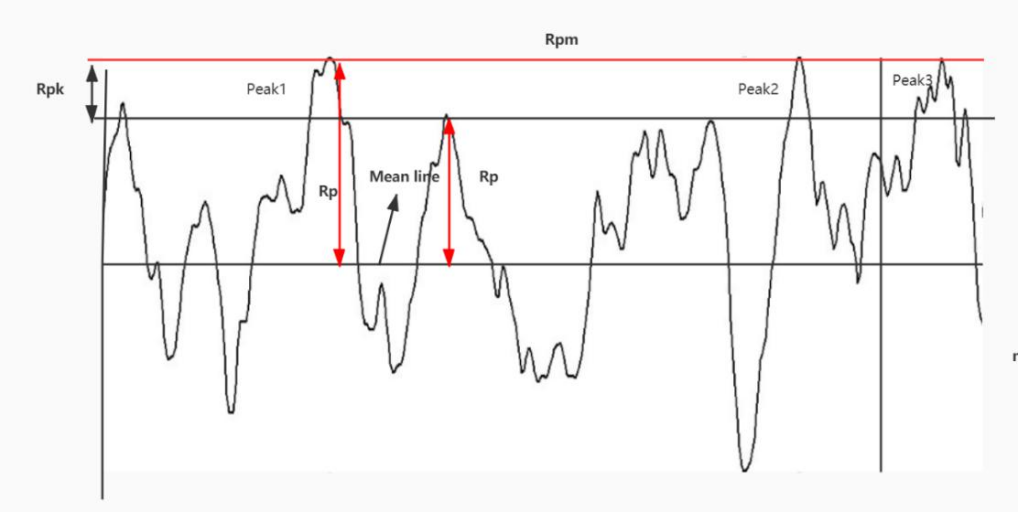

Figure 3.17. (a), (b) Definition of the height parameter, A1, Rpk, Rp, Rk, Rpk, Rvk, Rk, Mr1, Mr2, Mr1, Mr2 assessment.

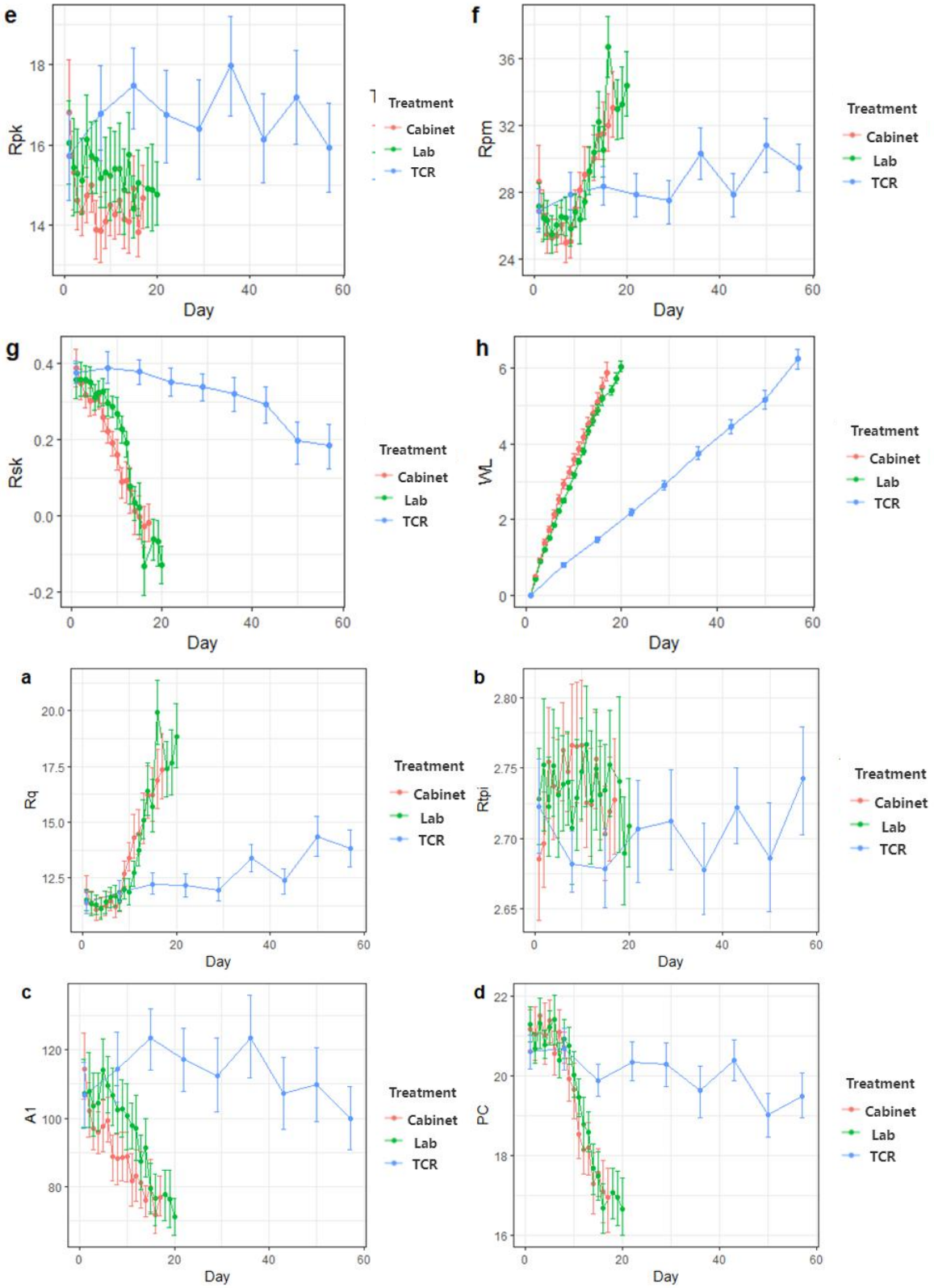

Figure 3.18. Line graphs of Skin topography parameters and RWL (Relative Weight Loss%) by Days in three treatments (Lab, Cabinet, and TCR).

The skin topography caused by shrivel can be quantified by two analytical technologies, one is surface structure's 2D profile, another is a statistical distribution on the basis of the 2D profile. The surface structure means the height of peak and valley for example Ra. the statistical distribution means, such as Rsk. The 2D profile describes surface structure from root mean square roughness (Rq), Average Maximum Profile Peak Height (Rpm), Peak Density (PC), Reduced Peak Height (Rpk), and skewness (Rsk), a material part micro (Rtpi), and material filled peak area (A1). The value of Rq, Rpm in 'SunGold™' increased with the storage time. The opposite trend was observed for PC, A1, and Rsk, whereas no obvious trend was observed in Rtpi, Rpk.

The fluctuation trend of surface topography characteristics in TCR is comparable to that in lab and cabinet room but changes the least based on storage time (Fig. 3.18). The magnitude and rate at which changes in skin parameters occurred were higher with a higher rate of weight loss (for lab and cabinet) and much lower for cool stored fruit.

Rq, as the root mean square average of the profile heights of the roughness profile (Eq.3.2), describes the skin roughness in a vertical direction. There was a significant difference in the mean Rq between fruit that had None, slight, moderate, and severe shrivel symptoms (Table 3.8). Greater Rq values could indicate a prominent surface structure, possibly resulted from more severe shrivel symptoms (e.g. higher peaks) from the vertical direction (Fig. 3.19) (Martinez et al., 2021). In this research, 73.7% non-shrivel 'SunGold™' kiwifruit has Rq< 13μm, with 62% possibility that slight symptoms has Rq at the range of 13~16 μm (Table 3.2). However, the threshold of Rq between shrivel moderate and severe symptoms is not clear. Thus, Rq can possibly describe the shrivel occurrence but difficult to clarify the shrivel categories in this research.

$$Rq=\sqrt{\frac{1}{lr}*\int_0^{lr} R^2(x)dx} \qquad \text{(Eq.3.2)}$$

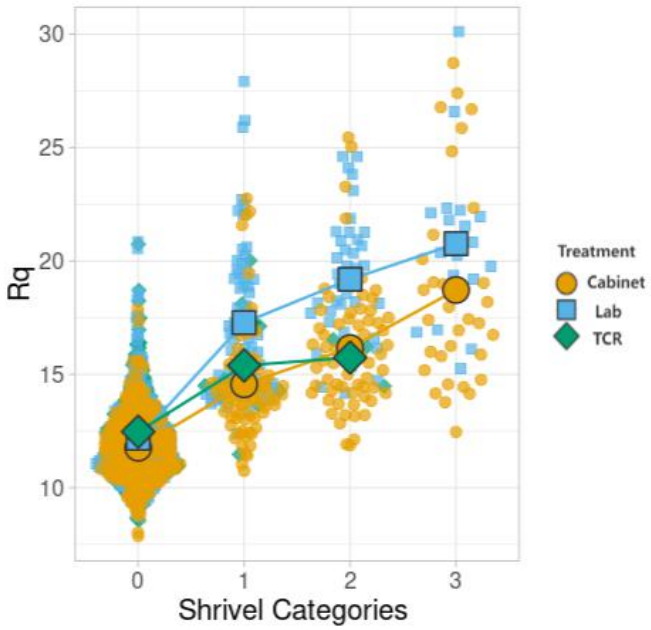

Figure 3.19. Rq (indication of the standard deviation of the distribution of surface heights in the line parameter) development base on the shrivel categories in this research.

Table 3.2. The threshold of Rq on shrivel categories (0=None, 1=slight, 2=moderate, 3=severe).

Rq (µm)	**0**		**1**		**2**		**3**	
(0, 13]	643	73.7%	16	10.7%	3	2.8%	0	0
(13, 16]	212	24.2%	93	62%	37	34.9%	11	21.6%
(16, 19]	23	2.63%	17	11.3%	42	39.6%	14	27.5%
(19, 23]	5	0.057%	24	20%	23	21.7%	25	49%
overall	876		150		106		51	

A1describes the peak cross-sectional area of skin surface topography (Fig. 3.20). The value of A1 is determined by Mr1(>0) and Rpk (>0) (Eq.3.3). The value of A1 shows a downtrend with increasing shrivel severity, with considerable changes amongst the first three stages but a slight reduction from moderate to severe shrivel symptoms (Fig. 3.20; Table 3.3). Lenticel size is in the range of 0.05~0.25mm^2. The fringe projection can identify the micrometer level structure. Thus, the lenticel structure can be captured by fringe projection and being a possible influential factor to the data collection of the surface topography caused by shrivel. In this case, a decrease value of A1 increased with shrivel symptoms possibly due to the reduction of the extent of the effect of lenticels on skin

surface topography. As the shrivel symptoms get severe, the peak number (PC) becomes lower, thus a less peak cross-sectional area of skin surface topography.

$$A1 = \frac{1}{2} * Rpk * Mr1 \qquad \text{(Eq.3.3)}$$

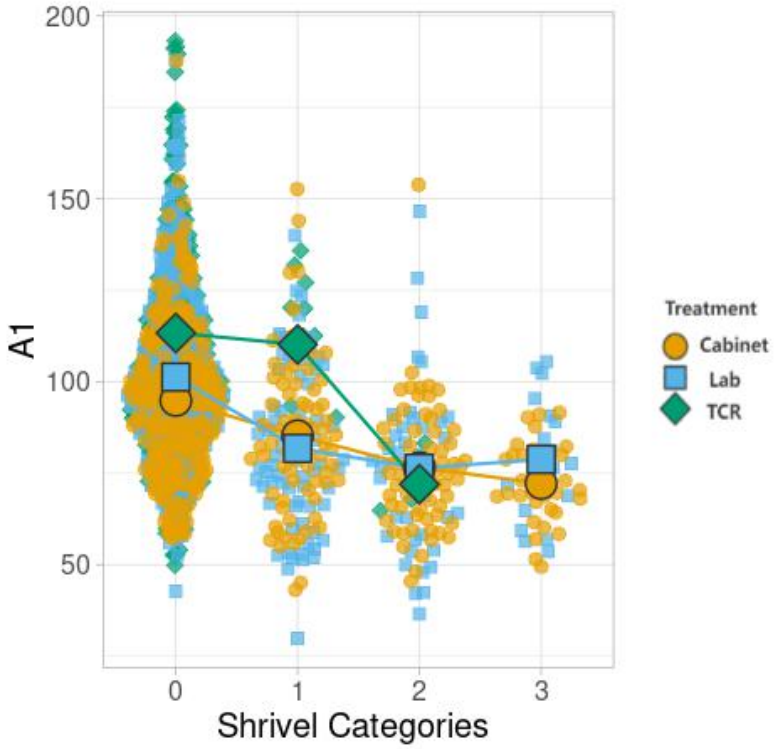

Figure 3.20. A1 (indication of the material filled peak area) development base on the shrivel categories in this research.

Table 3.3. The threshold of A1 on shrivel categories (0=None, 1=slight, 2=moderate, 3=severe).

A1 (µm)	**0**		**1**		**2**		**3**	
(190, 96]	494	56.4%	44	29.3%	15	14.2%	3	5.88%
(96, 76]	258	29.5%	52	34.7 %	36	34.0%	20	39.2%
(76, 60]	104	11.9%	32	21.3%	55	51.9%	19	37.3%
(60, 0]	26	3.00%	22	14.7%	22	20.8%	9	17.7%
overall	876		150		106		51	

PC is the peak number of the kiwifruit surface in the total measure distance. The peak heights were defined as the heights which are above a proportion of the calculated RZ values. RZ is the average maximum height of the roughness. In this research, PC is wrinkle volume on kiwifruit skin. A fixed height for PC, above 2% of Rz was considered (RZ value at 35~75µm from none to severe in this chapter). Hence, as the kiwifruit shrivel became severe, the average height of peak increased which would arise of the fixed height for PC and thus decreased the influence of the natural valley and peak from fruit skin. As in severity, peaks, and deep gauges (produced by wrinkles is around 15~17 µm), non-shrivel occurs at 8-10 µm, and shrivel occurs at > 10 µm. The mean height is far less than Rz as symptom develops. Therefore, as the shrivel symptoms get severer, the number of peaks on the skin surface could be decreased (Fig. 3.21). PC showed a high difference in diverse shrivel categories. The mean of PC decreased with increasing shrivel severity (Table 3.4).

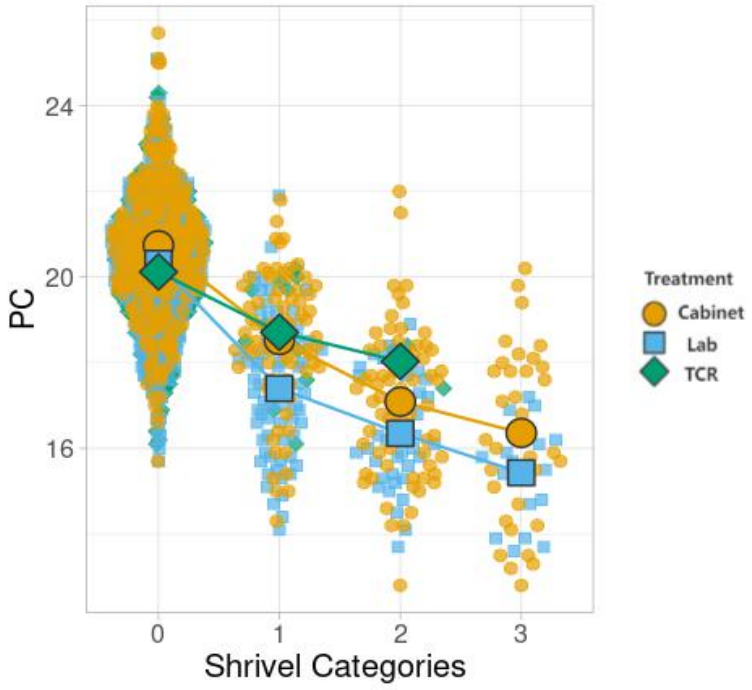

Figure 3.21. PC (indicating of the peak number on the measure distance of kiwifruit surface) development base on the shrivel categories in this research.

Table 3.4. The threshold of PC on shrivel categories (0=None, 1=slight, 2=moderate, 3=severe).

PC	0		1		2		3	
(26, 19]	717	81.9%	41	27.3%	7	6.6%	3	0
(19, 17.5]	145	16.6%	56	37.3 %	33	31.1%	10	19.6%
(17.5, 15.7]	32	3.7%	38	24.6%	39	36.8%	20	39.2%
(15.7, 13]	3	0.34%	16	10.7%	27	25.5%	22	43.1%
overall	876		150		106		51	

Rpm, a vertical parameter, is the average height of the largest profile peaks. In other words, Rpm describes the average height of the largest undulating skin hills caused by the wrinkled skin with shrivel symptom. Thus, the higher the Rpm is, the larger the skin hills could be, and thus possibly correlating to a more severe shrivel symptom (Fig. 3.22). The mean Rpm between none, slight, moderate, and severe shrivel symptoms differed significantly ($P<0.05$). (Table 3.5).

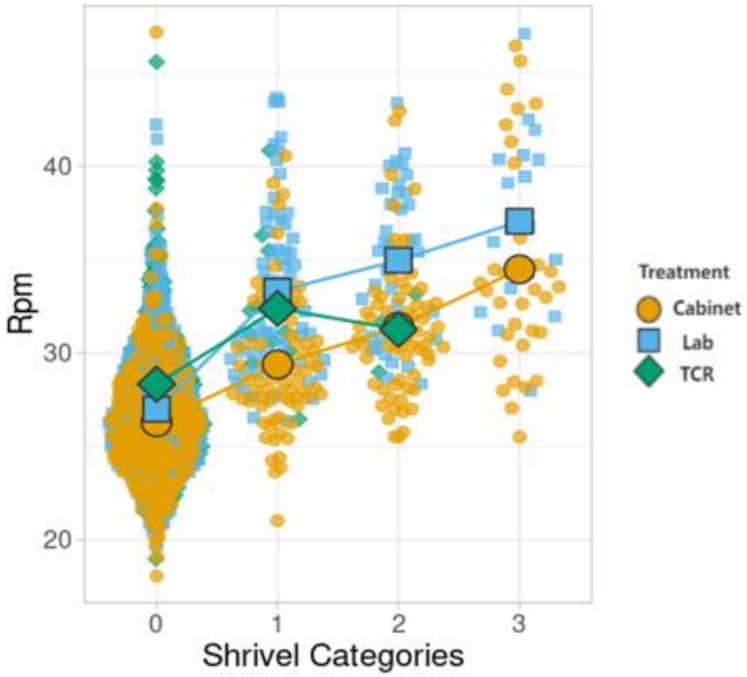

Figure 3.22. Rpm (the average height of the largest profile peaks) development base on the shrivel categories in this research.

Table 3.5. The threshold of Rpm on shrivel categories (0=None, 1=slight, 2=moderate, 3=severe).

Rpm (µm)	**0**		**1**		**2**		**3**	
(18,27]	454	51.8%	17	11.3%	3	2.83%	1	1.96%
(27, 31]	296	33.8%	68	45.3 %	37	34.9%	9	17.7%
(31, 35]	94	10.7%	41	27.3%	38	35.9%	21	41.2%
(35, 47.2]	31	3.54%	30	20%	29	24.06%	20	39.2%
overall	876		150		106		51	

Rpk, is the average height of the protruding peaks above the protruding core roughness profile. On the kiwifruit skin measurement, Rpk shows the average height of the undulating skin hills caused by the wrinkled kin with shrivel symptoms. Therefore, a higher average height of skin hills possibly describes a larger range rise and fall of skin, thus severer shrivel symptoms. However, based on the PCA result, Rpk was not regarded as an influential parameter to classify shrivel. Similarly, according to Table 3.7, shrivel categories cannot be statistically distinguished by Rpk into the none, slight and severe shrivel symptoms but can significantly be looked at the difference of moderate shrivel among shrivel categories. There is no obvious trend despite that the mean of Rpk for fruit with moderate shrivel severity showed a statistical difference (Fig 3.23). The result suggested that Rpk has no apparent tendency of indicating shrivel categories, as expected as the PCA result. Since Rpk describes the degree of difference between the greatest peak and the average, if the fruit surface shrivels evenly from the vertical direction, the severity of the shrivel does not affect the value of Rpk.

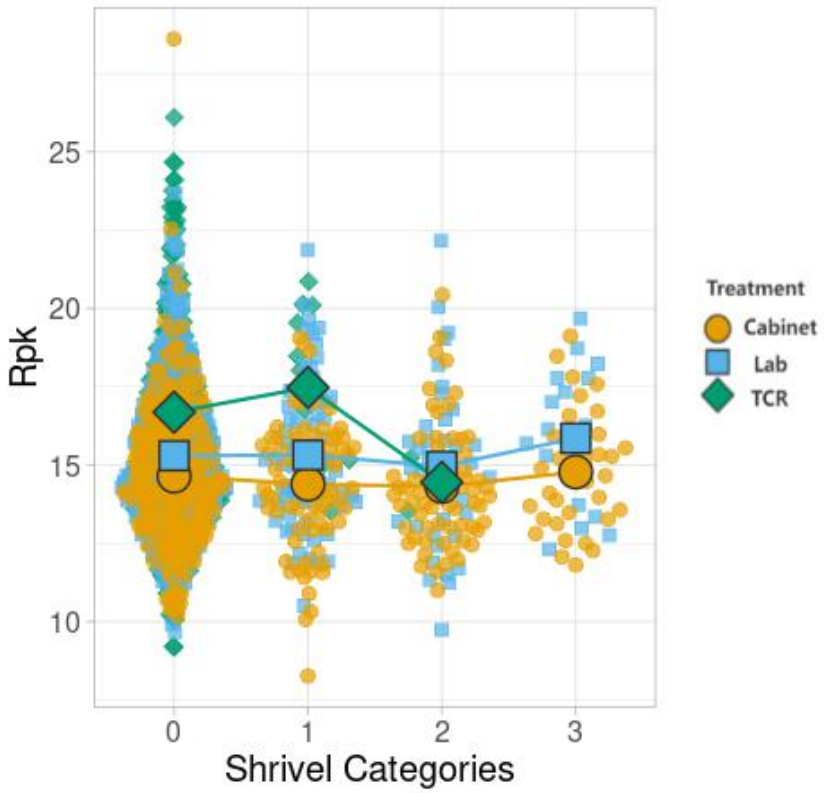

Figure 3.23. Rpk (the average height of the protruding peaks above the protruding core roughness profile) development base on the shrivel categories in this research.

Rsk, a vertical parameter, is a measure of the asymmetry of the amplitude density curve (Eq.3.4). On the kiwifruit surface measurement, it gives information on the morphology of the surface texture of kiwifruit. Statistically, Rsk is a skewness, which negative skew value highlights the risk of leaf tail events, while a positive skew refers to a longer or fatter tail on the right. The mean of positively skewed data will be greater than the median. A positive skewness explains that most of the measurement values are lower than the mean value, indicating a situation of an underestimate, and vice versa (Fig. 3.24a). In this research, a negative Rsk on the 'SunGold™' kiwifruit surface indicates the predominance of valleys on the fruit surface, and possibly explains severer shrivel symptoms (Fig. 3.24b). A positive Rsk indicates fewer deep valleys with many peaks, and Rsk closes to zero shows the same number of peaks as valleys (Fig. 3.24b) (Lai et al., 2019; Martinez et al., 2021). Thus, Rsk changed from being positive (with sound fruit) to zero (slight and some of the moderate) and then to negative (severe). The surface started with main peaks (possibly due to lenticels) to a large number of valleys as shrivel severity increased.

Rsk divided shrivel categories into none, slight, moderate significantly (P<0.05) but no clear threshold between moderate and severe shrivel symptoms. The average of Rsk is 0.29 in non-shrivel level, 0.052 in slight, -0.048 is moderate, and -0.107 in severe shrivel (Table 3.6). As the severer of shrivel symptom, a lower value of Rsk with the ranges at -1, 1, which is satisfied with the expectation of PCA. As Rsk lower than 0, means there are lots of peak (Fig. 3.22 b). the Rsk larger than 0 shows that the peak number is less, and most of the peak height are lower than mean line (Fig. 3.24a). Thus, Rsk could remarkably explain the shrivel categories from none to a moderate degree (Fig. 3.25).

$$\text{Rsk} = \frac{1}{Rq3} * \left[\frac{1}{lr} * \int_0^{lr} |R^3(X)|dx\right] \quad \text{(Eq.3.4)}$$

a.

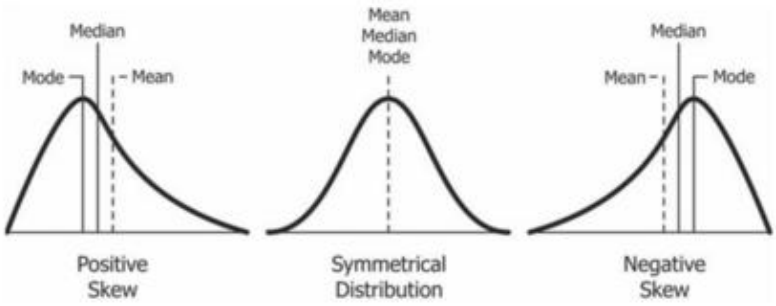

.

b.

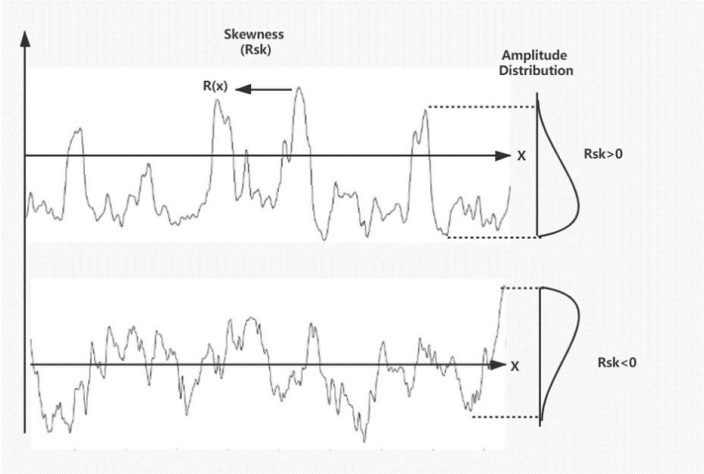

Figure 3.24. A graph of indicating positive skew, symmetrical distribution, and negative skew (a), and the meaning of Rsk (skewness) value on skin topography.

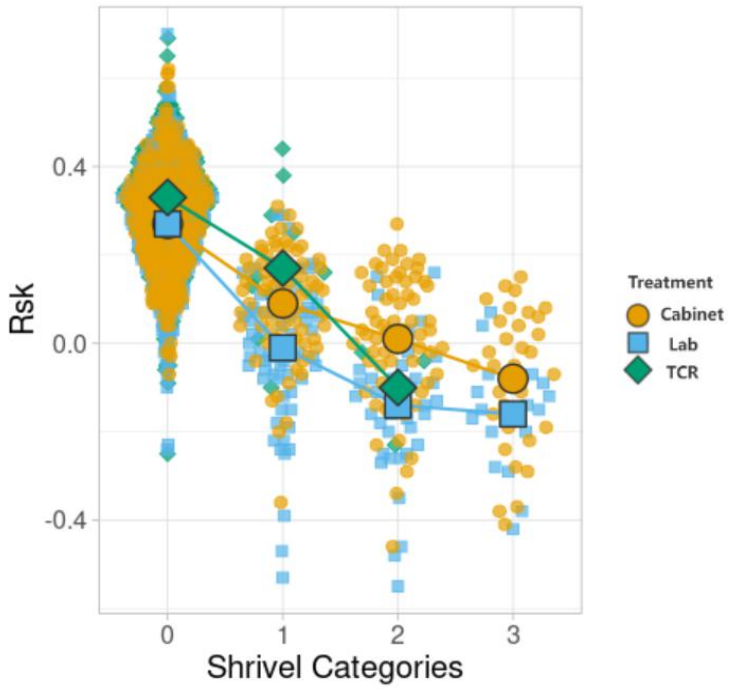

Figure 3.25. Rsk (measuring the asymmetry of the amplitude density curve) development base on the shrivel categories in this research.

Rsk	**0**		**1**		**2**		**3**	
(1, 0.3]	423	48.3%	2	1.33%	0	0%	0	0%
(0.3, 0.05]	402	45.9%	78	52 %	29	27.4%	8	15.7%
(0.05, -0.15]	37	4.22%	50	33.3%	39	36.8%	17	33.3%
(-0.1, -1]	6	0.68%	20	13.3%	38	35.9%	26	51%
overall	876		150		106		51	

Table3.6. threshold of Rsk on shrivel categories (0=None, 1=slight, 2=moderate, 3=severe).

Rtpi, a material part micro, is the ratio of the material part to the entire length. PCA results have suggested that Rtpi could not play a crucial role in determining the shrivel severity (Fig 3.26). According to Fig. 3.26, Rtpi did not vary with the severity of shrivel symptoms and failed to determine thresholds between shrivel categories. Also, the results of ANOVA have proved the implication that Rtpi cannot be applied in looking at the shrivel categories of 'SunGold™' kiwifruit (Table 3.7), which has proved the results in the PCA method.

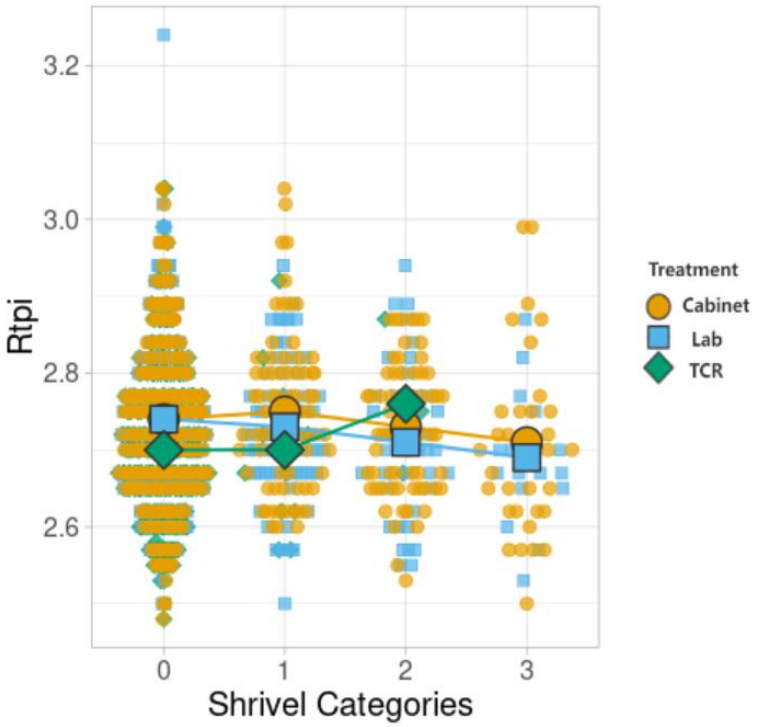

Figure 3.26. Rtpi (a material part micro, as the ratio of the material part to the entire length) development base on the shrivel categories in this research.

3.3.6 Shrivel Development and Relative Weight Loss, Weight Loss Rate

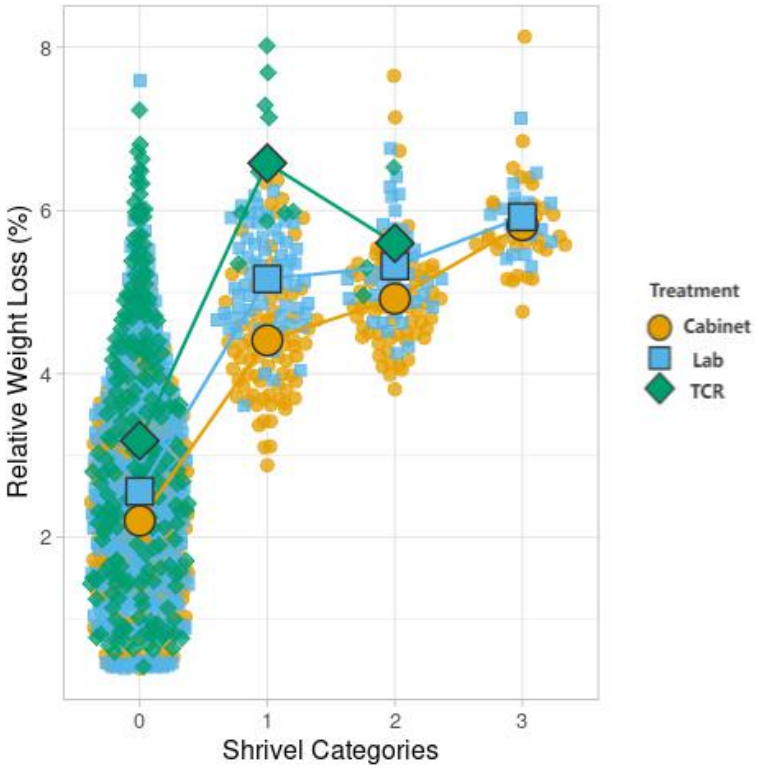

Figure 3.27. Relative Weight loss and proportion of fruit in each shrivel category for ''SunGold™' kiwifruit with differential shrivel severity after storage in cool store 1℃ and then three treatments (lab at 20℃, 52.9% RH; cabinet at 20℃, 47.4% RH; TCR at 1℃, 79.5% RH).

Shrivel occur at 4~5% relative weight loss with a weight loss rate of 14.5-16mg/h in the cabinet, 14-14.9 mg/h at the lab, and around 5mg/h in TCR. Statistically, relatively weight loss (RWL) shows a significant difference between fruit with none, slight, severe shrivel symptoms but no difference was observed between fruit with slight and Moderate symptoms (Table 3.7). The range of parameters in Table 3.7 shows the high possibility in value of parameters in each shrivel categories. The overall trend of relative weight loss increased with increasing shrivel severity. Without shrivel symptoms the average relative weight loss was 2.63%. The average weight loss was 4.90%, 5.08% and 5.56% respectively for fruit with slight, moderate, and severe shrivel symptoms. On the basis of the previous research, there is no significant difference of weight loss between none, slight and moderate shrivel, but a notable increase of weight loss from moderate to severe shrivel in 'Gold9' kiwifruit (Burdon et al., 2014).

'Gold9' kiwifruit tends to show shriveling with the weight loss in the range between 1% and 6%, even the fruit shrivel severity is not associated with weight loss (Burdon et al., 2014; Burdon et al., 2015). In this research, due to the fact that the fruit's initial weight is not at-harvest weight, the slight shrivel symptoms start to show at around 5% relative weight loss, whilst 6% relative weight loss was required for severe symptoms to display. However, the results still seem to be reasonable based on the previous research from Burdon et al. (2014); Burdon et al. (2015).

Table 3.7. Weight loss, skin topography parameters in each shrivel category for 'SunGold™' kiwifruit with different severity of shrivel after storage in the cabinet, lab, and TCR treatment. Values within a column not sharing a common letter differ at α=0.05 (P < 0.05), as analyzed by one-way ANOVA and Tukey.

Shrivel category	**Relative Weight loss (%)**	**Weight loss rate (mg/h)**	**Rq**	**Rtpi**	**A1**	**PC**	**Rpk**	**Rpm**	**Rsk**
None (0)	2.63[c]	15.3a	12.14d (10.92, 13.10)	2.728a (2.65, 2.8)	102.82a (85.37, 118.14)	20.39a (19.4, 21.4)	15.51a (13.54, 17.07)	27.15d (24.57, 29.27)	0.288a (0.20, 0.38)
Slight (1)	4.90[b]	14.4b	15.83c (13.86, 17.14)	2.735a (2.67, 2.80)	85.53b (70.97, 101.61	18.04b (16.90, 19.3)	15.03a (13.62, 19.30)	31.34c (28.06, 33.83)	0.052b (-0.03, 0.16)
Moderate (2)	5.08[b]	14.4b	17.24b (14.74, 18.76)	2.72a (2.65, 2.77)	76.37c (63.04 , 87.22)	16.85c (15.62, 17.88)	14.55b (13.03, 15.73)	32.66b (29.99, 35.44)	-0.048c (0.14, 0.07)
Severe (3)	5.86[a]	14.1b	19.44a (16.19, 21.89)	2.701a (2.64, 2.75)	74.54c (63.04, 87.22)	16.03d (15.62, 17.88)	15.2a (13.42, 16.65)	35.38a (31.36, 40.26)	-0.11c (-0.20, 0.01)
	Statistical analysis: ANOVA *P* values								
Shrivel category :	<2e-16 ***	0.00060 6 ***	<2e-16 ***	0.189	<2e-16 ***	<2e-16 ***	0.00205 **	<2e-16 ***	<2e-16 ***

3.4 Discussion

Fringe projection is a non-destructive technology that can be utilized to quantify surface topography data of fruit. It has been presented to identify and quantifiably characterize protruding and depressed features on fresh produce surfaces with high accuracy to the micrometer level. (Lai, et al., 2018 ; Lai, et al., 2019a ; Lai, et al., 2019b). This research successfully identified the correlation between skin topography and shrivel and weight loss. As such, fringe projection can be used to substitute manual visual inspection of fruit surface defects such as shrivel and can provide a quantification of fruit surface characteristics during postharvest storage.

3.4.1 Shrivel categories and Relative Weight Loss

Weight loss was regarded as a possible main factor in shrivel development during the postharvest period of kiwifruit. A variety of shrivel severity in kiwifruit was obtained by storing kiwifruit at different airflow rates and temperatures in this study. Regardless of the environments in the storage, kiwifruit shrivel outcomes were obtained under different relative weight loss. Therefore, the storage environment possibly influences the shrivel symptoms by impacting the weight loss (water loss) and rate of weight loss of kiwifruit. Water loss would be the main influencing factor on changes to shrivel symptoms for 'SunGold™' kiwifruit.

However, a limitation of this study is that the correlation between the shrivel and weight loss is set up based on ignoring the potential influence of treatments on the connection between shrivel and weight loss. In other words, temperature, humidity, the size of the storage room can all induce a different relationship between shrivel and weight loss.

This study confirms that relatively weight loss is highly associated with shrivel categories in 'SunGold™'. The result of this work is not totally in agreement with Burdon et al., 2014. Absolute weight loss of 'Gold9' among shrivel categories including None, Slight and Moderate was not significantly different but shows an obvious higher value in severe symptoms (Burdon et al.,2014). However, in this research, except for the measurable weight loss difference between severe and other shrivel degrees, a significant difference in relative weight loss can be seen between none shrivel and shrivelled fruit (fruit with shrivel severity greater than 1). The difference from the

previous research possibly results from the distinct standard of division in shrivel symptoms. The shrivel symptoms division was only based on a permanent location which the area was used to do skin parameter measurement by fringe projection. And in this position, squeezing and collisions that can lead to shrivel are avoided. Thus, during the division process, some fruit with shrivel occurrence in the unmeasurable area would not be considered as a shriveled fruit but the weight loss is still being measured.

3.4.2 Shrivel categories and Rate of Weight Loss

The kiwifruit shelf life would be extended by controlling the weight loss rate and monitoring the humidity and temperature in the storage environment. The 'SunGold™' kiwifruit with a higher weight loss rate tend to shrivel faster. It indicates that to prolong 'SunGold™'kiwifruit marketable quality, kiwifruit need be maintained a low respiration rate in the postharvest chain.

3.4.3 Shrivel severity and roughness response relationships

Our comparative analysis showed that overall skin surface topography and the shape of surface structure vary greatly among kiwifruit shrivel categories. The correlation between shrivel severity and skin topography seems more reliable in this study. In vertical parameters, Ra (average of the heights) and Rq (the differences of the height value), and Rpm (the average height of the largest peak) increased dramatically as the weight loss increase and shrivel symptoms get severer. But A1(a material-filled peak area), PC (peak number), and Rsk (skewness, indicating the number of peaks and valley) were found to correlated to shrivel symptoms negatively. Rpk, Rtpi were not found to have a causal effect on shrivel categories. Among all the parameters, Rq and PC indicate better results in classifying the shrivel categories.

Generally, shriveled 'SunGold™' kiwifruit had a value of Rq larger than 13. However, several fruit had Rq at 17 and showed no shrivel. Also, some kiwifruit that had an Rq value of 17, which had slight, moderate, or severe shrivel symptoms. Hence, there was not a very clear threshold of Rq value required for shrivel to occur. But considering that the one-way ANOVA and Tukey results, the mean of Rq value can be significantly distinguished between shrivel categories. As Rq value lower than 13, 73.7% possibility the 'SunGold™' kiwifruit has none-shrivel skin. Thus, at any given time

in postharvest storage, those fruit with more severe shrivel tended to have a higher Rq value than less shriveled fruit.

PC measures the peak number of the kiwifruit surface in the total measure distance. The likelihood of none-shrivel 'SunGold™' kiwifruit is 81.9% as the PC is at the range from 19 to 26. However, the PC value was not clear to classify the threshold of the others shrivel categories. Only 37.3 % 'SunGold™' with PC at (19, 17.5] has slight shrivel, 36.8% with PC at (17.5, 15.7] in moderate and PC at (15.7, 13] with 43.1% possibility in severe symptoms. In conclusion, an acceptable qualification of 'SunGold™' kiwifruit with the high commercial value might have a surface parameter in certain ranges, Rq < 13, PC >19.

3.4.4 Industry applications

Exploring the correlation between weight loss, shrivel symptom response, skin topography characteristics can help the industry enhance postharvest management. The results of this experiment build a correlation between surface topography and shrivel. It indicates shrivel occurrence using skin topography parameters possibly helps the industry estimate the release date of kiwifruit to avoid kiwifruit loss. According to the data, maintaining skin topography parameters Rq<13, PC>19 during the postharvest chain and storage would minimize shriveling degradation of kiwifruit.

The application of a cool storeroom with 1℃, atmosphere storage could prolong the shelf life of fruit by retaining weight. From the cell perspective, the properly low temperature (1℃) can retain the integrity of cells and the fruit firmness. The comparison of water loss in the TCR room (1℃) with subsequent shelf life at lab and cabinet at 20℃ suggested that weight loss increased slowly with 6% weight loss after 8 weeks. Nevertheless, fruit transferred to 20℃, weight loss increased by around 6% in 2 or 3 weeks. The rapidly mass loss could be due to the adverse effect of high temperature on cellular integrity, which increases the membrane permeability (Saltveit and Morris, 1990). Temperature affects permeability by affecting the activity of enzymes. The membrane permeability, in other words, is the possibility of substances into cellular, which the process can be divided into active transport and passive transport. A large part of the membrane transport substances relies on active transport, and active transport requires the participation of enzymes. Thus,

a proper temperature plays a vital role in cellular integrity and influences the weight loss of crops. Besides, the rapid mass loss in high temperatures could be due to the vapor pressure attributed to the temperature and relative humidity. Under the high temperature, EP cell in kiwifruit surface skin is more susceptible to lose water driven by the water vapor pressure between the ambient air and epidermis (DíazPérez et al., 2007). Therefore, a proper low temperature (1℃) in this experiment prolongs the shelf life of kiwifruit essentially in accord with the expectation. Thus, the cool store was always applied in fresh crops storage after harvest in the commercial supply chain.

Compared with the shrivel symptoms, the weight loss could be easier to monitor. Shrivel symptom is a sensory index that needs to be transferred to numerical values for directly monitoring. In this study, Rq and PC as skin topography parameters could essentially indicate the appearance of shrivel with the accuracy up to 73.7% and 81.9% approximately. Alternatively, this experiment suggested that the weight loss could indicate the shrivel symptom below the commercial standards. This would allow for the opportunity for correction of atmosphere throughout the commercial supply chain, or to redirect fruit batches to less distant markets. Further investigation possibly tends to focus on skin topography characteristics of the other kiwifruit cultivars to determine the proper atmosphere throughout the commercial supply chain. The results imply the possibility of quantitatively describing shrivel by looking at skin topographic parameters. Predicting the alteration of shrivel by skin topography parameters could be the next goal.

The hypothesis relationship between weight loss and skin topography traits for ‘SunGold™’ kiwifruit. In order to investigate the potential mechanism, the cellular level study including cellular resistance and the turgor microstructural changes needs to be analyzed in the next step. Also, the other vital index, for instance, firmness, possibly impacting on skin performance of shrivel symptoms responses could be measured.

3.5 Conclusion and Recommendations

This experiment identifies a new shrivel categories' classification and sets a shrivel library for the kiwifruit industry successfully. Compared with the previous shrivel identification, this study classifies shrivel categories is not only based on the certain measurements area but also consider the shrivel severity from the vertical and horizontal direction.

This experiment indicates that the shrivel symptoms responses induced by different storage temperatures and humidity could be essentially distinguished by weight loss. A relatively high temperature (20℃), and humidity could induce a severer shrivel symptom. At a given temperature, the humidity manipulated by the alteration of airflow can be applied in inducing kiwifruit with variable shrivel responses. The experiment setting in this study provides a potential possibility and suggestions for retaining kiwifruit quality after harvest to international markets in the commercial environment. But significantly, the shrivel responses to weight loss could need to be explored in other varieties to confirm the possibility for this experiment.

The hypothesis relationship between shrivel symptoms and skin topography characteristics is supported by these experimental results. Rq, indicating the degree of dispersion of surface height on kiwifruit wrinkled skin, as a possible representative of vertical parameters could describe shrivel categories essentially. As the weight loss increase, the skin topography gets wrinkled with a shrivel response during postharvest storage. Thus, retaining a low weight loss rate would be a way to maintain a sound quality of kiwifruit for commercial use. The sound quality of crops in the sale process needs to be guaranteed as the lousy appearance, decreasing the customers' preference, generating less profit.

In conclusion, this project develops fringe projection, a non-destructive technology, as a new measuring instrument to visualize the surface curvature of horticultural products. Fringe projection assess fruit surface roughness and identify and quantifiably characterize protruding and depressed features on fresh produce surfaces with high accuracy to the micrometer level. Thus, the fringe projection, quality control systems, could provide the industry with the opportunity to take corrective measures, by determining whether a fruit batch will have desirable skin topography characteristics for maintaining customer satisfaction in commercial use. The kiwifruit with sound

skin in the postharvest after storage and transportation could be exported to overseas markets. Therefore, this experiment provides evidence to indicate the possibility of ensuring acceptable kiwifruit skin standards for the marketplace.

Chapter 4. Recording kiwifruit Shrivel by Three-Dimensional Technology

4.1 Introduction

Shrivel is a common mechanism of failure for fruit that has lost a substantial amount of weight (Burdon et al., 2014). Surface topography variations on the micromillimeter scale may provide information on the development of these visual problems (East et al., 2016). The previous chapter demonstrated that shrivel incidence may be detected by measuring skin roughness. Thus, recording the skin wrinkle outcome in shrivel symptoms is critical to shrivel study.

Consistent detection and quantification of shrivel across a global supply chain is a challenge. While the previous chapters' work has utilised technological advancements in order to quantitatively describe shrivel symptoms, this technique requires fringe projection in order to describe shrivel symptoms that have significant cost barriers, and at this stage requires post processing of the data in order to determine the results, which adds significant time. Hence, while the work of the previous chapter demonstrates the potential of fringe projection to quantify shrivel accurately, the technology is more likely to be deployed in a laboratory and research setting in the immediate future.

Quality control within industry fresh produce systems is often done with little or simple equipment and relies heavily on visual comparison and even trained touch (for texture measurement). At industry sites, it is very common to find assessment tables surrounded by visual aid posters that assist quality assessors in identifying and scoring quality issues. For shrivel, photographic capture of symptoms is challenging due to its subtle nature (e.g. texture, shape, etc.). It is then theoretically possible that using physical representative models, which mimic real indicators of the incidence and severity of shrivel development, may be useful in providing guidance to quality assessors. Should physical models that represent certain indicators of disorder be able to be precisely manufactured to predetermined specifications, then these same models can be used across a supply chain and enable better symptom scoring. This may improve the data consistency across the quality assessment system. Thus, it is appropriate to use the 3D model to train the inspector.

3D scanning is a non-destructive tool that captures data by imaging the actual objects and bringing them into the digital pipeline. 3D scanning has been increasingly used in the assessment of horticultural products. For example, terrestrial laser scanning technique was applied to detect the structure of trees and fruit yield (Tamás, et al., 2011). However, previous 3D scanning has previously focused on large scale dimension and shape description rather than determination of the finer scale surface topography of the product. The consistently improving quality and resolution of 3D scanners provides the potential for capturing detailed surface topography of fruit.

Should high resolution topography data be captured through 3D scanning, then potential physical models of shrivel could be consistently reproduced through 3D printing (Varotsis, 2021). 3D printing processes print a three-dimensional object layer by layer to create a new object in a matter of hours. The Material Jetting-based 3D printing system uses support wax and plastic resin to build complex, low-resolution parts. The printing resolution can reach 32 microns. 3D printing technology has been increasingly used in the agriculture and horticulture fields in recent decades. For instance, a design and test of a gripper prototype by printing 3D models has been done for horticulture products by Russo et al. (2017). In kiwifruit, 3D printing technology has been used to design and manufacture the end-effector for mechanical kiwifruit harvest (Mu et al., 2017), and kiwifruit on-tree counting and yield estimation in the preharvest field (Mekhalfi et al., 2020). Huang et al. (2017) works at Massey University has done physical and thermal simulators, but his work focused on getting the macro scale dimensions and shape right rather than the finer. As a result, 3D printing technology has the ability to manufacture replicated fruit items for extensive uniform roll out across the supply chain as a constant visual help for quality graders.

The objectives of this work were to attempt to produce a physical replica of a 3D shrivel library for the kiwifruit industry and to determine the current possibility of using physical simulators as aids for grading shrivel severity in the quality assurance system.

4.2 Materials and Methodology

4.2.1 Experimental philosophy

In order to determine the likelihood of recreating 3D physical models of shrivel the following processes were conducted:

1. Kiwifruit with different shrivel symptoms were selected and placed into five shrivel categories. The former four levels were used in chapter 3 (Fig. 3.7). The fifth degree is added in this chapter for the whole shrivel fruit (Fig. 4.1).
2. A Fringe projection measurement of the microtopography of a specific location on the kiwifruit surface was conducted (Two images were collected from each fruit, and the imaging area has the same shrivel severity on the same fruit).
3. A visual image of the shrivel being considered was captured for future use.
4. A 3D scanner was used to capture the entire 3D surface of each kiwifruit.
5. Blender (version 2.79, Blender foundation, Amsterdam, Netherlands, 2020) was used to insert the sphere on the surface that identified the location of the scanning position of the fringe projection measurement.
6. A 3D printer was used to consequently print the 3D model of the kiwifruit from the 3D captured data.
7. The resulting 3D printed fruit models' surface roughness was again captured by fringe projection, enabling quantitative comparison of the surface roughness between the real fruit and the 3D printed fruit simulator.
8. Quantitative comparison of real and simulated fruit surface topography with methods established in chapter 3.

Figure 4.1. Selected representative kiwifruit showing the shrivel categories from level 0 to level 4 from left to right.

4.2.2 Fruit materials

18 ‘SunGoldTM’ kiwifruit (sized count 30) were divided into five shrivel severity groups (Fig. 4.1), 2 for none-shrivel (shrivel 0), and 4 each for slight shrivel (shrivel1), moderate (shrivel 2), and severe shrivel (shrivel 3 and 4 respectively).

4.2.3 Skin topography measurement by fringe projection

Skin topography measurement by fringe projection was carried out before three-dimensional scanning and after 3D printing. Details of the fringe projection process are described in chapter3 (Fig. 4.1).

4.2.4 Photo fruit

Kiwifruit were taken photos to record a visual appearance before doing the three-dimensional scanning and fringe projection. All the photos were taken using a Canon EOS 90D (EFS 15-18mm 3.5-5.6 lens) camera. Pictures were taken in a lightbox outfitted with D65 lighting that had been switched on at least 10 minutes prior to guarantee steady image capture.

4.2.5 Three-dimensional scanning

To record the entire form and size of each fruit, a desktop 3D scanner (EinScan-SE, Shing 3D Tech Co., Ltd, 2019) driven by ExScan S v3.0.0.1 was utilised. The EinScan-SE is a revolutionary 3D scanner with high-cost performance. The scanner's utilises laser triangulation technology and the single shot precision can approach 0.1mm. The device can scan items weighing less than 5 kg with minimum dimensions of 30×30×30 mm and maximum dimensions of 700x700x700mm. Digital 3D models scanned using the 3D scanner were saved as Obj,.mtl, and.jpg files, and all the three files are applied in adding sphere prior to 3D printing.

The EinScan-SE is made up of three major components: a structured light scanner, a revolving turntable, and a calibration board. The scanner head contains two monochrome cameras that can record the object's colours and surfaces, as well as one white light emitted in the centre (Lievendag,

2017). The generating process takes place without any physical contact with the items. The scanned item is placed on the turntable. The light scanner projects a pattern of light that strikes the object on the turntable.

During the scanning process, the scanner is stationary, and the turntable can move automatically, or the item can be moved by the user to perform a fixed scan that provides numerous angles that add up to 360 °. A single scan takes eight seconds, but a 360° scan takes two minutes. The scan turntable, on the other hand, revolve 8 to 180 times in a 360° scan. The less the angle changes each time, the better the scan quality, and hence the longer the scan will take. The scanner automatically aligns 3D data based on placement targets. After scanning, the patterns were merged to produce a complete 3D target object, which was then performed on ExScan S v3.0.0.1. Furthermore, because the EinScan-SE captured objective data with two cameras, the stereoscopic pair must be calibrated beforehand. The calibration finished three calibration processes as well as a white balance test in preparation for scanning a colourful item.

4.2.6 Adding location markers to the 3D scanned fruit

Kiwifruit shapes were generated digitally in blender (version 2.79, Blender foundation, Amsterdam, Netherlands, 2020). All three formats Obj, .mtl, and .jpg files of each fruit in the same directory were used in the sphere inserting process. Before importing the fruit file, the current kiwifruit model could import with a center which was offset a long way from their center of mass. Adjusting the position of the object to 0, 0, 0 by entering X, Y, Z values. After that, by clicking the 'Viewport Shading' button shown to view the object with texture was for locating the sphere. Axis button could be used to get views in different planes when placing markers.

To add the sphere to the updated model, a sphere had to be added to the scene. A radius of 1.0mm was used for the sphere by enlarging the add UV Sphere box and entering the necessary value. Adjust the coordinates in various perspectives until the sphere was at the desired location. About half of the sphere should be above and half below the fruit's surface. Next, the sphere was saved and moved to the proper position for repeating the procedure by establishing a union at each dot. The final 3D model was saved and exported as a STL.file for 3D printing.

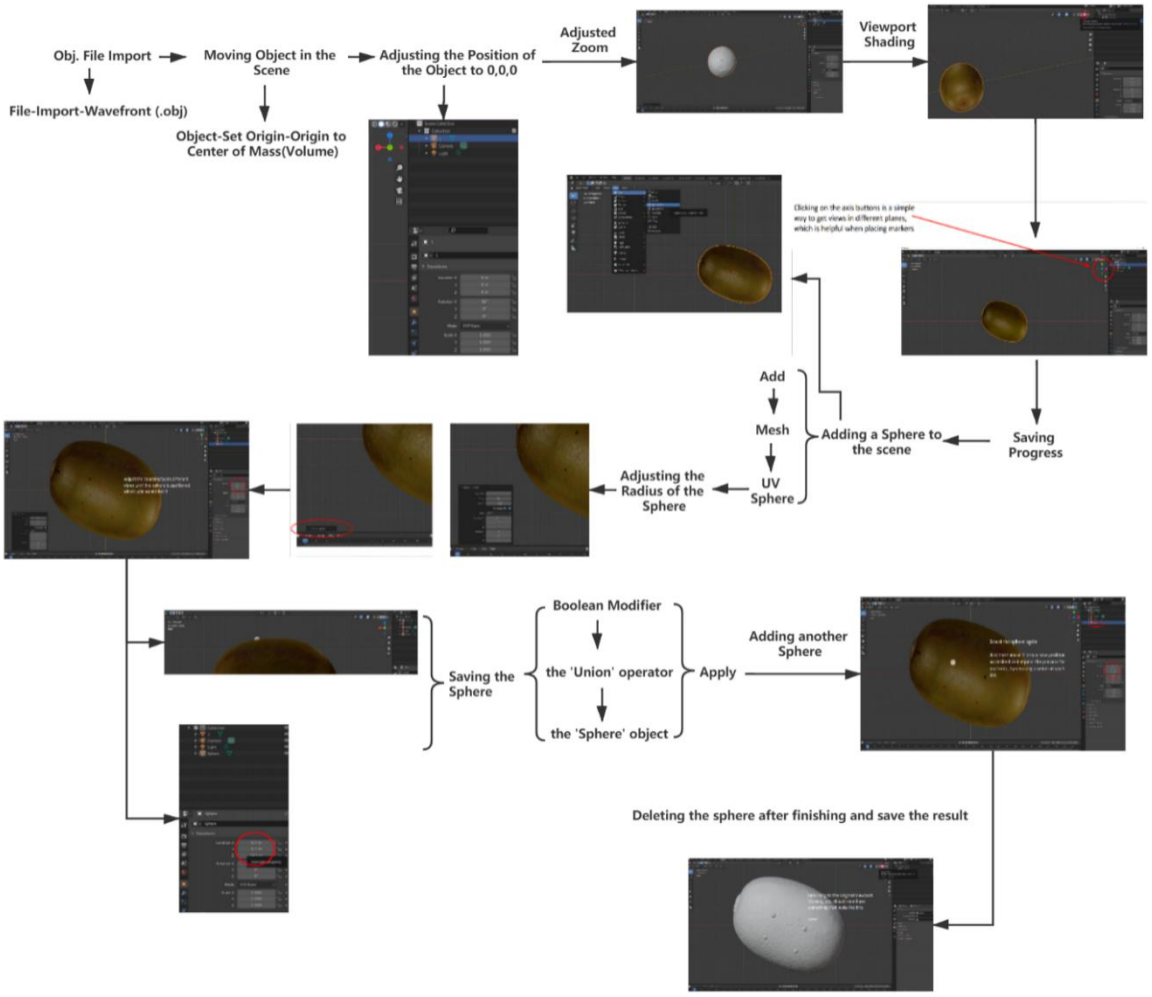

Figure 4.2. Workflow in adding sphere in 3D kiwifruit model by Blender (version 2.79, Blender foundation, Amsterdam, Netherlands, 2020).

4.2.7 3D printing

The kiwifruit model was saved as an STL. file for 3D printing after the position marking spheres were added. The 3D printing was done on a ProJet MJP 2500 Plus 3D printer (3D Systems, Rock Hill, SC, USA). The 3D printer created a Kiwifruit model with wax support, which was then delivered to the Project EasyClean system in steam mode to remove the support wax necessary for printing. (Fig. 4.4). The ProJet® MJP 2500 Series has a claimed resolution of 32 micrometres, which might allow for reproduction of specific information on the kiwifruit surface, such as lenticels and topography as impacted by shrivel development.

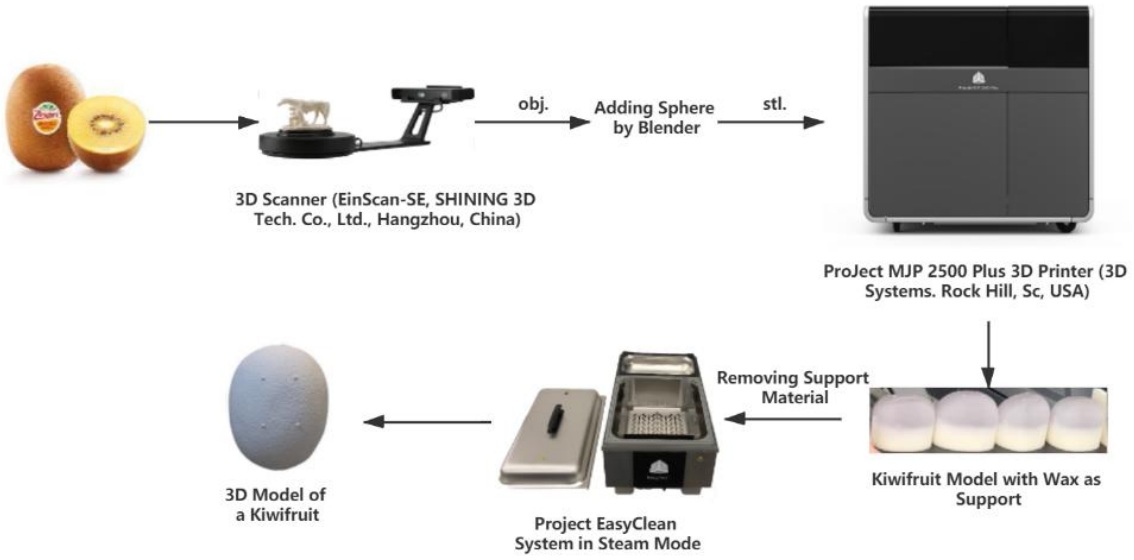

Figure 4.3. kiwifruit 3D scanning and adding sphere and printing process.

4.2.8 Three-dimensional fruit image analysis

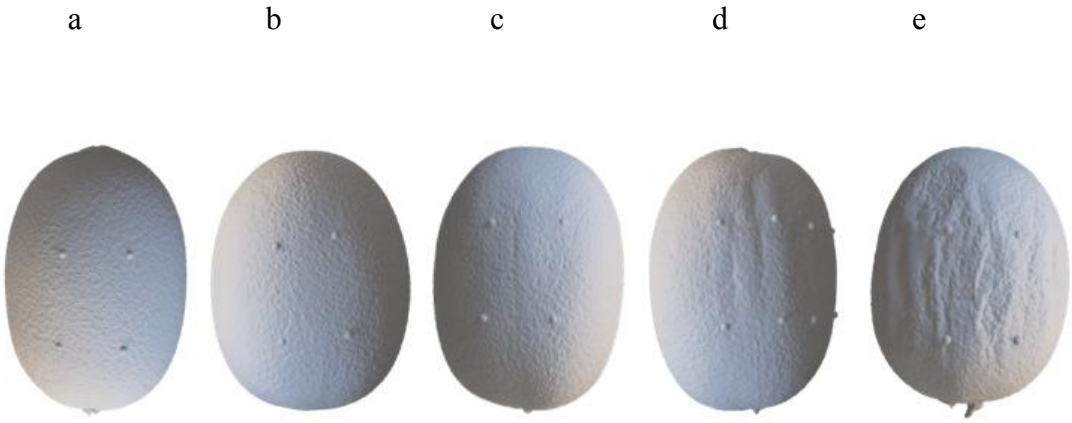

Figure 4.4. Selected representative 3D kiwifruit model image after sphere inserting showing the shrivel categories from level 0 to level 4 (a: level 0; b: level 1; c: level 2; d: level 3; e: level 4), the kiwifruit model is different fruit from above Fig. 4.1.

4.2.9 Quantitative analysis

In order to the performance of 3D technology, skin topography data collected from 3D printed fruit surface and real fruit were compared with the result in chapter 3. In chapter 3, skin line parameter has been classified into seven groups, and Rq, A1, PC, Rtpi, Rpk, Rpm, Rsk as representatives to describe shrivel. Thus, in this chapter, shrivel performance of printed fruit are described by comparing the seven parameters.

4.3 Results

4.3.1 Visual Comparison of Real to 3D printed model kiwifruit

Example topographical profiles of the real and 3D printed fruit are presented in Fig. 4.5. Overall, the reproduced fruit simulators demonstrated similar topography to the real fruit. In comparing the valley of topography caused by shrivel and the peaks caused by the overall topography, the fruit simulators resulted in very similar patterns especially in the cases of severe shrivel (Fig. 4.5d and h).

However, in this study fruit was only be scanned for one time, 3D scanner (EinScan-SE) with 0.1mm accuracy, 0.17mm~0.2mm resolution may loss some information of skin characterized on fruit surface. Also, noticeably, the lenticel in the 3D printed fruit is rougher than the real fruit (Fig. 4.5) as evidenced by the resolution of 3D printer is 32μm causing that peak and valley less than 32 μm cannot be identified (Table 4.1).

As shown in Fig. 4.5, the color of image describes the height level, height from -140 to 160 is with color from dark to light. As shrivel severity increased from level 1 to 4, the proportion of yellow and dark part became larger, which means that the height of peak and valley became large in both printed and real fruit. As shrivel became more severe, the lenticel, valley size and shape between 3D artificial fruit and real fruit tend to be similar. However, it is quite difficult to compare the resemblance of surface captured by fringe projection for shrivel levels 1 to level 3. The lenticels on 3D fruit surface are larger than those of real fruit (Fig. 4.5).

Table 4.1. The resolution comparision of Fringe projection, 3D scanner and 3D printer (ProJet MJP 2500 Plus 3D printer (3D Systems, Rock Hill, SC, USA))

Equipment	Fringe projection	3D scanner (EinScan-SE, Shing 3D Tech Co., Ltd, 2019)	3D printer (ProJet MJP 2500 Plus 3D printer (3D Systems, Rock Hill, SC, USA))
Resolution	x-y resolution: 26.83 μm. z(vertical) resolution: 2 μm	0.17mm~0.2mm	32μm resolution

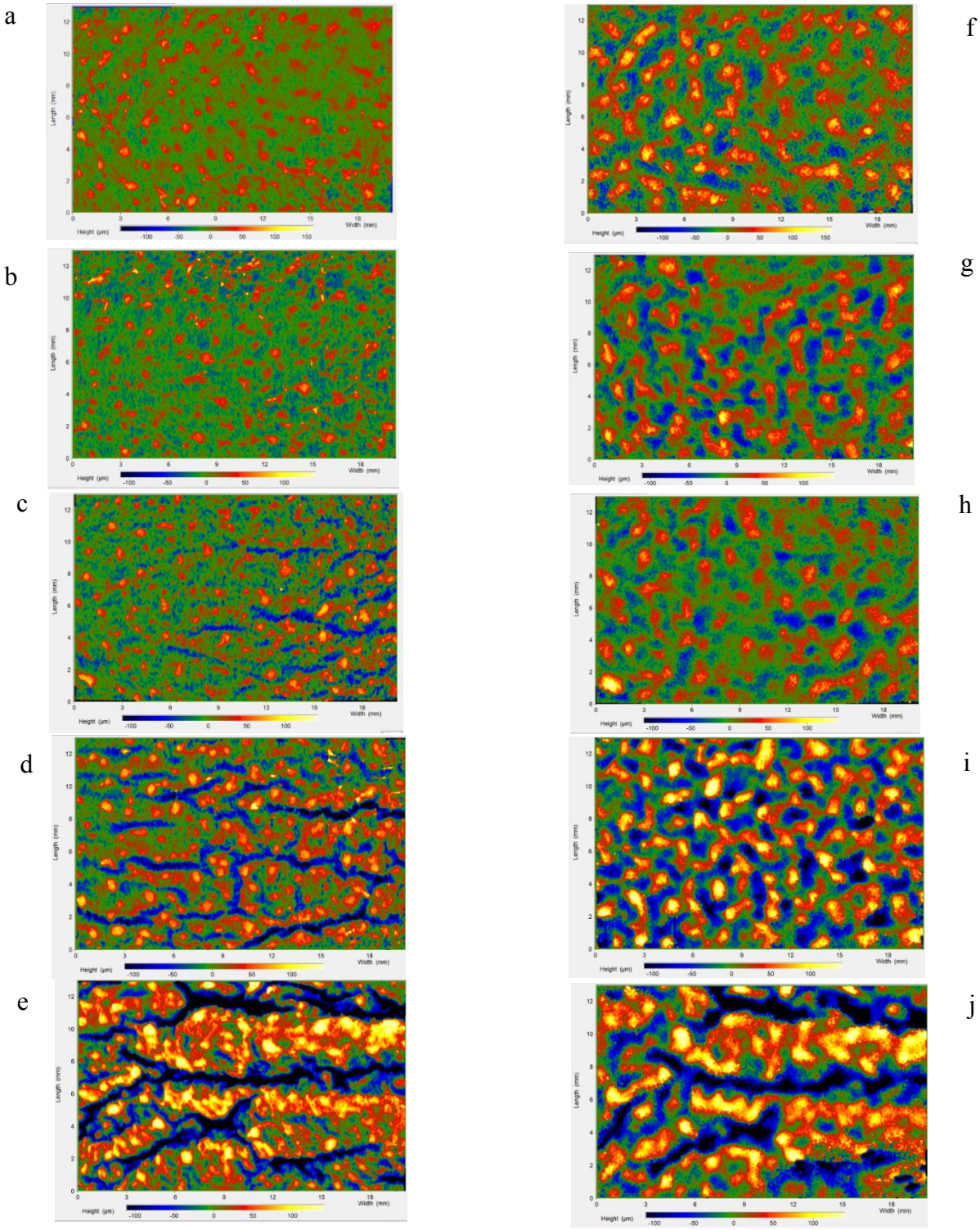

Figure 4.5. Selected representative (a-d) real and (e-h) 3D simulator kiwifruit 2D topographical images from fringe projection showing the shrivel categories. the x and y axis represent the width and length of 2D images and the colour bar indicates the height of the peak and valley. Vertical aligned images are for the same fruit with differing severity of (a, f) level 0, (b, g) level 1, (c, h) level 2, (d, i) level 3 and (e, j) level 4.

4.3.2 Quantitative comparison of real and simulated fruit surface topography

In this section, quantitative comparison between real and simulated fruit was analyzed by looking at seven skin surface parameters. The seven parameters were selected by chapter 3 (section 3.3.4; section 3.3.5). Thus, shrivel symptoms can be comprehensive analyzed.

Rq describes the root mean square average of the profile heights of the roughness profile, which means the degree of dispersion of surface height. The shrivel visualization is due to the difference of peak height and valley. According to Fig. 4.5, color difference increased with the shrivel symptoms from slight to severe, indicating a higher peak and deeper valley as shrivel became severer. The trend of Rq observed in this chapter is similar to that in chapter 3.3.6, which verify that the increasing Rq values reflect a larger difference between values of the peak, indicating an increase in shrivel severity.

According to Fig. 4.6, Rq of the 3D printed fruit increased with shrivel severity, similar to the real fruit. However, Rq of printed fruit was greater at no-shrivel (0), but less than real at high shrivel score of 4. 3D scanner and printer resolution and accuracy are high but possibly cannot identify all detailed information (such as slight roughness) on the skin surface. The value of Rq can be 8-12 μm in very slight shrivel, the depth resolution of fringe projection is 1.7 μm meaning can capture the Rq value clearly. Thus, the possibly of losing information due to the fringe projection equipment (Primos™ Lite, Canfield Image Systems, USA) system is excluded. The 3D surface of non-shrivel level could tend to have a higher roughness compared with real fruit skin due to the inaccuracy during the scanning process or printing and thus a less difference of peak height on the 3D surface indicated a higher value of Rq.

The resolution of 3D printer ProJet® MJP 2500 Series at 32 μm indicates that it can capture a slight peak above core that less than 32 μm. The value of Ra (average height of the roughness profiles) did not reach 32 μm from shrivel 0 to 4 on the kiwifruit surface in this chapter. However, given that the value Rmax (maximum roughness depth) and Rt (the maximum height of the roughness profile) are all larger than 32 μm, shows that only a part of information in vertical direction can be identified by 3D printer from fruit surface. The resolution of 3D scanner is 170μm, the resolution of the 3D scanner seems lower compared to fringe projector and 3D printer. Thus, the loss of information can

possibly occur during scanning and the printer only printed out the level of details recorded in the 3D model.

A1 is peak cross-sectional area, the accuracy of A1 is determined by Rpk and Mr1, Visibly, the area of printed lenticels from 3D profile is inaccurate and with a large number of smaller lenticels not identified by 3D printer due to the inaccuracy (Fig. 4.5b). For shrivel severity 4, the peaks are larger because of shrivel development, which would be easy to identify. Therefore, the value to A1 of 3D printed fruit is close to that of the real fruit at high shrivel severity scores (3 and 4).

$$\text{A1} = \frac{1}{2} * Rpk * Mr1 \qquad \text{Eq. 4.1}$$

Rsk describes the information of the surface texture of kiwifruit. The surface texture in the form of peaks and valleys, characterized by the height and spacing of these peaks and valleys. The 3D printed fruit returned similar Rsk values irrespective of the shrivel severity while in real fruit a dramatic reduction in Rsk values is observed (Fig. 4.6g), 3D printed fruit has a rougher surface compared with the 2D profile of real fruit (Fig. 4.5). Also, Rsk is determined by Ra and Rq, which is a vertical parameter. According to the above, Ra and Rq of 3D fruit are not accurate, indicating that 3D scanning, and printing technology cannot recognize the surface texture accurately possibly due to the resolution of 3D printer (32μm).

$$\text{Rsk} = \frac{1}{Rq3} * \left[\frac{1}{lr} * \int_0^{lr} |R^3(X)| dx\right] \qquad \text{Eq.4.2}$$

Rpm, a vertical parameter, is the average height of the largest profile peaks. Rpm is calculated by the largest profile peaks (Rp). The real fruit Rpm in none shrivel is 30μm, an become larger from slight to severe shrivel, thus can be identified at least from slight shrivel, which seems indicates that Rpm of 3D fruit in non-shrivel cannot match its in real fruit, however, failed to explain the big difference in shrivel level 4 (Fig.4.6; Fig.4.7).

PC is the number of peaks of the kiwifruit surface in the total measure distance, which is also calculated by R(x) (height). It is apparent that only height larger than 32μm can be printed by 3D printer, based on the definition of PC that the peak heights are the heights which are above a

proportion of the calculated RZ values (the average length between the peaks and valleys) (RZ value at 38~85μm from level0 to level 4 in real fruit in this research). Thus, PC should satisfy the expectation, however, still has a big error.

Rtpi, the ratio of the material part to the entire length on kiwifruit surface (Fig 4.6d), has been proved that it has no relevance to shrivel in chapter 3 by PCA and ANOVA method, as similar as the result in this chapter. The value of Rtpi is always at the range of 2.6~2.8.

Rpk, as a peak parameter, is the average height of the protruding peaks above the protruding core roughness profile. On the kiwifruit skin measurement, Rpk shows the average height of the undulating hills caused by the wrinkled skin as a result of shrivel symptoms.

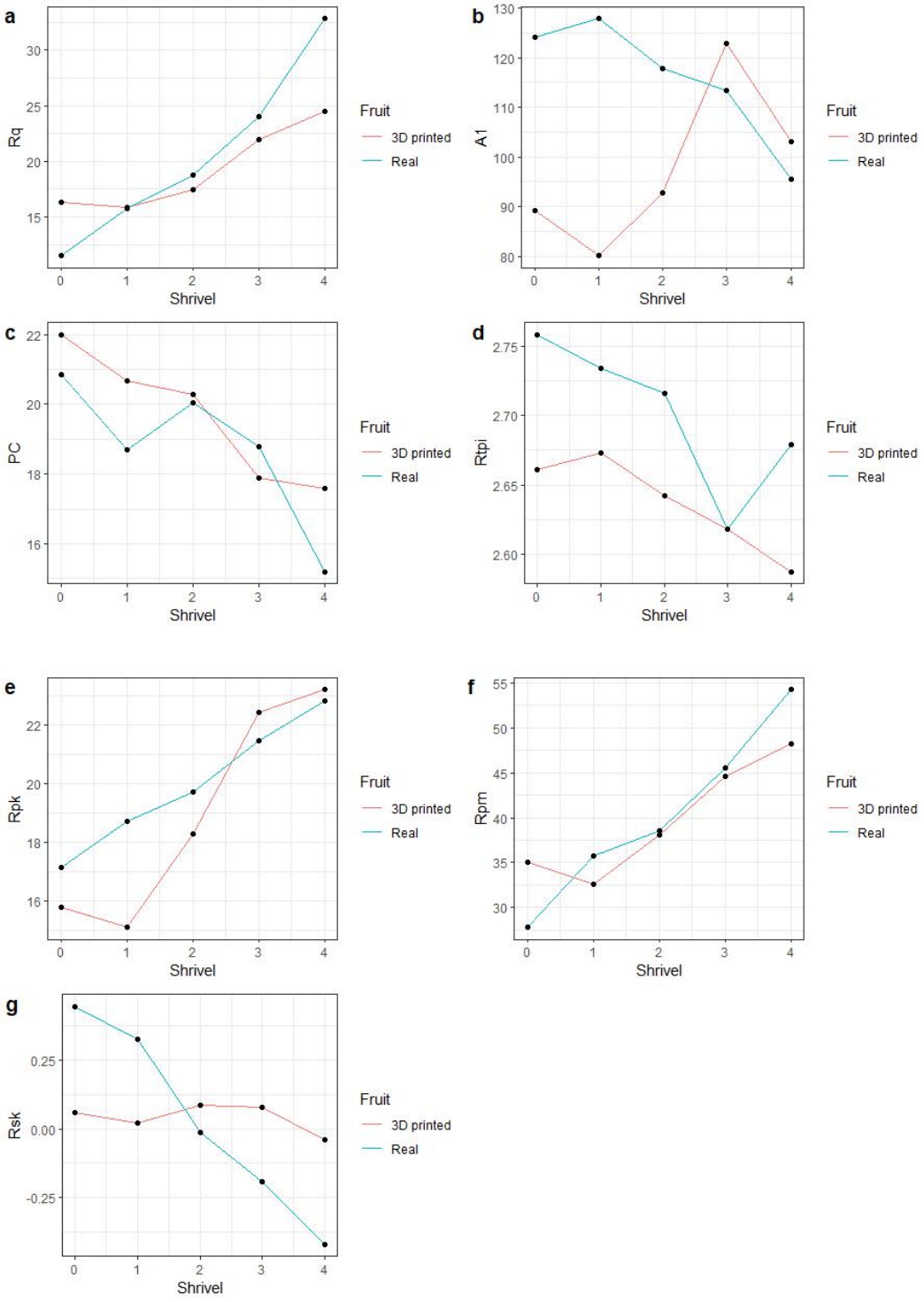

Figure 4.6. is a comparison of 3D fruit and real fruit in the average parameter values extracted from topographical data for each shrivel grade, including 18 kiwifruit, 2 fruit in shrivel level 1, 4 in each level from 1 to 4.

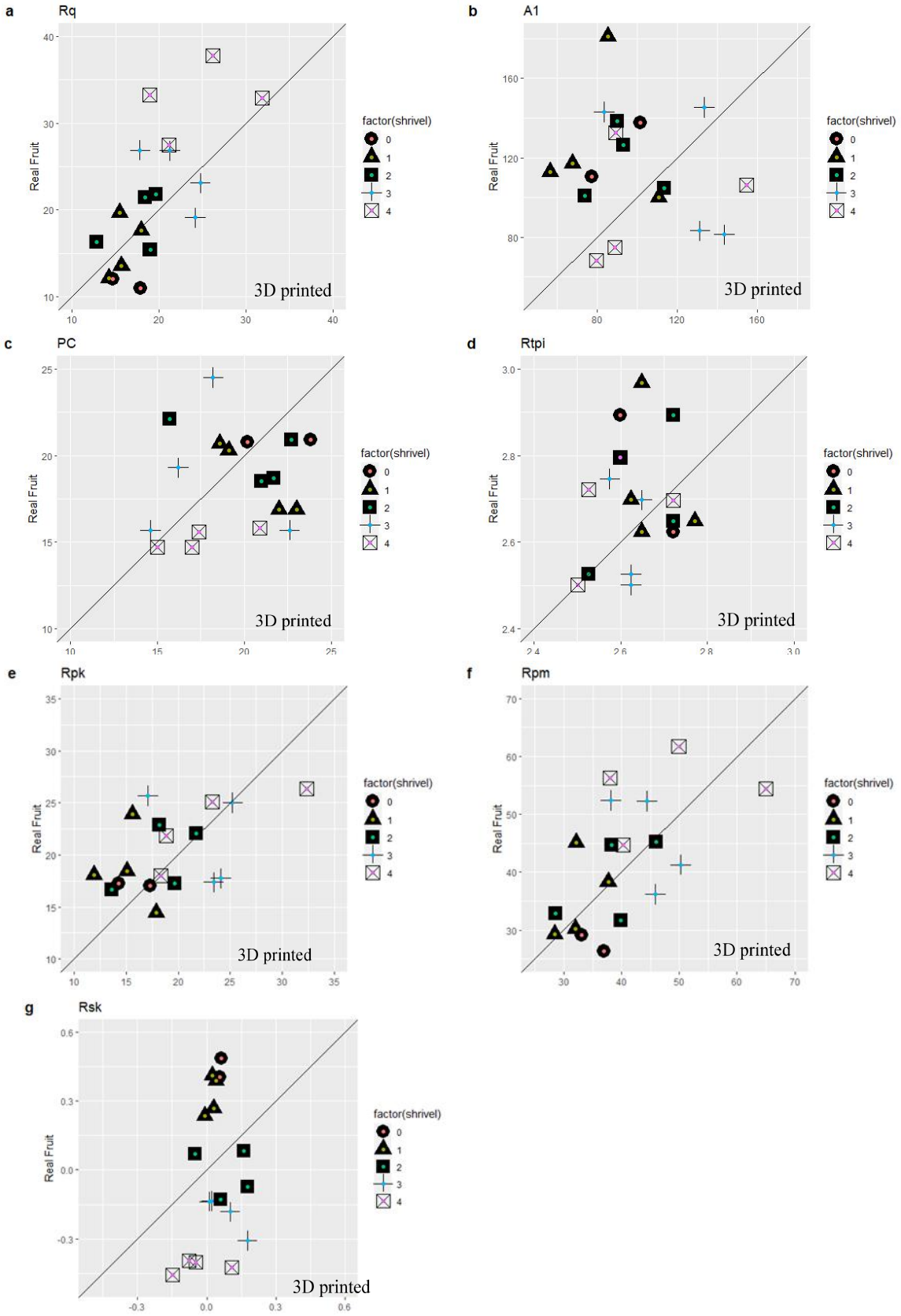

Figure 4.7. Scatter plots of parameters of kiwifruit in five shrivel categories in real and printed fruit.

4.4 Discussion

4.4.1 Reason for losing information in 3D fruit simulators (Resolution)

The objectives for this work were to attempt to produce a physical replicate 3D shrivel library for the kiwifruit industry and hence determine the current possibility of using physical simulators as aids for grading shrivel severity in the quality assurance system.

There was a lot of heterogeneity between stimulated fruit and real fruit in one of those characteristics, indicating that the data set didn't have adequate replication. The poor resolution of the 3D printer or 3D scanner, the high-temperature cleaning procedure, and light reflection during data collection utilising fringe projection for the 3D printed fruit might all contribute to this variation. Due to these circumstances, information on surface features were lost, especially for low shrivel severity. Furthermore, the substantial inaccuracies in the data might be explained by the fact that the 3D printed material has different surface properties (reflectivity, etc.) than real kiwifruit (Gorthi, Rastogi, 2010). Fringe projection uses white light scanning for collecting surface topography data. The transparent, plastic material reflects light and can cause the unaccounted surface topography identification (Gorthi, Rastogi, 2010).

High-quality watertight surface mesh for hiding the unaccounted data from the 3D scanning process can result in micro-topography structure loss. Also, the accuracy of the 3D scanner (EinScan-SE, Shing 3D Tech Co., Ltd, 2019) can only reach 0.1mm. Therefore, the data collection process was likely hindered by the resolution of the 3D scanner, leading to unaccounted small feature mapping. After obtaining the 3D printed fruit, the high-temperature cleaning process by Project EasyClean system in steam mode could potentially remove micro-scale surface data from the 3D fruit surface as a result of the cleaning process.

4.4.2 The application of 3D in the Horticulture industry

This study applied 3D technology to physically record kiwifruit shrivel topography. Shrivel symptoms change quickly and thus can be difficult to study. The 3D scanner brings shrivelled kiwifruit into the digital pipeline and captures the symptoms visibly online, which assists future study of fruit shrivel. The 3D printer reconstructed the digital 3D kiwifruit model to a physical object. These fruit simulators can potentially be used as references in quality system processes across an industry, around the world. However, in this experiment, the result was disadvantaged by the resolution of the scanner and printer, leading to a lower quality 3D mapping than expected, hence the ability to regenerate mild shrivel symptoms was reduced. However, this explanation cannot explain the phenomenon that some printed fruit match perfectly with their real fruit. Thus, without considering the accuracy and resolution issues, the printed kiwifruit would not be accurate enough to provide consistency in the data. In addition, since the scanner is light-based, the results may be skewed erratically by the specific angle at which the kiwifruit is reflecting the light at any given moment. This needs to be confirmed with a test. A reprint of the kiwifruit in a less reflective material or color may validate the reasons why the fruit simulators are so different to the real fruit.

Additionally, the 3D printed fruit cannot reflect the color of real fruit. The color of printed fruit is likely to influence the identification of shrivel from the observer. However, fruit with moderate, severe shrivels are clearly visible by naked eyes, therefore the printed fruit seems to be suitable to be used as visual aids to record the conditions of real fruit. Nevertheless, the cost of one printed fruit is also quite high at 200 NZD. The current shrivel severity scale was set up by visual observation of the researcher, which might not reflect general consumer perception or the industry quality standard. A more suitable scale needs to be further determined by sensory science to obtain more accurate categorization of shrivel symptoms in relation to consumers purchase decisions and/or industry grading thresholds.

4.5 Conclusion

This work demonstrates that 3D technology has the potential to be used as a technique to visualize and physically reproduce the micro topography of wrinkled skin symptoms that occur due to shrivel. However, accuracy of reproduction was not high. Amongst several skin parameters obtained from

skin topography using fringe projection, Rq, Rpk, Rpm and PC were found to be the significant indices to classify shrivel among severity categories. Using these parameters, surface profile of 3D printed fruit data matched well with real fruit. The quality of the 3D object is mainly determined by 3D scanner accuracy and 3D printing resolution. Also, in this experiment, the plastic material was applied in making the 3D object, which is transparent and tends to be reflective during the surface topography data collection process by fringe projection. More data collection needs to be carried out to reduce the large variability observed between fruit samples. A material which does not reflect light as much as the current material will be required to improve the accuracy of data capture using fringe projection.

In conclusion, more data collection needs to be done in the future to conclusively claim that printed models can be used as effective indications of shrivel symptoms from an analytical point of view.

Chapter 5. Discussion

5.1 Shrivel Symptoms

Shrivel symptom is a quality issue for the kiwifruit industry (Burden et al., 2014). For storage capability, there is inherent diversity across kiwifruit cultivars, orchard practice, harvest abilities, and so on. The variability results in difficulty to categorise different shrivel categories. This variability results in different shrivel propensities during storage. The kiwifruit industry relies on previous season information and at-harvest fruit quality measures to determine the possible storage time. Currently, subjective visual inspection was used in determining the variable shrivel performance before marketing. This research attempts to develop a mathematical descriptor to identify the shrivel severity of individual fruit based on quantitative analysis of surface roughness.

In this work, the fringe projection was used to capture the surface roughness characteristics of 'SunGold™' kiwifruit during shrivel development. The relationship between shrivel symptoms and surface parameter performance varies across kiwifruit cultivars. The size of lenticel tends to impact the expression of the surface parameters. As the general recommendations for actions to accurately measure the development of symptoms were that the evaluation of surface roughness changes based on shrivel development in a variety of kiwifruit cultivars, such as Red19, is in demand. Given that the shrivel level of *Actinidia deliciosa* var. *deliciosa* ('Hayward') is hardly measured by fringe projection due to its hair on the surface (Hallett & Sutherland, 2005), other technology which could need to be explored in the future.

Besides, East et al. (2016) demonstrated that fringe projection can be used in determining fruit surface qualification in other fruit, for example, apple, peach, banana, tomato, pear, orange, lemon, etc., some of which are susceptible to shrivel. No previous study has investigated the surface roughness response to shrivel among these fruit. Thus, the correlation between surface parameter and shrivel development possibly could be usefully explored in further research.

Identifying the threshold of shrivel occurrence using fringe projection is a potential technology to replace naked eyes for identifying shrivel incidence and severity in the fruit industry. $Rq < 13$, and $PC > 19$ was set up to be the threshold of shrivel occurrence in this research. To verify the accuracy of the threshold, sensory science needs to be done in the next step. Customer preference and tolerance to shrivel needs to be investigated for validating the shrivel classification in this research.

The advancement of non-destructive technology allows for the evaluation of individual fruit, the reduction of fruit waste, and the classification of fruit based on their unique features and characteristics. This allows for the creation of a subpopulation that may be targeted towards certain markets. Many packaging companies use non-destructive automated procedures in high-speed grading lines equipped with sensors in current grading systems (Nicola et al., 2014). Dielectric spectroscopy has been proposed as an improved approach for characterising kiwifruit quality indicators such as firmness, TSS, and pH during storage (Fazayeli et al., 2019). Lai et al. (2018) discovered that the fringe projection can assess shrivel development; the next step would be to determine the link between shrivel and kiwifruit maturity, quality, size or storability features for directly expressing fruit quality using the fringe projection.

5.2 Surface Parameter

The fringe projection has been used to measure and monitor changes on the surface due to changes in roughness profiles, such as dermatological tests on human skin in the last decade (Luebberding et al., 2014a; Luebberding et al., 2014b; Jaspers., 2006). Few previous studies have investigated fringe projection in the horticulture industry (East et al., 2016; Lai et al., 2018; Lai et al., 2019). In the research, the fringe projection was used to detect the surface parameter of kiwifruit during shrivel development. The vertical parameter (e.g. Rq as the representative), and wrinkle volume (e.g. PC) were considered as the most influential parameters in determining the shrivel appearance on the kiwifruit surface. It is encouraging to compare these parameters with that found by Luebberding et al. (2014a) who detect wrinkle depth (Overall average wrinkle depth, Average maximum wrinkle depth, Maximum largest wrinkle depth), percentage wrinkle area, and wrinkle volume to determine the skin wrinkle of humans, using fringe projection method (PRIMOS) method as similar as what we used in detecting kiwifruit skin topographic information.

5.3 Shrivel and Rate of Relative Weight Loss

Whilst many previous studies investigated the relationship between weight loss and shrivel, very little was found in the literature on the correlation between the rate of weight loss and shrivel. In this experiment, consistent with many studies of other crops, shrivel becomes apparent as the relative weight of kiwifruit diminishes. More importantly, the rate of relative weight loss declined with time for the fruit stored at normal temperature (20℃) with 45~55% RH, ambient, and the rate of fruit in the cool room (1℃, 70~80% RH) was consistently lower than in that normal temperature and 45~55%, which supports evidence from previous

observations on 'Gold 9' kiwifruit (Burdon et al., 2015). Nevertheless, the weight loss rate remained constant in cool storage in this research. Thus, cool storage can prolong the shelf life of fruit. As relative weight loss reached 6% for the cool stored fruit, most of the kiwifruit showed no shrivel. Meanwhile, fruit stored at normal temperature had severe shrivel with 6% relative weight loss. Thus, the absolute amount of relative weight loss cannot reflect the shrivel severity accurately. According to Burdon et al 2015, water status (free or bound water) fruit outer pericarp (OP) could be related to the rate of weight loss. The driving force that influences the rate of weight loss according to Fick's law of diffusion (Maguire et al., 2010). Its status that diffusion rate is proportional to both surface area and concentration difference, but inversely proportional to the membrane thickness. A cool temperature with relatively high RH% (70%, which is similar to kiwifruit internal water content) could maintain the water status stability compared with the normal temperature (50 RH %). The present study demonstrates that the rate of relative weight loss can influence shrivel severity in stored kiwifruit. To better understand the correlation between relative weight loss rate and shrivel development in kiwifruit, an observation on water status in the outer pericarp at variable weight loss rate is required.

5.4 3D Technology

Currently, the utilization of 3D technology is in its infancy. This experiment uses the naked eye to classify the shrivel categories initially. The 3D scanner (EinScan-SE, Shing 3D Tech Co., Ltd, 2019) was used to capture kiwifruit surface roughness at shrivel categories in this research. And a ProJet MJP 2500 Plus 3D printer (3D Systems, Rock Hill, SC, USA) reproduces the simulated fruit. In this research, fringe projection cannot demonstrate the excellent precision of fruit simulators reproduced by 3D scanning and printing technology. Nonetheless, the mistake was caused in significant part by the reflecting material. The 3D simulator accurately replicated the moderate and severe shrivel symptoms but difficult to identify slight shrivel from non-shrivel fruit when viewed with the naked eye. A material that results in a printed fruit that does not reflect light as much as the fruit which was printed is probably required. This may be the primary reason for the discrepancy. A test is required to validate this. A reproduction of the kiwifruit in a less reflective material or hue may confirm the reasons why the kiwifruit prints deviate so much from the actual kiwifruit.

Chapter 6. Conclusion

The main goal of the current study was to determine whether skin topography parameters detected by fringe projection can classify the shrivel categories and ascertain if 3D technology can accurately reproduce shrivelled kiwifruit at the micrometre level as a shrivel category.

The occurrence of shrivel defined by visual observation may be recognised using the structured light method, which offers microtopography information, according to this study. The structured light technique is useful in quantitatively describing shrivel objectively. This has the implication that fringe projection can be used to detect kiwifruit shrivel occurrences in place of manual visual inspection and can provide a quantification of fruit surface characteristics during postharvest storage. The findings will be of relevance to the kiwifruit industry for the development of a system to automatically filter sound kiwifruit for the market. In this study, a relative weight loss rate of 15.3 (mg/h) would preserve the 'SunGold^{TM}' kiwifruit surface quality, assuring non-shrivel occurrence after harvest. In this case, at approximately 80% possibility, a non-shrivelled kiwifruit could have an Rq value below 13 and a PC value above 19. The fact that this study only discovered the surface parameter of one kiwifruit cultivar, 'SunGold^{TM},' is a drawback. Other cultivars, such as Red19 and 'Gold9,' must be investigated in the future. Grower effects, such as fruit grown in different countries need to be investigated as well. More broadly, additional study is required to identify other quality indices that influence surface characteristics. Sensory science is conducted to determine the rate of relative water loss further.

This 3D scanning and printing technique is capable of reproducing 3D-printed kiwifruit in a range of shrivel categories but not accurately. This is the first attempt at merging fringe projection and 3D technology. The research suggests that reproducing the kiwifruit in a less reflective material may validate the reasons why the surface topography data from kiwifruit prints deviates so much from the genuine kiwifruit. Furthermore, because the current study is based on a limited sample size, the findings would require replication in the future. Using multiple surface roughness tests, possibly with a physical testing device. For example, Atomic Force Microscope (AFM), in addition to the light-based device, preparing multiple comparisons of kiwifruit with prints that are not reflective at all, comparing these with the control measuring technique, and then proceeding with an in-depth statistical analysis is the best course of action.

Reference

Bell, H. P. (1937). The protective layers of the apple. *Canadian Journal of Research*, *15*(8), 391-402.

Ben-Yehoshua, S., & Rodov, V. (2002). Transpiration and water stress. In *Postharvest physiology and pathology of vegetables* (pp. 143-197). CRC Press.

Ben-Yehoshua, S., Shapiro, B., Chen, Z. E., & Lurie, S. (1983). Mode of action of plastic film in extending life of lemon and bell pepper fruits by alleviation of water stress. *Plant physiology*, *73*(1), 87-93.

Berryman, F., Pynsent, P., Fairbank, J., & Disney, S. (2008). A new system for measuring three-dimensional back shape in scoliosis. *European Spine Journal*, *17*(5), 663-672.

Berardesca, E., Maibach, H. I., & Wilhelm, K. P. (Eds.). (2013). *Non invasive diagnostic techniques in clinical dermatology*. Springer Science & Business Media.

Blender Foundation. (2020). Blender 2.79 Reference Manual. Retrieved 18 March 2020, from https://docs.blender.org/manual/en/2.79/index.html.

Boyd, L., Barnett, A., Denny, J., Holmes, T., Ong, S., Sutherland, P., Minchin, P. (2011). Do some 'GOLD9' fruit shrivel more than others? *New Zealand Kiwifruit Journal, 210*, 9–15.

Burdon, J., Punter, M., Billing, D., Pidakala, P., & Kerr, K. (2014). Shrivel development in kiwifruit. *Postharvest biology and technology*, *87*, 1-5.

Burdon, J., Punter, M., Billing, D., Pidakala, P., & Kerr, K. (2015). Shrivel development in kiwifruit. *Acta Horticulturae, 1096*(2012), 309-312.

Burdon, J., & Clark, C. (2001). Effect of postharvest water loss on 'Hayward' kiwifruit water status. *Postharvest Biology and Technology*, *22*(3), 215-225.

Burton, W. G. (1982). *Post-harvest physiology of food crops*. Longman Group Ltd..

Creaform. (2015). An Introduction to 3D scanning ebook1. Retreived from http://www.slideshare.net/karikou2005/ebook1-an introductionto3dscanningen26082014

Celik, H. K., Rennie, A. E., & Akinci, I. (2011). Deformation behaviour simulation of an apple under drop case by finite element method. Journal of Food Engineering, 104(2), 293-298.

Chen, L. C., & Huang, C. C. (2005). Miniaturized 3D surface profilometer using digital fringe projection. *Measurement Science and Technology*, *16*(5), 1061.

Costa, G., Ferguson, R., Huang, H., & Testolin, R. (2017, September). Main changes in the kiwifruit industry since its introduction: present situation and future. In *IX International Symposium on Kiwifruit 1218* (pp. 1-16).

Diarte, C., Lai, P. H., Huang, H., Romero, A., Casero, T., Gatius, F., ... & Lara, I. (2019). Insights into olive fruit surface functions: a comparison of cuticular composition, water permeability, and surface topography in nine cultivars during maturation. Frontiers in plant science, 10, 1484.

Drummond, L. (2013). The composition and nutritional value of kiwifruit. *Advances in food and nutrition research*, *68*, 33-57.

East, A. R. (2011). Accelerated libraries to inform batch sale scheduling and reduce postharvest losses of seasonal fresh produce. *Biosystems engineering, 109*(1), 1-9.

East, A. R., Bloomfield, C., Trejo Araya, X., & Heyes, J. A. (2014, August). Evaluation of fringe projection as a method to provide information about horticultural product surfaces. In *XXIX International Horticultural Congress on Horticulture: Sustaining Lives, Livelihoods and Landscapes (IHC2014): 1119* (pp. 189-196).

East, A. R., Bloomfield, C., Trejo Araya, X., & Heyes, J. A. (2016). Evaluation of fringe projection as a method to provide information about horticultural product surfaces. *Acta Horticulturae, 1119*, 189-196.

FAOSTAT. 2020. Food and Agricultural Organisation of the United Nations. FAOSTAT statistical database. http://www.fao.org/faostat/en/#data/QCL

Fazayeli, A., Kamgar, S., Nassiri, S. M., Fazayeli, H., & De la Guardia, M. (2019). Dielectric spectroscopy as a potential technique for the prediction of kiwifruit quality indices during storage. *Information Processing in Agriculture, 6*(4), 479-486.

Feng, S., Zuo, C., Tao, T., Hu, Y., Zhang, M., Chen, Q., & Gu, G. (2018). Robust dynamic 3-d measurements with motion-compensated phase-shifting profilometry. *Optics and Lasers in Engineering, 103,* 127-138.

Ferguson, A. R. (2016). World economic importance. In *The Kiwifruit Genome* (pp. 37-42). Springer, Cham.

Gadelmawla, E. S., Koura, M. M., Maksoud, T. M., Elewa, I. M., & Soliman, H. H. (2002). Roughness parameters. *Journal of materials processing Technology*, *123*(1), 133-145.

Gaffney, J. J., Baird, C. D., & Chau, K. V. (1985). Influence of airflow rate, respiration, evaporative cooling, and other factors affecting weight loss calculations for fruits and vegetables. *ASHRAE transactions*, *91*(1), 690-707.

Gayed, A. A. N. A., Shaarawi, S. A. M. A., Elkhishen, M. A., & Elsherbini, N. R. M. (2017). Pre-harvest application of calcium chloride and chitosan on fruit quality and storability of 'Early Swelling'peach during cold storage. *Ciência e Agrotecnologia*, 41, 220-231.

Genovese, K., & Pappalettere, C. (2006). Whole 3D shape reconstruction of vascular segments under pressure via fringe projection techniques. *Optics and lasers in engineering*, *44*(12), 1311-1323.

Gorthi, S. S., & Rastogi, P. (2010). Fringe projection techniques: whither we are? *Optics and lasers in engineering, 48(*ARTICLE), 133-140.

Griffin, M. (2017, December 13). *Farmshelf: cost-effective custom parts for an urban farm system.* https://ultimaker.com/learn/farmshelf-cost-effective-custom-parts-for-an-urban-farm-system

Hallett, I. C., & Sutherland, P. W. (2005). Structure and development of kiwifruit skins. *International Journal of Plant Sciences*, *166*(5), 693-704.

Haleem, A., & Javaid, M. (2019). 3D scanning applications in medical field: a literature-based review. *Clinical Epidemiology and Global Health*, *7*(2), 199-210.

Hanafi, A., Gharbi, T., & Cornu, J. Y. (2005). In vivo measurement of lower back deformations with Fourier-transform profilometry. *Applied optics*, *44*(12), 2266-2273.

Hertog, M. L. A. T.., Ben-Arie, R., Róth, E., & Nicolaï, B. M. (2004). Humidity and temperature effects on invasive and non-invasive firmness measures. *Postharvest Biology and Technology, 33*(1), 79–91. https://doi.org/10.1016/j.postharvbio.2004.01.005

Hernandez, G., Craig, R., Tanner, D., & Rickett, P. (2012). Improving postharvest performance of 'Gold9'-curing and packaging. *New Zealand Kiwifruit Journal*, *214*(July/August), 20-23.

Holcroft, D. (2015). The Postharvest Education Foundation (PEF)Water Relations in Harvested Fresh Produce. *The Postharvest Education Foundation White Paper*, 15, 1-16.

Holloway, P. J. (1982). Structure and histochemistry of plant cuticular membranes: an overview. *The plant cuticle*.

New Zealand Horticulture. (2020). FreshFacts. https://www.freshfacts.co.nz/files/freshfacts-2020.pdf

Huang, H., Tunnicliffe, M., Shim, Y. M., & Bronlund, J. E. (2017, October). Model based development of fruit simulators. In *AIP Conference Proceedings* (Vol. 1896, No. 1, p. 150004). AIP Publishing LLC.

Keyence Corporation of America. (2012). Introduction to Surface Roughness Measurement, Keyence Corporation, New Jersey, USA

Jaspers, S. (2006). Fringe Projection for In Vivo Topometry. *Bioengineering of the skin: skin imaging and analysis, 137.*

Jaspers, S., Hopermann, H., Sauermann, G., Hoppe, U., Lunderstädt, R., & Ennen, J. (1999). Rapid in vivo measurement of the topography of human skin by active image triangulation using a digital micromirror device. *Skin Research and Technology*, *5*(3), 195-207.

Kaiser, H. F. (1960). The application of electronic computers to factor analysis. *Educational and psychological measurement*, *20*(1), 141-151.

Lai, Gwanpua, Bailey, Heyes & East. (2018). Skin topography changes during kiwifruit development. *Acta Horticulturae. 1218,* 427-433. http://doi. 10.17660/ActaHortic.2018.1218.59

Lai, P. H. L., Bailey, D., East, A., Gwanpua, S. G., & Heyes, J. (2019, May). Methodology of extracting microtopography of kiwifruit skin using fringe projection. In *2019 IEEE International Instrumentation and Measurement Technology Conference (I2MTC)* (pp. 1-5). IEEE.

Lendzian, K. J., & Kerstiens, G. (1991). Sorption and transport of gases and vapors in plant cuticles. *Reviews of environmental contamination and toxicology*, 65-128.

Lievendag, N. (2017). The beginners guide to 3D scanning & photogrammetry on a budget. *Retrieved from 3DScanExpert web site: https://3dscanexpert. com/beginnersguide-3d-scanning-photogrammetry*.

Lilley, F., Lalor, M. J., & Burton, D. R. (2000). Robust fringe analysis system for human body shape measurement. *Optical Engineering*, *39*(1), 187-195.

Li, Z. & Thomas, C. (2014). Quantitative evaluation of mechanical damage to fresh fruits. *Trends Food Sci. Technol. 35*, 138–150. https://doi.org/10.1016/j.tifs.2013.12.001.

López, D. Y., Martínez-García, A., & Gómez, Julián (2017). Apple quality study using fringe projection and colorimetry techniques. *Optik, 147*, 401-413.

Luebberding, S., Krueger, N., & Kerscher, M. (2014a). Quantification of age‐related facial wrinkles in men and women using a three‐dimensional fringe projection method and validated assessment scales. *Dermatologic Surgery, 40*(1), 22-32.

Luebberding, S., Krueger, N., & Kerscher, M. (2014b). Comparison of Validated Assessment Scales and 3D digital fringe projection method to assess lifetime development of wrinkles in men. *Skin Research and Technology, 20*(1), 30-36.

Lufu, R., Ambaw, A. & Opara, U. L. (2020). Water loss of fresh fruit: Influencing pre-harvest, harvest, and postharvest factors. *Scientia Horticulturae*, *272*. http://doi.10.1016/j.scienta.2020.109519

Lu, Y., Cohen, I., Zhou, X. S., & Tian, Q. (2007, September). Feature selection using principal feature analysis. In *Proceedings of the 15th ACM international conference on Multimedia* (pp. 301-304).

Martínez-García, A., & Gómez, J. (2017). Apple quality study using fringe projection and colorimetry techniques. *Optik, 147*, 401-413.

Martinez, A., Nguyen, D., Basson, M. S., Medina, J., Irschick, D. J., & Baeckens, S. (2021). Quantifying surface topography of biological systems from 3D scans. *Methods in Ecology and Evolution.*

Maguire, K. M., Banks, N. H., & Opara, L. U. (2001). Factors affecting weight loss of apples. *Horticultural reviews, 25*, 197-234.

Mazzaglia, A., Studholme, D. J., Taratufolo, M. C., Cai, R., Almeida, N. F., Goodman, T., ... & Balestra, G. M. (2012). Pseudomonas syringae pv. actinidiae (PSA) isolates from recent bacterial canker of kiwifruit outbreaks belong to the same genetic lineage. *PloS one, 7*(5), e36518.

Mekhalfi, M. L., Nicolò, C., Ianniello, I., Calamita, F., Goller, R., Barazzuol, M. & Melgani, F. (2020). Vision System for Automatic On-Tree Kiwifruit Counting and Yield Estimation. *Sensors. 20*(15), 4214. https://doi.org/10.3390/s20154214

Minchin, P., Snelgar, B. & Ong, S. (2013). Why do 'Gold9' fruit shrivel? *New Zealand Kiwifruit Journal, 217*, 38-42.

Mu, L., Liu, Y., Cui, Y., Liu, H., Chen, L., Fu, L., & Gejima, Y. (2017). Design of end-effector for kiwifruit harvesting robot experiment. In *2017 ASABE Annual International Meeting* (p. 1). American Society of Agricultural and Biological Engineers.

Mukama, M., Ambaw, A., & Opara, U. L. (2020). Advances in design and performance evaluation of fresh fruit ventilated distribution packaging: A review. F*ood Packaging and Shelf Life, 24*, 100472.

Nachimuthu, V. V., Robin, S., Sudhakar, D., Raveendran, M., Rajeswari, S., & Manonmani, S. (2014). Evaluation of rice genetic diversity and variability in a population panel by principal component analysis. *Indian journal of Science and Technology*, *7*(10), 1555-1562.

Ngo, T. D., Kashani, A., Imbalzano, G., Nguyen, K. T., & Hui, D. (2018). Additive manufacturing (3D printing): A review of materials, methods, applications and challenges. *Composites Part B: Engineering, 143,* 172-196.

Norhaimi, W. M. W., Sauli, Z., Aris, H., Retnasamy, V., Shahimin, M. M., & Vairavan, R. (2020, January). Fringe projection phase shift variance effects on breast height imaging. In *AIP Conference Proceedings* (Vol. 2203, No. 1, p. 020015). AIP Publishing LLC.

Olatunji, J. R., Redding, G. P., Rowe, C. L., & East, A. R. (2020). Reconstruction of kiwifruit fruit geometry using a CGAN trained on a synthetic dataset. *Computers and Electronics in Agriculture, 177*, 105699.

Park, H., Shah, C., & Shah, R. (2016). "An Enhanced Development of 3D Intra-Oral Scanner Using Fringe-Projection Technique for Dentistry." Proceedings of the ASME 2016 International Mechanical Engineering Congress and Exposition. Volume 2: Advanced Manufacturing. Phoenix, Arizona, USA. November 11–17, 2016. V002T02A036. ASME. https://doi-org.ezproxy.massey.ac.nz/10.1115/IMECE2016-66427

R Development Core Team. (2020). R: A language and environment for statistical computing. Vienna, Austria: R Foundation for Statistical Computing.

Rogge, S., Defraeye, T., Herremans, E., Verboven, P., & Nicolaï, B. M. (2015). A 3D contour based geometrical model generator for complex-shaped horticultural products. *Journal of Food Engineering, 157,* 24-32.

Rowe, S. H., & Welford, W. T. (1967). Surface topography of non-optical surfaces by projected interference fringes. *Nature*, *216*(5117), 786-787.

Russo, M., Ceccarelli, M., Corves, B., Hüsing, M., Lorenz, M., Cafolla, D., & Carbone, G. (2017). Design and test of a gripper prototype for horticulture products. *Robotics and Computer-Integrated Manufacturing*, *44*, 266-275.

Saltveit, M. E., & Morris, L. L. (1990). Overview on chilling injury of horticultural crops. *Chilling injury of horticultural crops*, *1*, 3-15.

Salvi, J., Pages, J. & Batlle, J. (2004). Pattern codification strategies in structured light systems. *Pattern Recognition,37*(4),827–49.

Salvi, J., Fernandez, S., Pribanic, T., & Llado, X. (2010). A state of the art in structured light patterns for surface profilometry. *Pattern recognition, 43*(8), 2666-2680.

Samara, A. M. (2005). Enhanced dynamic range fringe projection for micro-structure characterization. The University of North Carolina at Charlotte.

Santos, S., Soares, B., Leite, M., & Jacinto, J. (2017). Design and development of a customised knee positioning orthosis using low cost 3D printers. *Virtual and Physical Prototyping*, *12*(4), 322-332.

Serrano, M., Martínez‐Romero, D., Castillo, S., Guillén, F., & Valero, D. (2004). Effect of preharvest sprays containing calcium, magnesium and titanium on the quality of peaches and nectarines at harvest and during postharvest storage. *Journal of the Science of Food and Agriculture*, 84(11), 1270-1276.

Schroeder, C. A. & Fletcher, W. A. (1965). The Chinese Gooseberry (Actinidia Chinensis) in New Zealand. *Economic Botany, 21*(1), 81-92.

Shing 3D, (2019). 3D scanner user guide. Retrieved May 2020, from https://www.einscan.com/wp-content/uploads/2020/05/EinScan-SE-Guidebook.pdf.

Taglienti, A., Massantini, R., Botondi, R., Mencarelli, F., & Valentini, M. (2009). Postharvest structural changes of Hayward kiwifruit by means of magnetic resonance imaging spectroscopy. *Food Chemistry*, *114*(4), 1583-1589.

Tait, P. R., Rutherford, P., Driver, T., Li, X., Saunders, C. M., Dalziel, P. C., & Guenther, M. (2018). Consumer insights and willingness to pay for attributes: Kiwifruit in Shanghai, China. Lincoln University. AERU.

Talbot, M. T., & Baird, C. D. (1993). Psychrometrics and postharvest operations. *Circular (Florida Cooperative Extension Service) (USA). no. 1097.*

Tamás, J., Riczu, P., Nagy, G., Nagy, A., Jancsó, T., Nyéki, J., & Szabó, Z. (2011). Applicability of 3D laser scanning in precision horticulture. *International Journal of Horticultural Science*, *17*(4-5), 55-58.

Varotsis, A. B. (2021). *Introduction to FDM 3D printing*. https://www. hubs.com/knowledge-base/introduction-fdm-3d-printing

Vanneste, J. L. (2012). Pseudomonas syringae pv. actinidiae (Psa): a threat to the New Zealand and global kiwifruit industry. *New Zealand Journal of Crop and Horticultural Science, 40*(4), 265-267.

Villordon, A., Gregorie, J. C., & LaBonte, D. (2020). Direct measurement of sweetpotato surface area and volume using a low-cost 3D scanner for identification of shape features related to processing product recovery. *HortScience*, *55*(5), 722-728.

Wei, X., Xie, D., Mao, L., Xu, C., Luo, Z., Xia, M. & Lu, W. (2019). Excess water loss induced by simulated transport vibration in postharvest kiwifruit. *Scientia Horticulturae, 250*, 113-120.

Wyant, J. C., & Creath, K. (1992). Basic wavefront aberration theory for optical metrology. *Applied optics and optical engineering*, *11*(part 2), 28-39.

Xiao, S., Tao, W., & Zhao, H. (2015, December). A low-cost and portable realization on fringe projection three-dimensional measurement. In *MIPPR 2015: Pattern Recognition and Computer Vision* (Vol. 9813, p. 981304). International Society for Optics and Photonics.

Yin, Y., Wang, M., Gao, B. Z., Liu, X., & Peng, X. (2015). Fringe projection 3D microscopy with the general imaging model. *Optics express, 23*(5), 6846-6857.

Zhang, M., Liang, Y., & Chu, G. (2017). Applying silicate fertilizer increases both yield and quality of table grape (Vitis vinifera L.) grown on calcareous grey desert soil. *Scientia horticulturae*, *225*, 757-763.

Appendix. A PCA Factor Selection of Skin Line parameters

A.1. PC scores of the germplasm selected based on >1.0 each PCs

PCA (Principal Component Analysis) is widely used in feature reduction (Lu et al., 2007). In this section, PCA was used to classify the skin topography parameters (Fig.3.10). On the basis of the scree plot (Fig 3.11) and Table 4, PC1 loading was selected to perform the selected skin topography parameters with explanation of 60.8% of the total variation. In order to select the factors, Eigenvalue, Scree plot, total percent variance explained should be taken into account.

PCs with eigenvalues of at least 1.0 are accepted as the descriptor of the variance in a data set based on Kaiser rules (Kaiser, 1960). This is because an eigenvalue of 1 explains the same amount of variance as a single variable, and the reasoning is that only factors that explain at least the same amount of variance as a single variable are worth retaining. A cut-off of an eigenvalue of 1 would imply four factors. According to Appendix Table B.2, Eigenvalues of PC1 (19.46), PC2 (4.00), PC3 (1.42), PC4 (1.32), were higher than 1.0.

A.2. Scree Plot and Total Percent Variance Explained

The scree plot suggests either one or two factors due to the way the slope levels off twice. Also, after three PC tended to become straight with little variance seen in each PC, a curve line is produced. In comparison to the other 27 PCs, PC1 showed the most variance on the graph, followed by PC2 (Nachimuthu et al. 2014). Given that the reason for running the PCA is to reduce a large number of variables to describe a complex concept. Thus, a smaller number of factors would be selected. In this case, the curve that occurred PC1 that explains the maximum amount of variability in the data and should be selected (Fig. 3.11).

A.3. Explanation of Variances

The shrivel included in this investigation for PCA analysis on the 28 skin line topography traits, all the characters were estimated based on PC scores and presented in (see Appendix Table 1.) These scores can be utilized to propose precise selection indices whose intensity can be decided by

variability explained by each of the principal components. A high PC score for skin topography parameters in a particular component denotes high values for the variables in that parameter.

A.4. Grouping parameters

In PCA biplot, the angles between the vectors show how the characteristics correlate with one another. As two vectors are close, forming a small angle (less than 90°), the two variables they represent are positively correlated, and vice versa. The skin line parameters have been grouped by PCA from eight directions. In this section, the eight direction parameters would be described with the explanation and analysis of the influence of the parameters on shrivel categories. Rq Ra, Rz, Rt, Rc, Rmax, Rvm, Rvk, Rv, Rk, R3z, Rda, Rpm, Wt showed a small angle and thus was grouped. Similarly, Rku; A1; Rpk, Rp;Rpm, WL; S, Rtpi; WLR, PC; RI; M2, Rsk;Mr1 were grouped separately.

A.5. The importance of parameters in the direction in PCA

The detailed factor selection process is in Appendix A. The project values on each PC show the importance they have on that PC (the larger they are these absolute values, the more a specific variable contributes to that principal component). Therefore, in each group, a significant variance that has the most influential impact on shrivel was selected (Rq, WL, Rtpi, PC, Rsk, A1, Rp).

A.6. Relative weight loss and line parameters of skin topography

The correlation between the relative weight loss, shrivel and skin topography parameter is provided In Fig 3.11. As for the shrivel and skin line parameters, shrivel has a positively correlated with Rla, Rk, Rvm, Rsm, Rk, Wt, Rv, Rvk, Rp, Rpm, Rdq, Rda, Rt, Rmax, Rz, Rq, Rc, Ra, R3z, A2, Rtpi, but a negative correlation with Rpk, A1, Rku, Mr1, Rsk, Mr2, PC, Rl. Looking at the importance of the variables, Ra, Rq, Rmax, R3z, Rt, Rz, Rpm, Rv, Rvm, Rsm, Rda, Rdq, Rla, Rc, Wt, Rk, Rvk, A2 has a relatively high correlation with weight loss.

Appendix. B

Table B.1. List of contributing skin line parameters in this study.

S. No	Name of line parameters	Abb.	Explanation of the line parameters
1.	Average roughness vertical parameter	Ra	Ra is the mean of the absolute values of the profile heights of the roughness profile. Ra=$\frac{1}{lr}*\int_0^{lr} \|R(x)\|dx$
2.	Root mean square roughness vertical parameter	Rq	Rq is the Root mean square average of the profile heights of the roughness profile. Rq=$\sqrt{\frac{1}{lr}*\int_0^{lr} R^2(x)dx}$
3.	Maximum roughness depth vertical parameter	Rmax	Rmax is the largest height difference in a single measurement section (see Rz).
4.	Base roughness depth vertical parameter	R3z	The average of the single base roughness depths is R3z. The difference between the third highest profile peak and the third deepest profile valley within a single measurement segment is the single base roughness depth. This value is set to 0 if there are no three peaks or valleys in one of the single measurement portions.
5.	Maximum height of the roughness profile vertical parameter	Rt	Rt is the height difference between the highest point and the deepest valley in the whole measuring area.
6.	Average maximum height of the roughness vertical parameter	Rz	Rz is the mean of the individual roughness depths. The difference between the highest profile peak and the deepest profile valley within a single measurement segment is the single roughness depth.
7.	Height of the	Rp	Rp is the Height of the largest profile peak within the

	largest profile peak vertical parameter		total measurement section.
8.	Average height of the largest profile peaks vertical parameter	Rpm	Rpm is the average of the height profile peaks within the single measurement section.
9.	Depth of the largest profile valley vertical parameter	Rv	Rv is the depth of the largest profile valley within the total measurement section.
10.	Average depth of the profile valleys vertical parameter	Rvm	Rvm is the mathematics of the deepest profile valley inside each individual measurement distance divided by the total number of individual measurement distances.
11.	Skewness vertical parameter	Rsk	Rsk is a measure of the amplitude density curve's asymmetry. A surface with negative skewness has load bearing characteristics. Rsk=0 for normally distributed profile parameters. Rsk=$\frac{1}{Rq^3}$*[$\frac{1}{lr}$*$\int_0^{lr}$ $\|R^3(x)\|dx$]
12.	Kurtosis vertical parameter	Rku	Rku is a measure of the amplitude density curve's steepness. Rku=3 for normally distributed profile parameters. Higher values are associated with rougher roughness profiles. Rku=$\frac{1}{Rq^4}$*[$\frac{1}{lr}$*$\int_0^{lr}$ $\|R^4(x)\|dx$]
13.	Average spacing of the roughness profile elements (horizontal parameter)	Rsm	The average distance between the profile components Xs is denoted by Rsm. Rsm is calculated using the following counting thresholds: in the vertical direction, 1% of the total measurement section. Rsm=$\frac{1}{n}$ *$\sum_{i=1}^{n} Xsi$

14.	Average peak distance (horizontal parameter)	S	S denotes the centre distance between the roughness profile's profile peaks. Unless otherwise specified in the settings, the minimum height for a peak is set to 0. A horizontal counting threshold can also be configured in the options.
15.	Average slope of the roughness profile mixed parameter in the vertical and horizontal directions.	Rda	Rda is the arithmetic average of the local profile slopes. Rda=$\int\left\|\frac{dr}{dx}\right\|dx$
16.	Root mean square slope of the roughness profile mixed parameter	Rdq	Rdq is the Root mean square value of the local profile slopes. Rdq= $\sqrt{\int(\frac{dr}{dx})^2 dx}$
17.		Rla	Rla is derived from Rdq and is calculated from the below named formula. Rla=$2*\pi*(\frac{Rq}{Rdq})$
18.	Material part micro	Rtpi	This parameter is designed to be used with the reference plane and cut-depth settings. It is calculated using the roughness profile. The sectional plane at which the section begins is defined by the reference plane. If the bearing part ratio of the reference plane is 5%, then the height of this plane is also 5%. The cut-depth lowers the evaluation section plane by the specified amount below the reference plane.

			The material part micro is therefore the material part to total length ratio. This parameter is expressed as a percentage. For example, if the cut-depth is set to 0, Rpti will be equal to the value of the reference plane (save for rounding errors within point resolution (For example, if the profile includes just 100 points, the results will be accurate to 1%).
19.	Maximum height of waviness profile	Wt	Wt is the height of the greatest profile peak minus the depth of the largest profile valley in the waviness profile.
20.	Peak number	PC	PC is the number of peaks in the total measurement distance. A fixed height for PC, above 2% of Rz.
21.	Bearing part Mr1	Mr1	Mr1 is the percentage of the bearing portion that separates the projecting peaks from the core roughness profile. This parameter and the six that follow are derived from a roughness profile calculated in line with the filter method defined in DIN EN ISO 13565-1. This filtering method is used to eliminate grooves. More information on how to calculate this and the six following parameters is provided further below.
22.	Bearing part Mr2	Mr2	Mr2 is the bearing part in percent which separates the deep valleys from the core roughness profile.
23.	Core roughness depth	Rk	Rk is the depth of the core roughness profile.
24.	Reduced peak height	Rpk	Rpk is the average height of the protruding peaks above the protruding core roughness profile.
25.	Reduced valley depth	Rvk	Rvk is the average depth of the profile valleys below the core roughness profile.

26.	Material filled peak area	A1	The formula described below is used to compute A1. There is no resulting area according to the formula below—in order to acquire the area, the computed parameter must be multiplied by the entire measurement section. A1=$\frac{1}{2}$*Rpk*Mr1
27.	Empty valley area	A2	A2 is calculated using the formula shown below. According to the below shown formula, there is not yet a resultant area- in order to obtain the area, the calculated parameter must be multiplied by the total measurement section. A2=$\frac{1}{2}$*Rvk*(100-Mr2)

Table B.2. List of contributing skin surface parameters in this study.

S. No	Name of surface parameters	Abb.	Explanation of the surface parameters
1.	Arithmetic Roughness vertical parameter	Sa	Sa is the arithmetic mean of the surface roughness. Sa=$\frac{1}{nx*ny} * \sum_{i=1}^{nx} \sum_{j=1}^{ny} R(xi,yi)$
2.	Quadratic Roughness vertical parameter	Sq	The arithmetic mean of surface roughness is denoted by Sq. If more than one measuring surface is designated, Sq is the average of the separate measuring surfaces. Sq=$\sqrt{\frac{1}{nx*ny} * \sum_{i=1}^{nx} \sum_{j=1}^{ny} R^2\,(xi,yi)}$
3.	Maximum stretching of the roughness profile vertical parameter	Smax	On the whole measuring field, this is the height difference between the highest peak and the lowest valley.
4.	Ten-point height vertical parameter	Sz	Sz is the mean of the 5 highest peaks and 5 deepest valleys from the entire measuring field. Sz =

			$\frac{\sum_{i=1}^{5}\lvert Rpi\rvert+\sum_{i=1}^{5}\lvert Rvi\rvert}{10}$
5.	Greatest roughness depth of the single measuring field vertical parameter.	St	The biggest height difference in a single measurement field is denoted by St. If the number of the single measurement field is equal to one. then St=Stm=Smax.
6	Averaged roughness depth of the single measuring fields (vertical parameter)	Stm	The difference between maximum and minimum is produced for each individual measurement surface using the Stm computation. These are totalled and then divided by the number of individual measurement surfaces.
7.	Height of the greatest profile peak vertical parameter	Sp	Sp is the height of the greatest profile peak in the entire measuring field.
8.	Mean of the height of the profile peak vertical parameter	Spm	Spm is the arithmetic mean of the highest profile peak inside a single measurement field multiplied by the number of single measuring fields.
9.	Depth of the greatest profile valley vertical parameter	Sv	Sv is the depth of the greatest profile valley within the entire measuring field.
10.	Mean of the depths of the profile valleys vertical parameter	Svm	Svm is the arithmetic mean of the deepest profile valley within a single measurement field multiplied by the number of single measuring fields.
11.	Skewness (vertical parameter)	Ssk	Ssk is a measure of the amplitude density curve's asymmetry. A surface with a negative skewness has a favourable carrying behaviour. For a typical profile value dispersion, Ssk=0.

			Ssk=$\frac{1}{nx*ny*Sq^3}$*$\sum_{i=1}^{nx}\sum_{j=1}^{ny} R^3\,(xi,yj)$
12.	Slope (vertical parameter)	Sku	Sku is a measure for the sloe of the amplitude density curve. For a normal dispersion of profile values, Sku=3.Sku=$\frac{1}{nx*ny*Sq^4}$*$\sum_{i=1}^{nx}\sum_{j=1}^{ny} R^4\,(xi,yj)$
13.	Middle distance of the profile peaks horizontal parameter	S	S denotes the middle distance between the roughness profile's profile peaks. The number 0 represents the minimum height for a peak. A horizontal counting threshold may still be configured in the settings.
14.	Arithmetic mean o the profile slope of the roughness profile mixed parameter	Sda	Sda is the arithmetic mean of the local profile slope in x- and y-direction.
15.	Quadratic mean of the profile slope of the roughness profile mixed parameter	Sdq	Sdq is the quadratic mean of the local profile in x-and y-direction.
16.		Sla	Sla is derived from sda and is calculated through the below formula. Sla=2*π*($\frac{Sa}{Sda}$)
17.	Number of peaks	PC	Pc is the total number of peaks in the measurement route. There is a setting parameter available for this parameter, which is given in the text under the description of the window elements further above.
18.	Surface surplus of the curved surface	Sdr	Sdr is the surplus of the curved surface to the even evaluation surface. This value is given in percent.

	vertical parameter		Sdr=$\frac{Ao-Ae}{Ae} * 100\%$
19.	Depth of the roughness core	Sk	Sk is the height difference between the material portions M1 and M2.
20.	Reduced peak height	Spk	Spk is the height of the projecting peaks in the centre of the material section M1.
21.	Reduced scoring depth	Svk	Svk is the middle depth of the valleys which lie under the material portion M2.
22.	Material-filled peak surface	V1	V1 is computed using the formula below. The formula alone does not generate a surface. To obtain a surface, multiply the computed value by the total measurement field. V1=$\frac{1}{2}$*Rpk*Mr1
23.	Empty valley area	V2	V2 is computed using the formula below. The formula alone does not generate a surface. To obtain a surface, multiply the computed value by the total measurement surface.

Appendix. C

Table C.1. Rotated Component Matrix[a] of Line Parameters

	1	2	3	4	5
Rq	.962				
Rc	.961				
Rz	.958				
Rt	.954				
Ra	.954				
Rmax	.948				
Rvm	.947				
Rvk	.941				
Rv	.939				
Wt	.932				
A2	.927				
Rk	.909				
R3z	.893			.332	
Rla	.890		-.406		
Rpm	.876			.339	
Rsm	.853		-.347		
PC	-.820		.482		
Rdq	.810			.530	
Rda	.800			.548	
Mr2	-.761	.330			
Rp	.745	.433		.323	
Rsk	-.672	.669			
WL	.592	-.302	-.397		-.364
A1		.944			
Rpk		.862			
Mr1	-.550	.702			
Rku		.404	.752		

Rtpi			-.420		
Rl				-.566	
S					.847
WLR		-.306			.582
weight	-.322				.357

Extraction Method: Principal Component Analysis.

Rotation Method: Varimax with Kaiser Normalization.

Rotation converged in 24 iterations.

Suppress small coefficients option with the Absolute value below".3".

Table C.2.Total Variance Explained of Line Parameters

Total Variance Explained

Component	Initial Eigenvalues			Extraction Sums of Squared Loadings			Rotation Sums of Squared Loadings		
	Total	% of Variance	Cumulative %	Total	% of Variance	Cumulative %	Total	% of Variance	Cumulative %
1	18.898	65.166	65.166	18.898	65.166	65.166	17.526	60.433	60.433
2	3.724	12.840	78.006	3.724	12.840	78.006	3.530	12.173	72.606
3	1.399	4.823	82.829	1.399	4.823	82.829	2.418	8.339	80.945
4	1.041	3.590	86.420	1.041	3.590	86.420	1.588	5.475	86.420
5	.930	3.206	89.625						
6	.827	2.852	92.477						
7	.781	2.695	95.172						
8	.361	1.245	96.417						
9	.300	1.033	97.450						
10	.176	.606	98.056						
11	.130	.447	98.504						
12	.115	.398	98.901						
13	.078	.268	99.169						
14	.069	.237	99.406						
15	.047	.163	99.570						
16	.041	.143	99.712						
17	.031	.108	99.820						
18	.013	.045	99.865						
19	.008	.029	99.894						
20	.008	.028	99.922						
21	.007	.023	99.944						
22	.005	.016	99.960						
23	.004	.015	99.975						
24	.003	.011	99.986						
25	.002	.009	99.994						
26	.001	.005	99.999						
27	.000	.001	100.000						
28	2.038E-9	7.027E-9	100.000						
29	1.347E-9	4.644E-9	100.000						

Extraction Method: Principal Component Analysis.

Table C.3. Component Transformation Matrix of line parameters

Component	1	2	3	4	5
1	.969	-.105	-.093	.204	-.005
2	.105	.892	.391	.134	-.150
3	.022	.439	-.816	-.240	.288
4	.001	.007	.291	.154	.944
5	.223	-.007	.296	-.927	.060

Extraction Method: Principal Component Analysis.

Rotation Method: Varimax with Kaiser Normalization.

Table C.4. Correlation Matrix of line parameter

Correlation Matrix[a]

		Ra	Rl	Rq	Rmax	R3z	Rt	Rz	Rp	Rpm	Rv	Rvm	Rsk	Rku	Rsm	S	Rda	Rdq	Rla	Rc	Rlpi	Wt	PC	Mr1	Mr2	Rk	Rpk	Rvk	A1	A2
Correlation	Ra	1.000	-.371	.998	.941	.962	.949	.988	.729	.906	.940	.975	-.707	-.324	.796	.201	.895	.887	.882	.992	-.128	.898	-.826	-.587	-.675	.981	.211	.913	-.157	.880
	Rl	-.371	1.000	-.370	-.352	-.355	-.351	-.370	-.290	-.351	-.336	-.357	.235	.141	-.292	-.054	-.366	-.362	-.297	-.375	.042	-.277	.292	.184	.200	-.360	-.088	-.313	.026	-.299
	Rq	.998	-.370	1.000	.953	.958	.960	.994	.748	.917	.946	.977	-.694	-.279	.795	.193	.900	.895	.873	.994	-.141	.900	-.815	-.573	-.683	.973	.237	.921	-.133	.890
	Rmax	.941	-.352	.953	1.000	.899	.996	.967	.838	.915	.947	.937	-.614	-.108	.725	.163	.888	.908	.773	.953	-.213	.859	-.715	-.513	-.666	.890	.327	.923	-.052	.890
	R3z	.962	-.355	.958	.899	1.000	.907	.953	.702	.877	.897	.938	-.700	-.357	.720	.192	.914	.900	.807	.954	-.112	.837	-.774	-.585	-.634	.955	.168	.853	-.187	.815
	Rt	.949	-.351	.960	.996	.907	1.000	.974	.837	.919	.954	.946	-.627	-.106	.731	.160	.894	.912	.781	.960	-.211	.868	-.722	-.526	-.672	.900	.320	.927	-.065	.894
	Rz	.988	-.370	.994	.967	.953	.974	1.000	.780	.935	.948	.976	-.673	-.204	.762	.178	.924	.924	.828	.992	-.166	.882	-.774	-.561	-.682	.956	.267	.919	-.111	.888
	Rp	.729	-.290	.748	.838	.702	.837	.780	1.000	.911	.633	.650	-.190	.162	.551	.077	.757	.804	.551	.754	-.335	.627	-.530	-.182	-.399	.671	.672	.605	.340	.571
	Rpm	.906	-.351	.917	.915	.877	.919	.935	.911	1.000	.798	.836	-.392	-.040	.702	.135	.887	.903	.738	.918	-.245	.779	-.710	-.330	-.516	.865	.537	.759	.186	.718
	Rv	.940	-.336	.946	.947	.897	.954	.948	.633	.798	1.000	.979	-.782	-.239	.730	.184	.848	.847	.802	.943	-.114	.882	-.729	-.644	-.731	.904	.083	.978	-.278	.950
	Rvm	.975	-.357	.977	.937	.938	.946	.976	.650	.836	.979	1.000	-.804	-.291	.750	.193	.887	.877	.830	.974	-.106	.890	-.764	-.667	-.740	.951	.084	.959	-.287	.936
	Rsk	-.707	.235	-.694	-.614	-.700	-.627	-.673	-.190	-.392	-.782	-.804	1.000	.543	-.521	-.173	-.605	-.564	-.638	-.687	-.065	-.673	.568	.847	.721	-.735	.398	-.775	.698	-.771
	Rku	-.324	.141	-.279	-.108	-.357	-.106	-.204	.162	-.040	-.239	-.291	.543	1.000	-.275	-.150	-.198	-.125	-.420	-.259	.221	-.259	.436	.442	.135	-.424	.432	-.193	.497	-.153
	Rsm	.796	-.292	.795	.725	.720	.731	.762	.551	.702	.730	.750	-.521	-.275	1.000	.184	.512	.517	.927	.808	-.097	.841	-.895	-.391	-.574	.781	.226	.742	-.039	.723
	S	.201	-.054	.193	.163	.192	.160	.178	.077	.135	.184	.193	-.173	-.150	.184	1.000	.132	.137	.224	.194	.043	.174	-.227	-.172	-.114	.212	-.084	.181	-.136	.173
	Rda	.895	-.366	.900	.888	.914	.894	.924	.757	.887	.848	.887	-.605	-.198	.512	.132	1.000	.991	.591	.900	-.168	.713	-.561	-.520	-.553	.875	.247	.789	-.106	.748
	Rdq	.887	-.362	.895	.908	.900	.912	.924	.804	.903	.847	.877	-.564	-.125	.517	.137	.991	1.000	.581	.899	-.187	.712	-.551	-.484	-.552	.854	.295	.795	-.058	.758
	Rla	.882	-.297	.873	.773	.807	.781	.828	.551	.738	.802	.830	-.638	-.420	.927	.224	.591	.581	1.000	.859	-.054	.877	-.945	-.508	-.628	.878	.160	.801	-.140	.775
	Rc	.992	-.375	.994	.953	.954	.960	.992	.754	.918	.943	.974	-.687	-.359	.808	.194	.900	.899	.859	1.000	-.149	.894	-.811	-.570	-.679	.966	.232	.919	-.136	.890
	Rlpi	-.128	.042	-.141	-.213	-.112	-.211	-.166	-.335	-.245	-.114	-.106	-.065	-.221	-.097	.043	-.168	-.187	-.054	-.149	1.000	-.125	.048	-.016	.084	-.098	-.326	-.116	-.210	-.112
	Wt	.898	-.277	.900	.859	.837	.868	.882	.627	.779	.882	.890	-.673	-.259	.841	.174	.713	.712	.877	.894	-.125	1.000	-.795	-.556	-.684	.880	.177	.890	-.170	.870
	PC	-.826	.292	-.815	-.715	-.774	-.722	-.774	-.530	-.710	-.729	-.764	.568	.436	-.895	-.227	-.561	-.551	-.945	-.811	.048	-.795	1.000	.455	.500	-.834	-.152	-.710	.117	-.627
	Mr1	-.587	.184	-.573	-.513	-.585	-.526	-.561	-.182	-.330	-.644	-.667	.847	.442	-.391	-.172	-.520	-.484	-.508	-.570	.016	-.556	.455	1.000	.577	-.658	.397	-.635	.784	-.627
	Mr2	-.675	.200	-.683	-.666	-.634	-.672	-.682	-.399	-.516	-.731	-.740	.721	.135	-.574	-.114	-.553	-.552	-.628	-.679	.084	-.684	.500	.577	1.000	-.612	.006	-.770	.302	-.832
	Rk	.981	-.360	.973	.890	.955	.900	.956	.671	.865	.904	.951	-.735	-.424	.781	.212	.875	.854	.878	.966	-.098	.880	-.834	-.658	-.612	1.000	.128	.863	-.250	.817
	Rpk	.211	-.088	.237	.327	.168	.320	.267	.672	.537	.083	.084	.398	.432	.226	-.084	.247	.295	.160	.232	-.326	.177	-.152	.397	.006	.128	1.000	.067	.864	.046
	Rvk	.913	-.313	.921	.923	.853	.927	.919	.605	.759	.978	.959	-.775	-.193	.742	.181	.789	.795	.801	.919	-.116	.890	-.710	-.635	-.770	.863	.067	1.000	-.284	.985
	A1	-.157	.026	-.133	-.052	-.187	-.065	-.111	.340	.186	-.278	-.287	.698	.497	-.039	-.136	-.106	-.058	-.140	-.136	-.210	-.170	.117	.784	.302	-.250	.864	-.284	1.000	-.294
	A2	.880	-.299	.890	.890	.815	.894	.888	.571	.718	.950	.936	-.771	-.153	.723	.173	.748	.758	.775	.890	-.112	.870	-.672	-.627	-.832	.817	.046	.985	-.294	1.000

a. This matrix is not positive definite.

Table C.5. Rotated Component Matrix[a] of surface Parameters

	Component				
	1	2	3	4	5
Sc	.956	.153			.104
Sa	.954	.132	.147		
Sk	.950	.120	.152		
Sq	.933	.215	.208		
Svk	.899	.275	-.103		.147
V2	.899	.275	-.103		.147
Sda	.814	.224	.119	.205	.167
Sdr	.745	.448	.133	.201	.165
Sla	.455		.154		-.119
Sku	-.142	.935			-.144
St	.290	.833	.235	.211	.316
Stm	.290	.833	.235	.211	.316
Sv	-.482	-.818			-.141
Svm	-.482	-.818			-.141
Ssk	-.415	-.815	.328		
Sdq	.603	.695		.121	.155
Sp		.501	.485	.452	.382
Spm		.500	.483	.451	.385
V1	.213		.927		
Spk	.213		.927		
S			.122	-.930	
PC				.928	
Smax					.880
Sz	.497	.223			.721

Extraction Method: Principal Component Analysis.

Rotation Method: Varimax with Kaiser Normalization.

a. Rotation converged in 8 iterations.

Table C. 6. Component Transformation Matrix of surface parameters

Component	1	2	3	4	5
1	.762	.573	.153	.098	.240
2	-.602	.569	.187	.468	.245
3	.089	-.475	.806	.244	.239
4	-.195	.330	.497	-.759	-.174
5	-.102	-.118	-.211	-.369	.892

Extraction Method: Principal Component Analysis.

Rotation Method: Varimax with Kaiser Normalization.

Appendix. D

The development of Kiwifruit skin topography parameter (Ra, Rl, Rq, Rmax, R3z, Rt, Rz, Rp, Rpm, Rv, Rvm, Rsk, Rku, Rsm, S, Rda, Rdq, Rla, Rc, Rtpi, Wt, PC, Mr1, Mr2, Rk, Rpk, Rvk, A1, A2) in three treatments (lab at 20℃, 52.9% RH; cabinet at 20℃, 47.4% RH; TCR at 1℃, 79.5% RH).

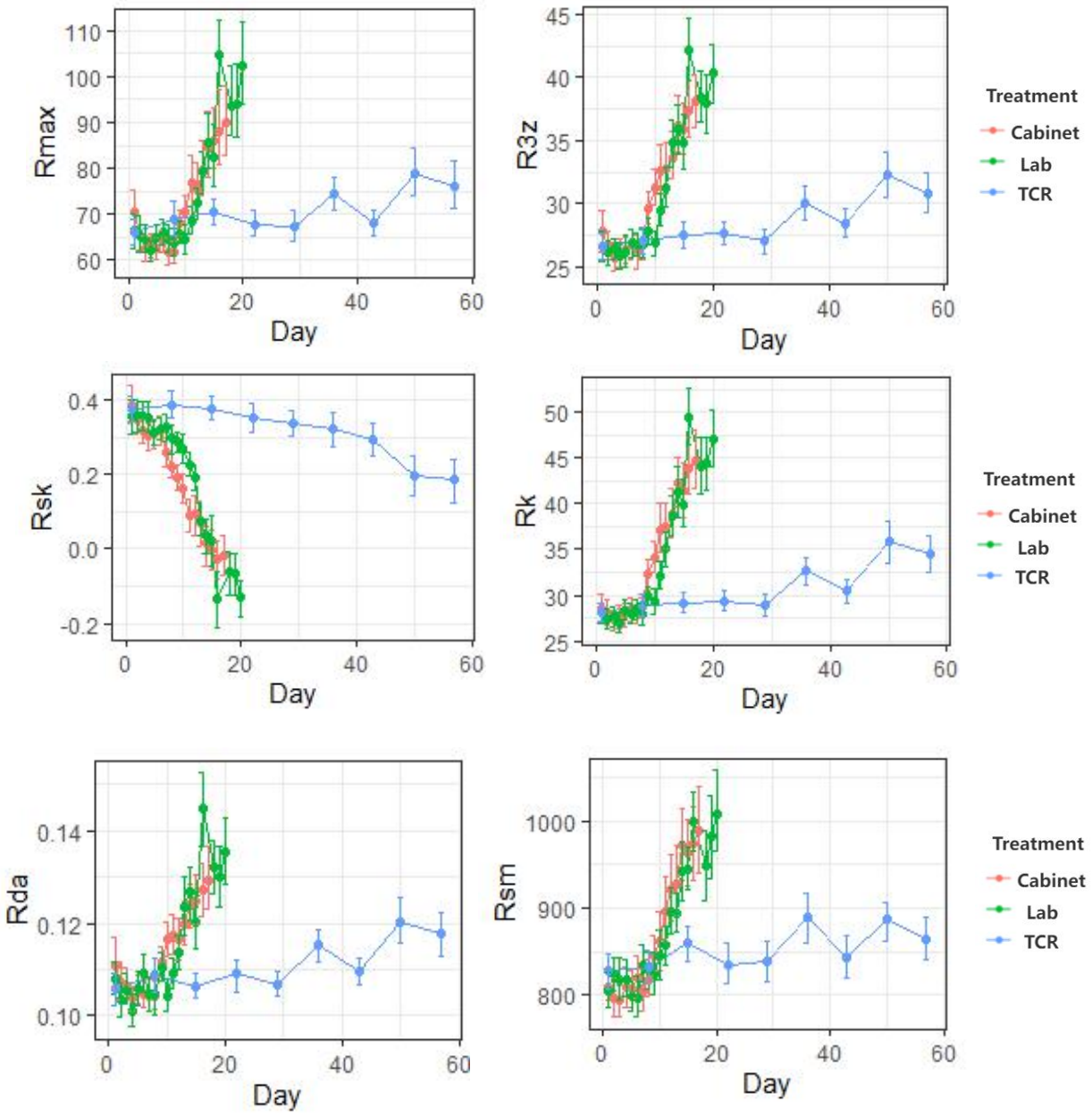

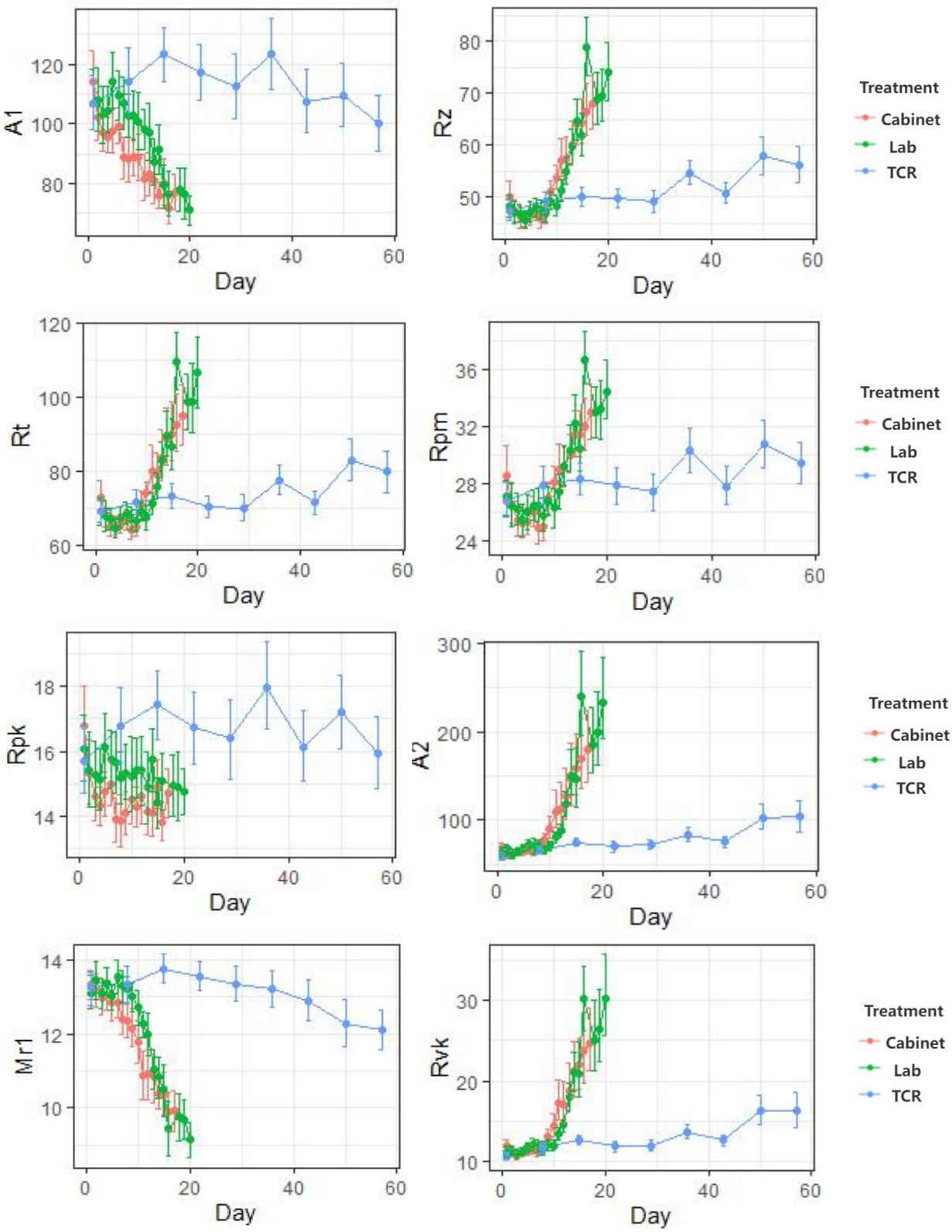
A1
Rz
Rt
Rpm
Rpk
A2
Mr1
Rvk
Day
Treatment
Cabinet
Lab
TCR

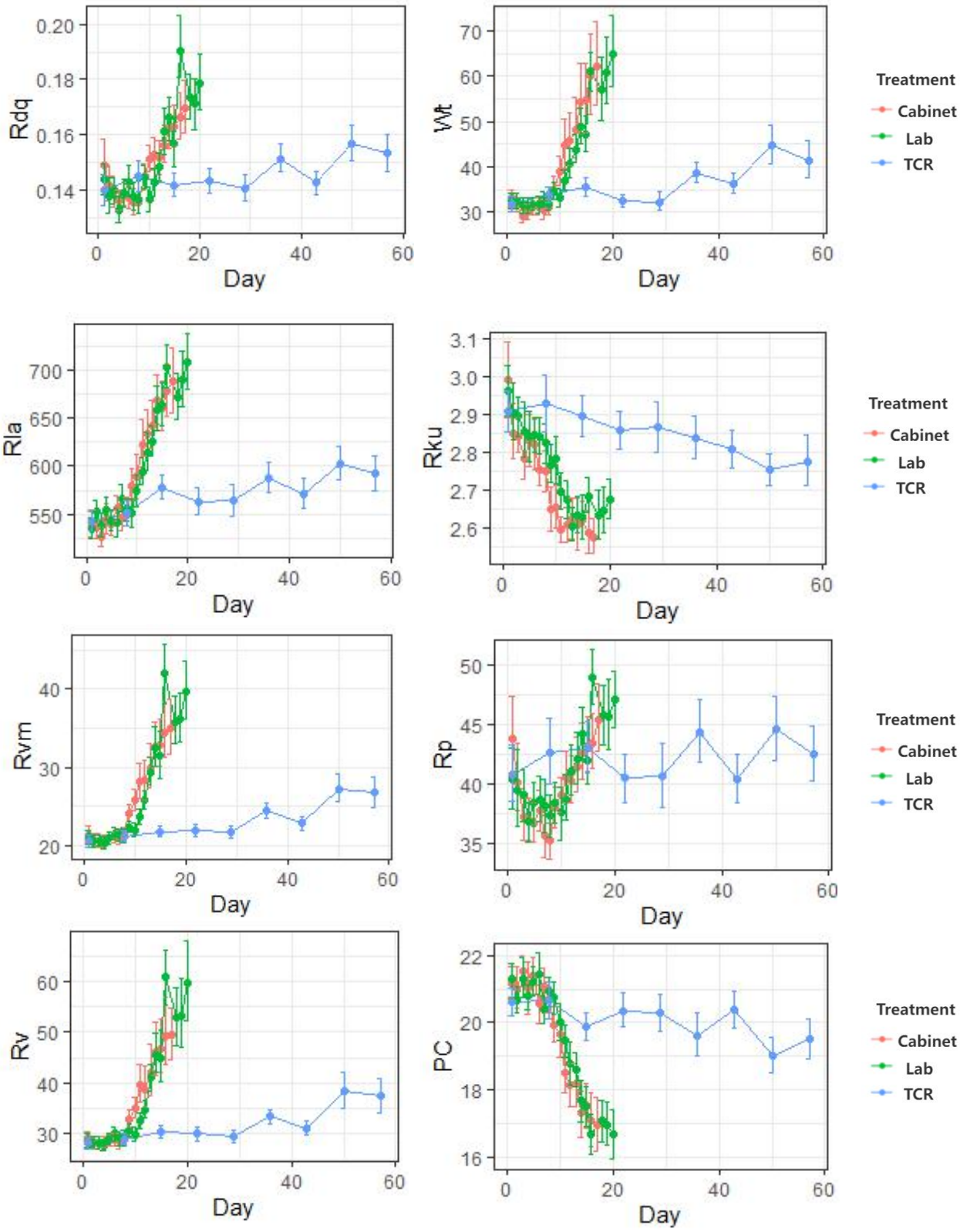
Rdq
Wt
Rla
Rku
Rvm
Rp
Rv
PC
Day
Treatment
Cabinet
Lab
TCR

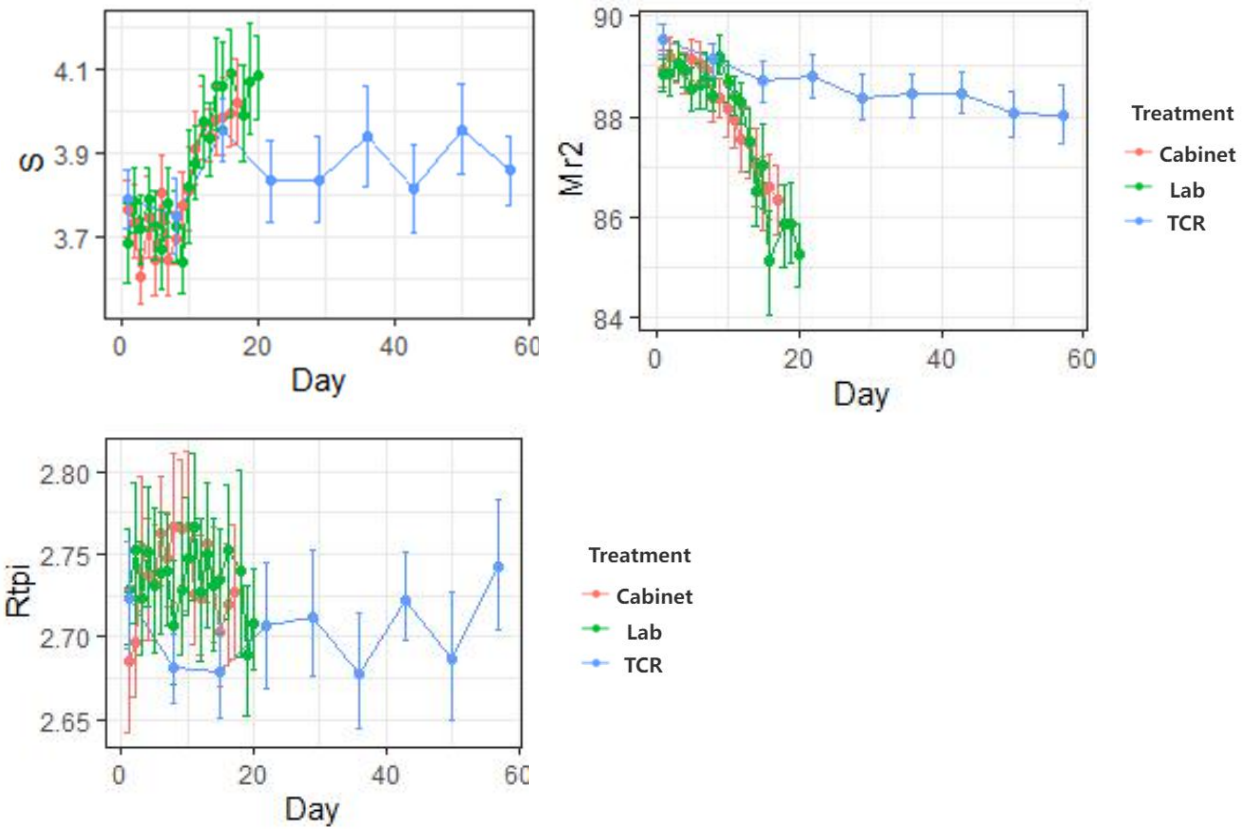
S
4.1
3.9
3.7
0
20
40
60
Day
Mr2
90
88
86
84
0
20
40
60
Day
Treatment
Cabinet
Lab
TCR
Rtpi
2.80
2.75
2.70
2.65
0
20
40
60
Day
Treatment
Cabinet
Lab
TCR

Appendix. E

The correlation of Kiwifruit skin topography parameter (Ra, Rl, Rq, Rmax, R3z, Rt, Rz, Rp, Rpm, Rv, Rvm, Rsk, Rku, Rsm, S, Rda, Rdq, Rla, Rc, Rtpi, Wt, PC, Mr1, Mr2, Rk, Rpk, Rvk, A1, A2) and Relative weight loss % in three treatments (lab at 20℃, 52.9% RH; cabinet at 20℃, 47.4% RH; TCR at 1℃, 79.5% RH).

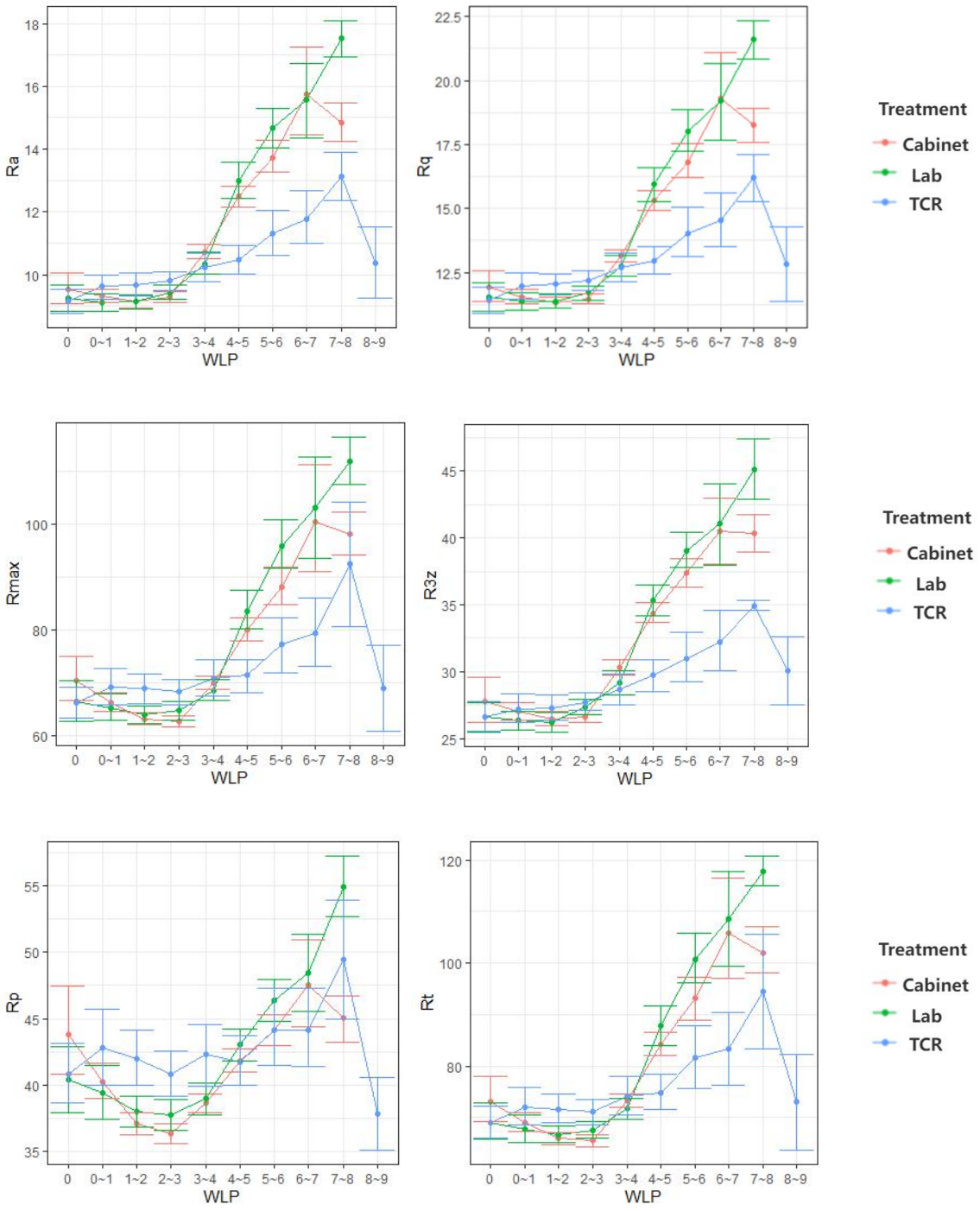

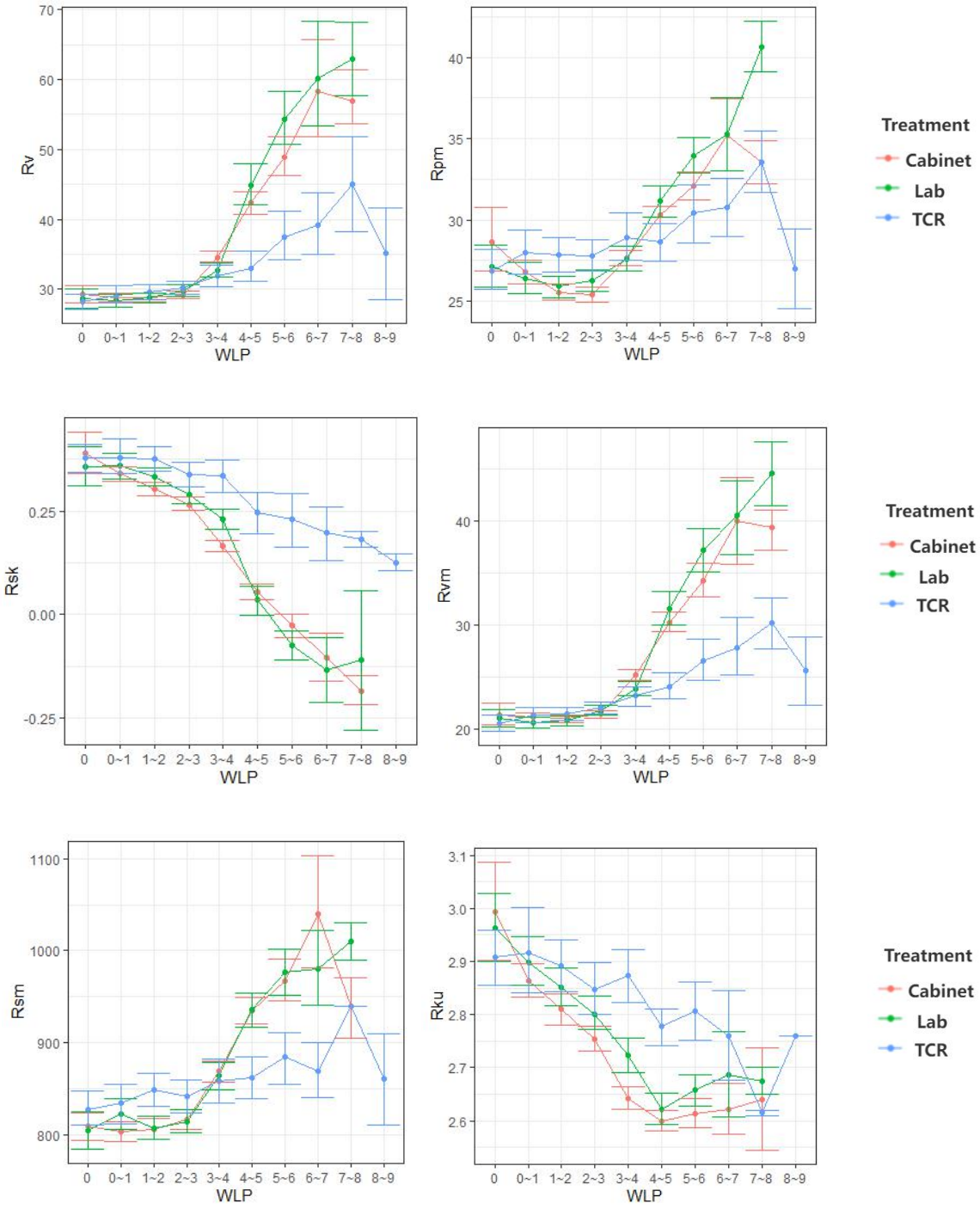
Rv
Rpm
Rsk
Rvm
Rsm
Rku
WLP
0
0~1
1~2
2~3
3~4
4~5
5~6
6~7
7~8
8~9
Treatment
Cabinet
Lab
TCR

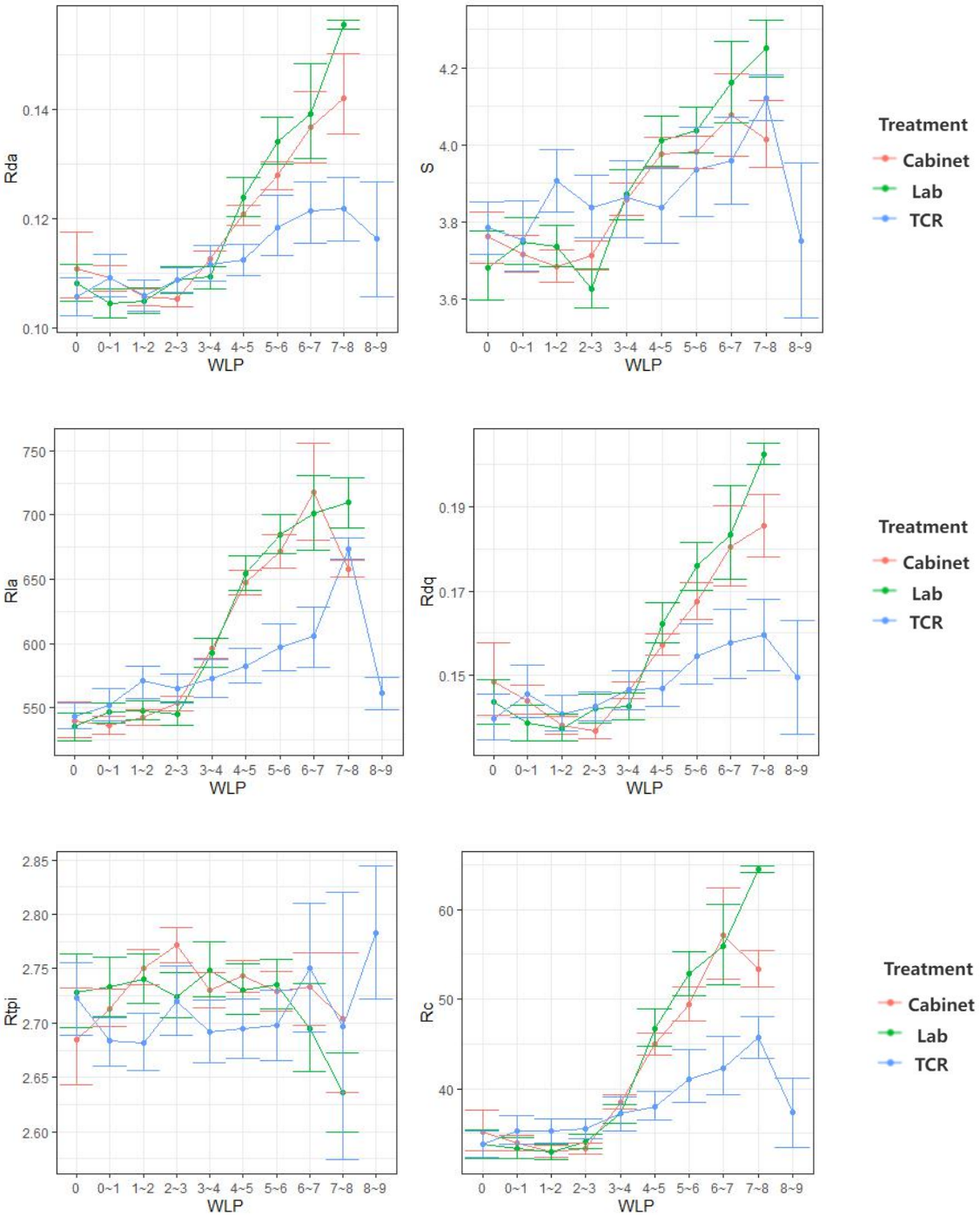
Rda
0.14
0.12
0.10
S
4.2
4.0
3.8
3.6
Rla
750
700
650
600
550
Rdq
0.19
0.17
0.15
Rtpi
2.85
2.80
2.75
2.70
2.65
2.60
Rc
60
50
40
0 0~1 1~2 2~3 3~4 4~5 5~6 6~7 7~8 8~9
WLP
Treatment
Cabinet
Lab
TCR

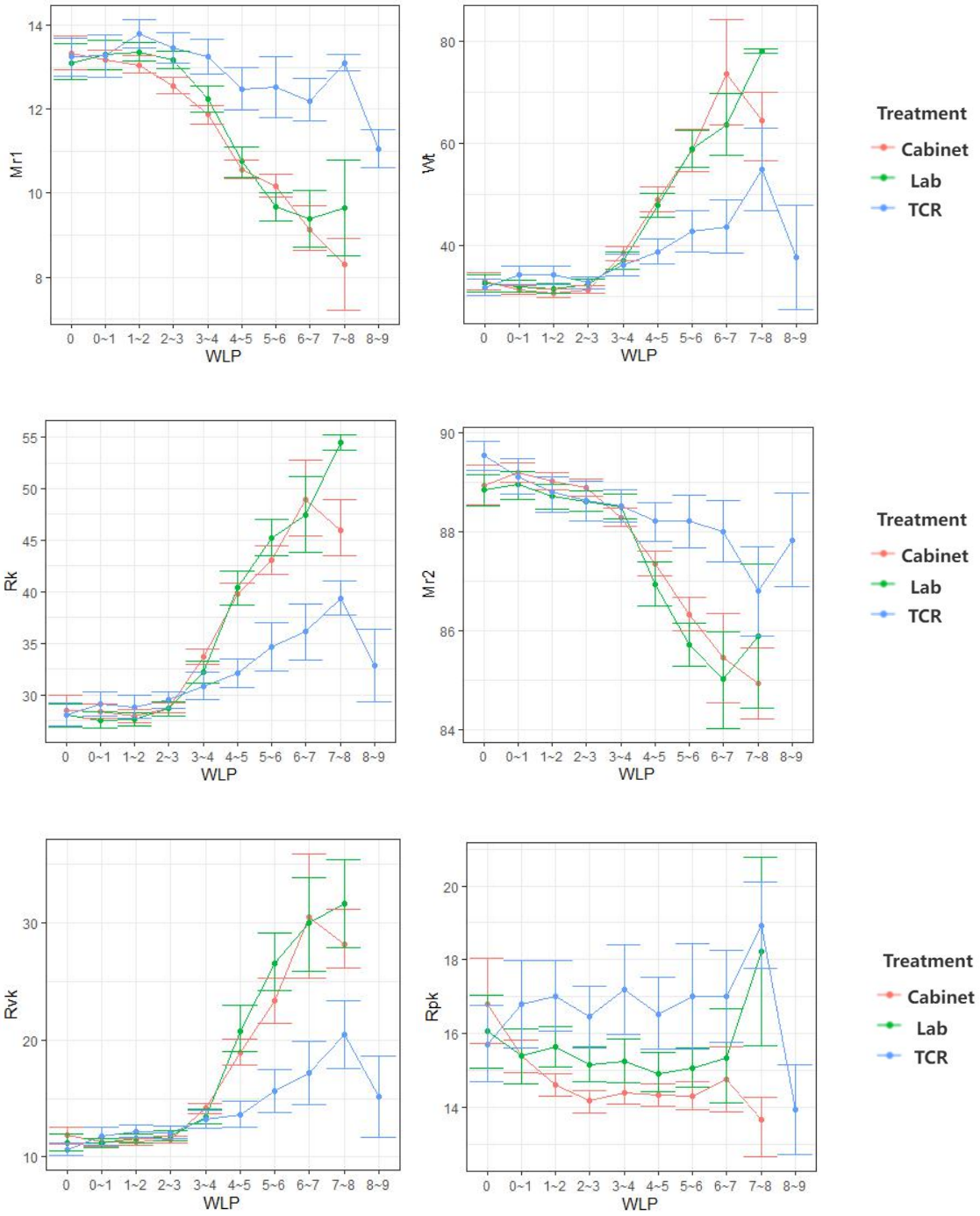
Mr1
Wt
Rk
Mr2
Rvk
Rpk
WLP
0
0~1
1~2
2~3
3~4
4~5
5~6
6~7
7~8
8~9
Treatment
Cabinet
Lab
TCR

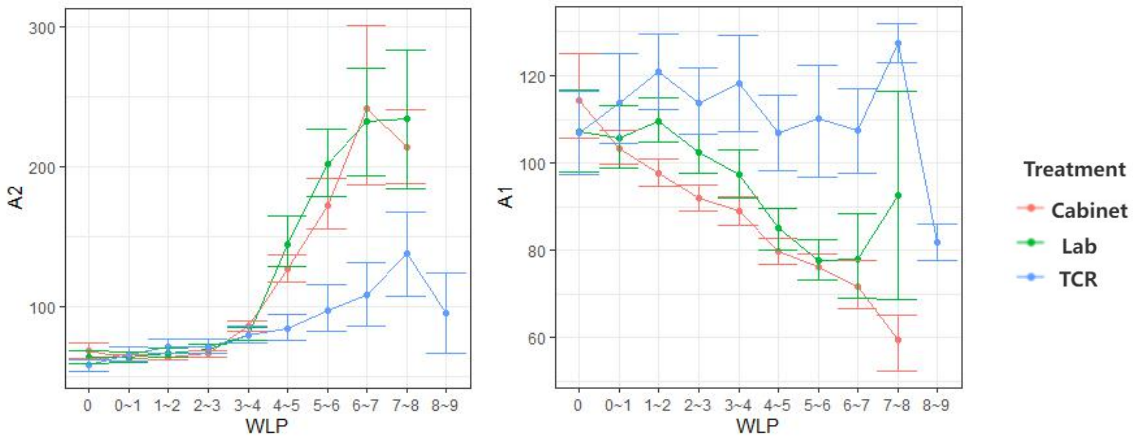
A2
300
200
100
0
0~1
1~2
2~3
3~4
4~5
5~6
6~7
7~8
8~9
WLP
A1
120
100
80
60
0
0~1
1~2
2~3
3~4
4~5
5~6
6~7
7~8
8~9
WLP
Treatment
Cabinet
Lab
TCR